

**ICE NUCLEATING PARTICLES IN THE CANADIAN ARCTIC**

by

Victoria Emilie Irish

MPhil, Cambridge University, 2010

MChem, First class honours, Durham University, 2008

A DISSERTATION SUBMITTED IN PARTIAL FULFILLMENT OF  
THE REQUIREMENTS FOR THE DEGREE OF

DOCTOR OF PHILOSOPHY

in

THE FACULTY OF GRADUATE AND POSTDOCTORAL STUDIES  
(Chemistry)

THE UNIVERSITY OF BRITISH COLUMBIA  
(Vancouver)

November 2018

© Victoria Emilie Irish, 2018

The following individuals certify that they have read, and recommend to the Faculty of Graduate and Postdoctoral Studies for acceptance, the dissertation entitled:

Ice Nucleating Particles in the Canadian Arctic

---

submitted by Victoria Irish in partial fulfillment of the requirements for

the degree of Doctor of Philosophy

in Chemistry

**Examining Committee:**

Allan Bertram

Supervisor

Kristin Orians

Supervisory Committee Member

Supervisory Committee Member

Phillip Austin

University Examiner

Philippe Tortell

University Examiner

**Additional Supervisory Committee Members:**

Supervisory Committee Member

Supervisory Committee Member

## Abstract

Ice nucleating particles (INPs) in the Arctic can influence climate and precipitation in the region; yet our understanding of the concentrations and sources of INPs in this region remain uncertain. The following dissertation investigates 1) the properties and concentrations of INPs in the sea surface microlayer and bulk seawater samples collected in the Canadian Arctic, and 2) the source region of measured concentrations of INPs in the Canadian Arctic marine boundary layer. All measurements were made in the Canadian Arctic on board the *CCGS Amundsen* during the summers of 2014 and 2016.

INPs were ubiquitous in the microlayer and bulk seawater samples, and were likely heat-labile biological materials between 0.2 and 0.02  $\mu\text{m}$  in diameter. There was a strong negative correlation between salinity and freezing temperatures, and a strong positive correlation between the fraction of meteoric water in each sample and freezing temperatures, possibly due to INPs associated with terrestrial run-off. Spatial patterns of INPs and salinities in 2014 and 2016 were similar. However the concentrations of INPs were higher on average in 2016 compared to 2014, and INP concentrations were enhanced in the microlayer compared to bulk seawater in several samples collected in 2016.

Average concentrations of INPs measured in the Canadian Arctic marine boundary layer fell within the range of INP concentrations measured in other marine boundary layer locations. The ratio of measured mineral dust surface area to sea spray surface area ranged from 0.03 to 0.09. Based on these ratios, and the ice active surface site densities of mineral dust and sea spray aerosol determined in previous laboratory studies, mineral dust is a more important contributor to the INP population than sea spray aerosol for the samples analysed. Based on particle dispersion

modelling, the source of INPs in the Canadian Arctic marine boundary layer during the summer of 2014 was from continental regions such as the Hudson Bay area, eastern Greenland, or northwestern continental Canada.

## **Lay Summary**

Ice nucleating particles (INPs) are atmospheric particles that catalyse the formation of ice crystals in clouds. INPs influence cloud properties, including cloud lifetimes, and thus impact the Earth's radiative properties and hydrological cycle. Warming in the Arctic will melt sea ice, glaciers, and permafrost, thereby increasing the amount of erodible soil and the surface area of the ocean that is exposed to the atmosphere. Since erodible soil and the ocean are potential sources of INPs to the atmosphere, the effects of warming in the Arctic on the population of INPs in the atmosphere are unknown. The research presented in this dissertation investigates the concentrations, properties and sources of INPs in the Canadian Arctic. The results from this research can be used in numerical models for predicting future climate in this region.

## Preface

Chapter 2 is a co-authored peer-reviewed journal article. Chapters 3 and 4 are co-authored journal articles under peer-review. My contributions to each research chapter are detailed below.

Chapter 2 (first author on a published journal article): Victoria E. Irish, Pablo Elizondo, Jessie Chen, Cédric Chou, Joannie Charette, Martine Lizotte, Luis A. Ladino, Theodore W. Wilson, Michel Gosselin, Benjamin J. Murray, Elena Polishchuk, Jonathan P. D. Abbatt, Lisa A. Miller, and Allan K. Bertram: Ice nucleating particles in Canadian Arctic sea surface microlayer and bulk seawater, *Atmos. Chem. Phys.*, **17**, 10583-10595, 2017

- I formulated research questions and designed research project with help from my supervisor,
- I collected microlayer and bulk seawater samples with help from Dr. M. Lizotte in the field during the summer of 2014,
- I performed ice nucleation experiments with help from P. Elizondo,
- I performed data analysis of ice nucleation experiments with help from P. Elizondo,
- I prepared all figures for publication, and
- I wrote the paper with guidance from my supervisor.
- Additional contributions from co-authors include:
  - Dr. M. Gosselin and J. Charette provided bacteria and phytoplankton data,
  - Dr. M. Lizotte provided dimethyl sulfide concentration data,
  - Dr. T. W. Wilson and Dr. B. J. Murray provided some of the INP data, bacteria abundance, and salinity data from the Arctic and Atlantic,

- Dr. E. Polishchuk and J. Chen gave valuable advice, and provided storage space for the samples and the heating block, and
- Dr. L. Miller provided microlayer sampling training, equipment for the field, and valuable suggestions to the manuscript.

Chapter 3 (first author on a journal article submitted to a peer-reviewed journal): Victoria E. Irish, Sarah Hanna, Yu Xi, Matthew Boyer, Elena Polishchuk, Jessie Chen, Jonathan P. D. Abbatt, Michel Gosselin, Rachel Chang, Lisa Miller, Allan K. Bertram: Revisiting properties and concentrations of ice nucleating particles in the sea surface microlayer and bulk seawater in the Canadian Arctic during summer.

- I formulated research questions and designed research project with help from my supervisor,
- I collected microlayer and bulk seawater samples with help from M. Boyer and Dr. R. Chang in the field during the summer of 2016,
- I performed most ice nucleation experiments,
- I performed data analysis of ice nucleation experiments,
- I prepared most figures for publication, and
- I wrote the paper with guidance from my supervisor.
- Additional contributions from co-authors include:
  - Dr. S. Hanna provided satellite chlorophyll *a* measurements and prepared the chlorophyll *a* correlation plots,
  - Y. Xi carried out the ice nucleation experiment for non-colligative effects of seawater salts on the freezing temperature of the samples,
  - Dr. M. Gosselin provided bacteria and phytoplankton abundance data,

- Dr. L. Miller provided equipment for microlayer sampling in the field, and valuable suggestions to the manuscript, and
- Dr. E. Polishchuk and J. Chen gave valuable advice, and provided storage space for the samples and the heating block.

Chapter 4 (first author on a journal article submitted to a peer-reviewed journal): Victoria E. Irish, Sarah Hanna, Megan Willis, Swarup China, Jennie Thomas, Jeremy Wentzell, Ana Cirisan, Meng Si, Richard Leitch, Jennifer Murphy, Jonathan P. D. Abbatt, Alex Laskin, Eric Girard, Allan K. Bertram: Ice nucleating particles in the marine boundary layer in the Canadian Arctic during summer 2014

- I formulated research questions and designed research project with help from my supervisor,
- I collected aerosol samples in the field during the summer of 2014 and 2016,
- I performed ice nucleation experiments,
- I performed data analysis of ice nucleation experiments,
- I performed HYSPLIT back trajectory analysis,
- I prepared most figures for publication, and
- I wrote the paper with guidance from my supervisor.
- Additional contributions from co-authors include:
  - Dr. S. Hanna, Dr. M. Willis, and Dr. J. Thomas carried out all FLEXPART back trajectory analysis, and Dr. S. Hanna carried out in-depth HYSPLIT trajectory analysis,
  - Dr. S. China, and Dr. A. Laskin performed CCSEM-EDX analysis, and
  - Dr. J. Wentzell provided HONO concentration data.

# Table of Contents

<b>Abstract.....</b>	<b>iii</b>
<b>Lay Summary .....</b>	<b>v</b>
<b>Preface.....</b>	<b>vi</b>
<b>Table of Contents .....</b>	<b>ix</b>
<b>List of Tables .....</b>	<b>xiv</b>
<b>List of Figures.....</b>	<b>xvi</b>
<b>List of Symbols .....</b>	<b>xxiv</b>
<b>List of Abbreviations .....</b>	<b>xxvi</b>
<b>Acknowledgements .....</b>	<b>xxviii</b>
<b>Dedication .....</b>	<b>xxx</b>
<b>Chapter 1: Introduction .....</b>	<b>1</b>
1.1 Atmospheric aerosol .....	1
1.1.1 Types of atmospheric aerosol .....	2
1.1.1.1 Sea spray aerosol.....	2
1.1.1.2 Mineral dust .....	4
1.2 Climatic impact of aerosols .....	4
1.3 Ice nucleation in the atmosphere.....	5
1.3.1 Mechanisms .....	5
1.3.2 Climatic impact of INPs.....	7
1.3.3 Sources of INPs.....	9
1.3.3.1 Sea spray as a source of INPs .....	9

1.3.3.2	Mineral dust as a source of INPs .....	10
1.3.4	The Arctic as a region of interest for climate .....	10
1.4	Overview of dissertation .....	11
<b>Chapter 2: Ice nucleating particles in Canadian Arctic sea surface microlayer and bulk seawater .....</b>		<b>13</b>
2.1	Introduction.....	13
2.2	Experimental .....	15
2.2.1	Sampling locations and collection methods.....	15
2.2.2	Ice nucleation properties of the samples.....	17
2.2.2.1	Droplet freezing technique and INP concentrations .....	17
2.2.2.2	Heating tests.....	18
2.2.2.3	The size of the INPs.....	18
2.2.2.4	Corrections for freezing temperature depression.....	19
2.2.3	Phytoplankton and bacterial abundance.....	19
2.2.4	Dimethyl sulfide (DMS) measurements .....	20
2.2.5	Statistical analysis.....	20
2.3	Results and Discussion .....	21
2.3.1	INPs in the microlayer and bulk seawater .....	21
2.3.2	Properties of the INPs.....	30
2.3.2.1	Heat-labile biological material.....	30
2.3.2.2	Size of INPs .....	31
2.4	Summary and conclusions .....	33

**Chapter 3: Revisiting properties and concentrations of ice nucleating particles in the sea surface microlayer and bulk seawater in the Canadian Arctic during summer.....35**

3.1	Introduction.....	35
3.2	Experimental.....	36
3.2.1	Collection methods.....	36
3.2.1.1	Automated sampler method.....	37
3.2.2	Ice nucleation properties of the samples.....	39
3.2.2.1	Droplet freezing technique and INP concentrations.....	39
3.2.2.2	Heating and filtration tests.....	39
3.2.2.3	Corrections for freezing temperature depression.....	40
3.2.3	Bacterial and phytoplankton abundance.....	41
3.2.4	Fraction of meteoric water from stable oxygen isotope data.....	41
3.2.5	Chlorophyll <i>a</i> satellite data.....	42
3.2.6	Statistical analysis.....	43
3.3	Results and Discussion.....	43
3.3.1	Concentrations of INPs.....	43
3.3.2	Effect of heating and filtering the samples.....	47
3.3.3	Spatial patterns of INPs in the Canadian Arctic.....	48
3.3.4	Correlations with biological and physical properties of the microlayer and bulk seawater.....	51
3.3.4.1	Chlorophyll <i>a</i> satellite data correlations.....	55
3.4	Conclusions.....	55

**Chapter 4: Ice nucleating particles in the marine boundary layer in the Canadian Arctic during summer 2014.....57**

4.1 Introduction..... 57

4.2 Experimental..... 58

4.2.1 Sampling locations..... 58

4.2.2 Quantification of INPs..... 60

4.2.2.1 Micro-orifice single stage impactor..... 60

4.2.2.2 Droplet freezing technique..... 61

4.2.3 Effect of ship emissions on measured INP..... 64

4.2.4 Particle dispersion modelling..... 65

4.2.5 Statistical analyses..... 66

4.2.6 Computer controlled scanning electron microscopy with energy dispersive X-ray spectroscopy (CCSEM-EDX)..... 66

4.3 Results and Discussion..... 67

4.3.1 Measured INP concentrations..... 67

4.3.2 Measured ratios of mineral dust surface area to sea salt surface area..... 69

4.3.3 Particle dispersion modelling..... 71

4.4 Conclusions..... 75

**Chapter 5: Conclusions and future work.....77**

5.1 Concentrations and properties of INPs in the microlayer and bulk seawater in the Canadian Arctic..... 77

5.2 Measurements of INPs in the marine boundary layer in the Canadian Arctic..... 79

5.3 Avenues for future research..... 80

<b>References.....</b>	<b>84</b>
<b>Appendices.....</b>	<b>103</b>
Appendix A.....	103
A.1 Classical nucleation theory: homogeneous ice nucleation.....	103
A.2 Classical nucleation theory: heterogeneous ice nucleation.....	104
Appendix B.....	107
B.1 Corrections for freezing temperature depression .....	107
Appendix C.....	116
C.1 Non-colligative effects of seawater on freezing temperatures .....	116
Appendix D.....	126
D.1 Calculation of $n_s$ -values of Niemand et al. (2012) and DeMott et al. (2016) .....	126

## List of Tables

Table 2.1: Sampling times and geographic coordinates for the eight stations investigated during July-August 2014 in the Canadian Arctic.....	15
Table 2.2: Correlation analyses between chemical or physical properties of bulk seawater and T <sub>10</sub> -values for the bulk seawater samples. Numbers in bold represent correlations that are statistically significant ( $p < 0.05$ ). .....	24
Table 3.1: Sampling times and geographic coordinates for the eleven stations investigated.....	37
Table 3.2: Correlations between biological and physical properties of microlayer and bulk seawater and T <sub>10</sub> -values for 2016. Values in bold indicate results that are statistically significant. The symbol n/a represents correlations for which there were no data.....	52
Table 4.1: Correlation coefficients (R), p and n values for correlation analysis between [INP] (L <sup>-1</sup> ) at -15, -20, and -25 °C and the time the air mass spent over different surface types within 0-300 m of the surface. Numbers in bold indicate correlations that are statistically significant ( $p < 0.05$ ). .....	74
Table B.1: Conditions at sampling stations. ....	108
Table B.2: Correlation analyses between chemical or physical properties of bulk seawater and T <sub>50</sub> -values for the bulk seawater samples. Numbers in bold represent correlations that are statistically significant ( $p < 0.05$ ). .....	109
Table B.3: Correlation analyses between phytoplankton and bacterial abundance in the microlayer and bulk seawater and T <sub>10</sub> -values for the microlayer and bulk seawater. ....	109
Table C.1: Conditions at sampling stations. ....	117
Table D.1: Dates, times, and locations of sampling. ....	127

Table D.2: Total number of particles analysed, and fractions of the total number of particles classified as either dust or sea salt using CCSEM-EDX..... 128

## List of Figures

Figure 1.1: Illustration of the generation of sea spray particles enriched in surface-active marine material from bubbles bursting at the air-sea interface. Adapted from Wilson et al. (2015). .....	3
Figure 1.2: Schematic of different modes of ice nucleation (Pruppacher and Klett (1997)).....	6
Figure 1.3: Schematic diagram illustrating the probable effects of an increase in INPs on mixed phase clouds and ice clouds. Adapted from DeMott et al. (2010).....	7
Figure 2.1: A) locations of current and previous studies of INPs (immersion mode) in the microlayer. B) Locations of current and previous studies of INPs (immersion mode) in bulk seawater or mixtures of bulk seawater and microlayer. Dates and coordinates for samples in the current study can be found in Table 2.1.....	14
Figure 2.2: Fraction of droplets frozen (in the immersion mode) versus temperature. A) and B) correspond to the microlayer and bulk seawater, respectively. Each set of line and markers represents the results for 3 repeat experiments of a sample or “blank”, adding up to a total of between 45 to 60 freezing events in each set. Also included are the respective “blank” samples and ultrapure water. Each data point corresponds to a single freezing event in the experiments. All microlayer and bulk seawater freezing points have been corrected for freezing point depression to account for dissolved salts in seawater (Section 2.2.2.4). The uncertainty in temperature is not shown but is $\pm 0.3$ °C.....	22
Figure 2.3: $T_{10}$ -values for microlayer and bulk seawater samples. All data have been corrected for freezing point depression. Boxes represent the 25 <sup>th</sup> , 50 <sup>th</sup> and 75 <sup>th</sup> percentiles, and whiskers represent the minima and maxima. ....	23

Figure 2.4: The concentrations of INPs,  $[INP(T)]$ , in A) the microlayer, and B) bulk seawater samples. All data, including those from other studies, are corrected for freezing point depression. Upper and lower limits to  $[INP(T)]$  ( $L^{-1}$ ) associated with the current study describe the statistical uncertainty due to the limited number of nucleation events observed in the freezing experiments (Koop et al. (1997))..... 26

Figure 2.5: Correlation plots with a 1:1 line for reference. A) Freezing temperatures for microlayer and bulk seawater samples in this study. All error bars represent the 95 % confidence intervals of the  $T_{10}$ -values from 3 replicate experiments. All data have been corrected for freezing point depression. B)  $T_{10}$ -values for microlayer and bulk seawater samples from Wilson et al. (2015). All data have been corrected for freezing point depression. C) Bacterial abundance in the microlayer and bacterial abundance in the bulk seawater in this study. There was only one reliable microlayer sample from station 7 for bacterial abundance; therefore, the percentage error for this station was assigned the maximum percentage error from the other bacterial abundance. D) Bacterial abundance in the microlayer and bacterial abundance in the bulk seawater from Wilson et al. (2015)..... 27

Figure 2.6: Effect of heating on the fraction frozen for unfiltered samples from A) the microlayer, and B) bulk seawater. Each data point corresponds to one droplet freezing event, and all data have been corrected for freezing point depression. The uncertainty in temperature is not shown but is  $\pm 0.3$  °C..... 30

Figure 2.7:  $T_{10}$ -values as a function of filter pore size in A) microlayer samples, and B) bulk seawater samples. Filter pore sizes were 10, 0.2, and 0.02  $\mu m$ . Error bars are the 95 % confidence intervals of the  $T_{10}$ -values from 3 replicate experiments. All data have been corrected for freezing point depression. .... 32

Figure 3.1: Map showing locations of microlayer and bulk seawater sampling in 2014 (pink) and 2016 (blue). ..... 36

Figure 3.2: Comparison of the concentrations of INPs, [INP(T)], in A) the microlayer, and B) bulk seawater samples from the 2014 study (dark pink squares) and the 2016 study (blue triangles). All data are corrected for freezing point depression. Error bars represent the statistical uncertainty due to the limited number of nucleation events observed in the freezing experiments (Koop et al., 1997). ..... 46

Figure 3.3: Relationship between  $T_{10}$ -values for microlayer and bulk seawater samples with a 1:1 line for reference. Data points are the average  $T_{10}$ -values from three repeat experiments. Error bars are the 95 % confidence interval for three repeat experiments. .... 47

Figure 3.4: Spatial patterns of (A, B)  $T_{10}$ -values, and (C, D) salinities in (A, C) 2016 and (B, D) 2014 for bulk seawater. .... 49

Figure 3.5: A) Map showing regions of similar sampling locations in 2014 (pink) and in 2016 (blue). Sampling sites in 2014 that were near sampling sites in 2016 were paired together (indicated with boxes in the figure) and assigned letters A-F. Although there are two stations in box A for 2016, we only used data for the station that was closest to the one in 2014. Relationships between B)  $T_{10}$ -values, and C) salinities for microlayer and bulk seawater samples in 2014 and 2016 for similar sampling locations. The letters plotted in B) and C) indicate the locations in A). Red letters represent bulk seawater data and blue letters represent microlayer data. .... 50

Figure 3.6: Relationships between biological and physical properties of bulk seawater and  $T_{10}$ -values for the 2016 study. .... 52

Figure 3.7: Relationships between the fraction of meteoric water in each sample, and the  $T_{10}$ -values and  $T_{50}$ -values for bulk seawater for the 2016 study. Note that a negative  $f_{MW}$  was generated for one station (station 4) due to the definition of our seawater end-member. .... 53

Figure 3.8: Correlation plot between chlorophyll  $a$  concentrations derived from satellite imagery from the GlobColour project and the  $T_{10}$ -values of microlayer and bulk seawater for 2016. .... 55

Figure 4.1: Locations of sampling. Blue circles around the red dots indicate the locations of samples used in DeMott et al. (2016). Information on specific geographical coordinates is given in Table D.1 (Appendix D). ..... 59

Figure 4.2: Plot of  $[INP]$  ( $L^{-1}$ ) as a function of temperature ( $^{\circ}C$ ) for A) the blanks, B) the samples, and C) the blanks and samples. The  $[INP]$  ( $L^{-1}$ ) of 11 blanks are shown in A and C. Each blank was performed on a separate hydrophobic glass substrate. Error bars are not shown to improve the visibility of the data in the plot. Error bars in the x direction are  $\pm 0.3$   $^{\circ}C$  for each data point. Error bars in the y direction were calculated using nucleation statistics following Koop et al. (1997); the errors for our measured  $[INP]$  ( $L^{-1}$ ) are reported in Fig. D.6 (Appendix D). ..... 68

Figure 4.3: Plot of  $[INP]$  ( $L^{-1}$ ) as a function of temperature including a comparison to field results from several recent field studies in marine environments reported in DeMott et al. (2016). The purple diamonds represent averages of the data reported in this study at -15, -20, and -25  $^{\circ}C$ . Error bars are the standard error of the mean. Other coloured circles represent INP measurements from field studies in marine environments reported in DeMott et al., (2016), with the locations indicated in the legend. .... 69

Figure 4.4: A) Ratios of the surface area of mineral dust to the surface area of sea salt measured by CCSEM-EDX (blue circles). Ratios of predicted  $[INP(T)]_{MD}$  to the predicted  $[INP(T)]_{SS}$

calculated using CCSEM-EDX measurements (red circles) at B) -25 °C, C) -20 °C, and D) -15 °C. .... 71

Figure 4.5: Top row: Average FLEXPART-WRF footprint potential emission sensitivities (PES) plots for A) all sampling days, B) the 36 % of samples with the highest [INP(T)] (L<sup>-1</sup>), and C) the 36 % of samples with the lowest [INP(T)] (L<sup>-1</sup>). Black circles indicate the ship’s position at the sampling mid-time. Middle row: Maps showing the ratios of D) plot B to plot A, and E) plot C to plot A. Bottom row: Maps showing the surface cover type on F) the first day of sampling (14<sup>th</sup> July), and G) the last day of sampling (12<sup>th</sup> August). Bare land, open water, sea ice, and snow cover are shown as beige, dark blue, light blue, and white, respectively. The NSIDC data classifies each 4 x 4 km grid cell as one covered by sea, land without snow, sea ice, or snow-covered land. In these plots, white represents snow-covered land, light blue represents sea ice, dark blue represents open water, and beige represents bare land. Note that for this study, lakes are included in the bare land category. .... 73

Figure A.1 Change in  $\Delta G_i$  as a function of the radius of the ice embryo.  $\Delta G_i^*$  is the activation energy required for a critical cluster of water molecules to form an ice embryo; the radius,  $r^*$ , is the critical radius. .... 104

Figure B.1: Photo of sampling with the glass plate (Harvey and Burzell, 1972). .... 110

Figure B.2: Correlation plots between chemical and physical properties, and T<sub>10</sub>-values in the bulk seawater. R and p values can be found in Table 2.2 in the main text. .... 111

Figure B.3: Sample locations and monthly average chlorophyll *a* concentrations for sampling during the current study. Chlorophyll *a* concentrations were obtained from the NASA Ocean Biology Distributed Active Archive Centre (OB.DAAC). .... 112

Figure B.4: Sample locations and monthly average chlorophyll *a* concentrations for sampling during the Wilson et al. (2015) study in the Arctic. Chlorophyll *a* concentrations were obtained from the NASA OB.DAAC..... 113

Figure B.5: Sample locations and monthly average chlorophyll *a* concentrations for sampling during the Wilson et al. (2015) study in the Atlantic. Chlorophyll *a* concentrations were obtained from the NASA OB.DAAC..... 114

Figure B.6: Plots of the fraction of droplets frozen (in the immersion mode) versus temperature for samples filtered with 10  $\mu\text{m}$ , 0.2  $\mu\text{m}$  and 0.02  $\mu\text{m}$  filters in A) the microlayer, and B) bulk seawater. Each set of line and markers represents results for 3 repeat experiments of each sample or “blank”, adding up to a total of between 45 to 60 freezing events in each set. All microlayer and bulk seawater freezing points have been corrected for freezing point depression to account for dissolved salts in seawater (Section 2.2.4). The uncertainty in temperature is not shown but is  $\pm 0.3$   $^{\circ}\text{C}$ ..... 115

Figure C.1: Photo of the automated sampling catamaran being lowered to the side of the zodiac. Photo credit: Robin Bénard..... 118

Figure C.2: Plots comparing the  $T_{50}$ -values and  $T_{10}$ -values for duplicate samples not frozen or stored (i.e. fresh) and samples stored at  $-80$   $^{\circ}\text{C}$  for up to six months. A) Microlayer samples and B) bulk seawater samples. Data points are the average  $T_{50}$ -values and  $T_{10}$ -values from three repeat experiments. Error bars are the 95 % confidence interval for three repeat experiments. With experimental variability, all microlayer and bulk seawater samples lie within the 1:1 line  $\pm 2$   $^{\circ}\text{C}$ ..... 119

Figure C.3: Fraction of droplets frozen (in the immersion mode) versus temperature in A) the microlayer, and B) bulk seawater. Each set of line and markers represents the results for 3 repeat

experiments of a sample or a sample passed through a 0.02  $\mu\text{m}$  filter, adding up to a total of between 45 to 60 freezing events in each set. Each data point corresponds to a single freezing event in the experiments. Also included are the results for ultrapure water and for ultrapure water sampled through the automated sampler (procedural blanks). All microlayer and bulk seawater freezing points have been corrected for freezing point depression to account for dissolved salts in seawater. The uncertainty in temperature is not shown but is  $\pm 0.3$   $^{\circ}\text{C}$ . The freezing properties of the samples after 0.02  $\mu\text{m}$  filtration may still contain some small particles ( $< 0.02$   $\mu\text{m}$  in diameter) that can act as INPs (Dreischmeier et al., 2017; O’ Sullivan et al., 2015)..... 120

Figure C.4: Preliminary data comparing the fraction of frozen droplets from the glass plate method to the fraction of frozen droplets from the automated sampling method. Data from stations 9 and 11 are used. Data are not corrected for freezing point depression..... 121

Figure C.5: Effect of heating on the fraction frozen curves for unfiltered samples from A) the microlayer, and B) bulk seawater. Each data point corresponds to one droplet freezing event. All data have been corrected for freezing point depression..... 122

Figure C.6: Fraction of droplets frozen as a function of filter pore size in A) microlayer samples, and B) bulk seawater samples. Filter pore sizes used in the experiments were 10  $\mu\text{m}$  (yellow diamonds), 0.2  $\mu\text{m}$  (red circles) and 0.02  $\mu\text{m}$  (blue triangles). All data have been corrected for freezing depression. .... 123

Figure C.7: Spatial patterns of (A, B)  $T_{10}$ -values and (C, D) salinities in (A, C) 2016 and (B, D) 2014 for the microlayer..... 124

Figure C.8: Plot of the  $T_{10}$ -values of microlayer sample from station 4 as a function of salinity. The salinity was adjusted by adding solutions of Instant Ocean in ultrapure water to the samples. Data points represent averages and error bars represent the 95 % confidence intervals of 3 repeat

experiments. Light blue circles represent  $T_{10}$ -values uncorrected for freezing point depression. Dark blue triangles represent  $T_{10}$ -values after correcting for freezing point depression by the presence of salts as described in Section 2.3.3. Red pentagons represent  $T_{10}$ -values for solutions of Instant Ocean in ultrapure water, after correcting for freezing point depression. .... 125

Figure D.1: A) Air temperature, B) wind speed, and C) relative humidity (RH) during sampling. .... 129

Figure D.2: Photo of the MOSSI (top shelf), and TSP inlet on the bridge of the CCGS *Amundsen*. .... 129

Figure D.3: Comparison of  $[INP]$  ( $L^{-1}$ ) when the wind direction measured on the ship was coming from the bow of the ship (between  $0-90^\circ$  and  $270-360^\circ$ , where  $0^\circ/360^\circ =$  bow of ship) and when the minute average wind speed was higher than 2.5 m/s (in red) to the  $[INP]$  ( $L^{-1}$ ) when the wind direction was from the stern of the ship (between  $90^\circ-270^\circ$ ) or when the minute average wind speed was less than 2.5 m/s (in black). Error bars represent the 95 % confidence interval. .... 130

Figure D.4: WRF domain used in FLEXPART ..... 131

Figure D.5: CCSEM-EDX particle classification scheme. Numbers represent atomic percentage. .... 131

Figure D.6: Time series of  $[INP(T)]$  ( $L^{-1}$ ) at A)  $-15^\circ C$ , B)  $-20^\circ C$ , and C)  $-25^\circ C$ . Error bars were calculated using nucleation statistics following Koop et al. (1997). .... 132

Figure D.7: Plots for correlation analyses between the time the air mass spent over different surface types within 0-300 m of the surface and  $[INP(T)]$  at A)  $-15^\circ C$ , B)  $-20^\circ C$ , and C)  $-25^\circ C$ . Correlation statistics for analyses can be found in Table 4.1. .... 133

## List of Symbols

[INP(T)]	Concentration of INPs at T
[INP(T)] <sub>MD</sub>	Concentration of INPs at T from mineral dust
[INP(T)] <sub>SS</sub>	Concentration of INPs at T from sea spray
#INP(T)	Number of INPs at T
%	Percentage
°C	Degrees Celsius
°N/°W	Degrees North/degrees West
cm	Centimetre
g	Gram
kg	Kilogram
km	Kilometre
L	Litre
ln	Natural logarithm
log	Logarithm to the base of 10
m	Metre
min	Minute
mL	Millilitre
mm	Millimetre
mW	Milliwatt
MΩ	Mega ohm
nm	Nanometre

$N_o$	Total number of droplets
$N_s$	Number of spots in the field of view
$n_s(MD)$	Ice active surface site density for mineral dust from (Niemand et al., 2012)
$n_s(SS)$	Ice active surface site density for sea spray from (DeMott et al., 2016)
$N_u(T)$	Number of unfrozen droplets
p	Probability value
R	Correlation coefficient
s	Seconds
$S_{MD}$	Total surface area for mineral dust measured by CCSEM-EDX
$S_{SS}$	Total surface area for sea salt measured by CCSEM-EDX
T	Temperature
$T_{10}$	Temperature at which 10 % of droplets have frozen by
$T_{50}$	Temperature at which 50 % of droplets have frozen by
Tg	Teragram
V	Volume
W	Watt
yr	Year
$\mu\text{L}$	Microlitre
$\mu\text{m}$	Micrometre

## List of Abbreviations

BP	Bandpass
BS	Beaufort Scale
CCD	Charged-coupled device
CCGS	Canadian Coast Guard Ship
CCN	Cloud Condensation Nuclei
CCSEM-EDX	Computer Controlled Scanning Electron Microscopy - Energy Dispersive X-ray
CFDC	Continuous Flow Diffusion Chamber
DAWT	Dalhousie Aerosol Water Tank
DFT	Droplet Freezing Technique
DMS	Dimethyl sulfide
ECMWF	European Centre for Medium-Range Weather Forecasts
EMSL	Environmental Molecular Sciences Laboratory
EOS	Earth Observing System
EPS	Extracellular Polymeric Substances
ERC	European Research Council
ESDIS	Earth Science Data and Information System
FLEXPART-WRF	FLEXible PARTicle dispersion model - Weather Research and Forecasting
HDPE	High Density Polyethylene
INP	Ice Nucleating Particle

IPCC	Intergovernmental Panel on Climate Change
LANCE	Land, Atmosphere Near real-time Capability for EOS
MODIS	Moderate Imaging Spectrometer
MOSSI	Micro-Orifice Single Stage Impactor
MOUDI	Micro-Orifice Uniform Deposit Impactor
NASA OB.DAAC	National Aeronautics and Space Administration Ocean Biology Distributed Active Archive Centre
NERC	Natural Environment Research Council
NETCARE	NETwork on Climate and Aerosol: addressing key uncertainties in Remote Canadian Environments
PBAP	Primary Biological Aerosol Particle
PES	Potential Emission Sensitivity
PNNL	Pacific Northwest National Laboratory
PTFE	Polytetrafluoroethylene
RH	Relative Humidity
SOA	Secondary Organic Aerosol
TEM	Transmission Electron Microscopy
TSP	Total Suspended Particulate
UTC	Coordinated Universal Time
VIIRS	Visible/Infrared Imager Radiometer Suite
YG	Yellow Green

## Acknowledgements

Words cannot express the gratitude I feel towards my supervisor, Allan Bertram, for guiding me through the ups and downs of my PhD. The support and kindness he shows all his students never falters and I consider myself extremely fortunate to have met and known him.

I would like to thank all my current and past colleagues in the Bertram group. A special thank you goes to Meng Si and Ryan Mason for showing me the ropes when I first started. Also to Dagny Ullmann, Erin Evoy, and Adrian Maclean for their friendship over the years.

I would like to thank all the Chemistry department facilities for their assistance. Without the hard work of the Mechanical and Electrical Engineering shops I would not have had functional instruments to deploy in my field campaigns. I would also like to thank Jessie Chen and Elena Polishchuk in the bioservices for their support.

This research was made possible through contributions from numerous individuals and scientific institutions, listed below:

- Chapters 2 and 3: I would like to thank the scientists, officers, and crew of the CCGS *Amundsen* for support during the expeditions in 2014 and 2016; Lucius Perreault for land-based support with the microlayer sampler; Allison Lapin, Eugene Shen, Hang Nguyen for help with INP analysis; Mélanie Simard, Joannie Charette, Aude Boivin-Rioux and Claude Belzile for flow cytometry analysis; and Drs. Dennis A. Hansell and Wenhao Chen for providing Reference Materials. I would also like to thank Lisa Miller, Martine Lizotte, and Michel Gosselin for helpful advice and discussions on oceanography. The Natural Sciences and Engineering Research Council of Canada and Fisheries and Oceans Canada for funding of the NETCARE project, support from The European Research Council, (ERC 648661 MarineIce) and the Natural Environment

Research Council (NERC, NE/K004417/1). GlobColour data (<http://globcolour.info>) used in this study has been developed, validated, and distributed by ACRI-ST, France.

- Chapter 4: I acknowledge the use of data products from the Land, Atmosphere Near real-time Capability for EOS (LANCE) system operated by the NASA/GSFC/Earth Science Data and Information System (ESDIS) with funding provided by NASA/HQ. A portion of the research used the Chemical Imaging Initiative at Pacific Northwest National Laboratory (PNNL), a multi-program national laboratory operated by Battelle for the U.S. Department of Energy under Contract DE-AC05-76RL01830. The work was performed at EMSL (Ringgold ID 47937 and 48781), a DOE Office of Science User Facility sponsored by the Office of Biological and Environmental Research.

I want to thank all my friends who have supported me throughout my PhD in Canada. All the fun trips we have had together on weekends away have helped me go into the lab during the week with a healthy and happy mindset.

I want to thank my mum and dad. My mum fostered a sense of curiosity within me from an early age, and my dad always challenged me intellectually growing up. I miss you both so much, and I thank you every day for the life you have given me. I also want to thank my brother for always supporting me.

Finally I want to thank Steve, my rock; without you I would not have been able to carry on with my PhD after my parents passed away last November. You are such a patient, understanding, and wonderfully caring person, and I am so lucky to have met you.

*In memory of my mother and father, and to Steve.*

## Chapter 1: Introduction

### 1.1 Atmospheric aerosol

Atmospheric aerosol is defined as a suspension of liquid or solid particles in air (Seinfeld and Pandis, 2006). The term particle is often interchanged with the term aerosol (Finlayson-Pitts and Pitts Jr., 2000) and this practice is used throughout this dissertation. Atmospheric aerosol is emitted or formed in the atmosphere as primary or secondary aerosol, and ranges in diameter from approximately 0.01  $\mu\text{m}$  to greater than 10  $\mu\text{m}$ . Primary aerosol is emitted directly into the atmosphere from natural or anthropogenic sources, with natural sources contributing 98 % to the global aerosol flux (Gieré and Querol, 2010). Sea spray, mineral dust, and primary biological aerosol particles (PBAPs) are examples of important sources of natural primary aerosols emitted directly into the atmosphere. Sea spray and mineral dust contribute 84 % and 13 %, respectively, to all natural fluxes of primary aerosol in the atmosphere (Gieré and Querol, 2010). Secondary aerosol is formed by reaction of gaseous species found in the atmosphere, followed by condensation of low volatility products from the reactions. An example of the formation of a common secondary aerosol particle is the oxidation of volatile organic compounds followed by condensation of the oxidised products to form secondary organic aerosols (SOA) (Seinfeld and Pandis, 2006).

Number concentrations of atmospheric aerosol varies between  $10^2$  and  $10^8 \text{ cm}^{-3}$  depending on location (Seinfeld and Pandis, 2006). Examples of number concentrations of aerosol from different locations (ranging from highest to lowest) are polluted urban cities ( $10^5$  to  $10^8 \text{ cm}^{-3}$ ); rural continental regions ( $10^3$  to  $10^4 \text{ cm}^{-3}$ ); and marine environments ( $10^2 \text{ cm}^{-3}$ ) (Finlayson-Pitts and Pitts Jr., 2000; Seinfeld and Pandis, 2006). Remote environments such as

the Arctic can have number concentrations as low as  $10^1$  to  $10^2$   $\text{cm}^{-3}$  during winter months (Ström et al., 2003; Tunved et al., 2013).

### **1.1.1 Types of atmospheric aerosol**

Types of atmospheric aerosol include, but are not limited to particles resulting from volcanic eruptions, forests, dust storms, and oceans. Primary biological particles such as fungi, pollen, bacteria, algae, and viruses can also become airborne as aerosol. Furthermore, anthropogenic particles in the atmosphere result from activities such as traffic, biomass burning, and mining (Gieré and Querol, 2010). This research focuses on sea spray aerosol and mineral dust.

#### **1.1.1.1 Sea spray aerosol**

Estimates for global emissions of sea salt are approximately 10,000 Tg/yr (Gieré and Querol, 2010). Sea spray aerosol is emitted into the atmosphere from the ocean by the bubble bursting mechanism (Blanchard and Keith, 1963). Bubbles form in the ocean by waves breaking, and by the impact of rain and snow at the surface (Blanchard and Woodcock, 1957). The bubbles then rise through the bulk seawater column, scavenging and carrying surface-active marine material. Upon reaching the sea surface microlayer (herein referred to as microlayer) the bubbles will eject the surface-active marine material into the atmosphere via jet or film droplets as illustrated in Fig. 1.1. The microlayer is the interface between the ocean and the atmosphere. The thickness of the microlayer is  $< 1$  mm (Liss and Duce, 1997), and the physical and chemical properties of the microlayer are different from bulk seawater (Zhang et al., 2003). For example,

the concentration of organic material is often enhanced in the microlayer compared to in bulk seawater (Wurl et al., 2009). This research focuses, in part, on the microlayer and bulk seawater.

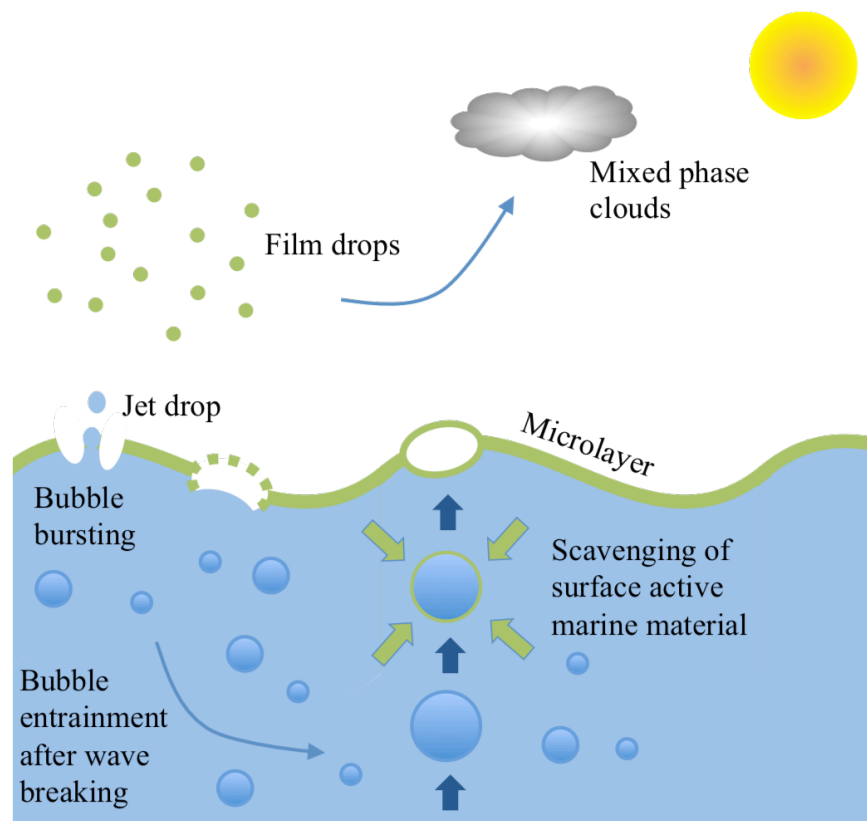


**Figure 1.1: Illustration of the generation of sea spray particles enriched in surface-active marine material from bubbles bursting at the air-sea interface. Adapted from Wilson et al. (2015).**

The composition and size of sea spray aerosol determines its role in atmospheric processes. Sea spray aerosol can be composed of inorganic salts and organic matter, such as colloids and marine aggregates (Ault et al., 2013). The chemistry of sea spray aerosol, and the types and amount of organic material emitted into the atmosphere is largely controlled by biological processes in the ocean (Ault et al., 2013; Cochran et al., 2017; Collins et al., 2013).

### **1.1.1.2 Mineral dust**

Atmospheric mineral dust particles are mainly composed of quartz, feldspar, calcite, illite, kaolinite, montmorillonite, and chlorite (Murray et al., 2012). Global emissions of mineral dust are estimated to be between 1000 and 4000 Tg/yr with ~90 % of emissions originating in the Northern Hemisphere (Boucher et al., 2013; Gieré and Querol, 2010; Murray et al., 2012; Seinfeld and Pandis, 2006; Tanaka and Chiba, 2006; Usher et al., 2003). Most mineral dust emissions come from dry, arid regions that undergo a lot of erosion. Therefore, mineral dust emissions in the Northern Hemisphere are dominated by Saharan dust, and mineral dust emissions in the Southern Hemisphere are dominated by Australian dust (Tanaka and Chiba, 2006). The range in estimated global dust emissions comes from the uncertainty associated with the complex process of raising dust into the atmosphere.

## **1.2 Climatic impact of aerosols**

Atmospheric aerosol plays an important role in our climate by directly and indirectly modifying radiative forcing in the Earth-atmosphere system. The term radiative forcing is used to quantify the extent to which a certain factor has an impact on climate change. The Intergovernmental Panel on Climate Change (IPCC) defines radiative forcing as the difference in energy supplied to the Earth-atmosphere system between present day (circa 2011) and the 'Industrial Era' (1750), given in watts per square meter ( $\text{W/m}^2$ ) (IPCC, 2014). A positive radiative forcing relates to a net warming effect, and a negative radiative forcing relates to a net cooling effect. Negative radiative forcing can result when certain types of particles, such as sulfate particles, directly reflect solar radiation, and positive radiative forcing can be observed

when particles, such as soot particles, directly absorb solar radiation (Andreae and Rosenfeld, 2008; Boucher et al., 2013; Finlayson-Pitts and Pitts Jr., 2000; Seinfeld and Pandis, 2006).

In addition to directly affecting the Earth-atmosphere radiative balance, atmospheric aerosols can indirectly influence the radiative balance through modifying cloud properties. The Twomey effect occurs when particles in the atmosphere increase or decrease the size and number of water droplets within clouds such that their optical properties are altered; this is also known as the cloud albedo effect (Lohmann and Feichter, 2005; Twomey, 1991). Furthermore, a change in size and number of water droplets or ice crystals in clouds can influence the precipitation rates in clouds and thus their lifetime (Albrecht, 1989). Particles that affect cloud water droplets are termed cloud condensation nuclei (CCN), and particles that catalyse ice crystal formation via ice nucleation in the atmosphere are termed ice nucleating particles (INPs). The main focus of this research is on INPs in the Arctic.

### **1.3 Ice nucleation in the atmosphere**

#### **1.3.1 Mechanisms**

Ice can form in clouds by homogeneous or heterogeneous ice nucleation. Homogeneous ice nucleation refers to ice nucleation in the absence of an INP and becomes important below approximately  $-33\text{ }^{\circ}\text{C}$  (Herbert et al., 2015; Koop and Murray, 2016). Heterogeneous ice nucleation refers to ice nucleation initiated by an INP. For the interested reader, an explanation of classical nucleation theory, which is used to explain homogeneous and heterogeneous ice nucleation, is available in Appendix A. INPs are a small subset of atmospheric aerosols (about 1 in  $10^6$  particles act as INPs (Rogers et al., 1998)) that can catalyse the formation of ice crystals in clouds at warmer temperatures than for homogenous ice nucleation (DeMott et al., 2010).

Atmospheric aerosols that act as INPs tend to have a number of characteristics that contribute to their ability to nucleate ice: 1) they are insoluble, 2) they have a size comparable to or larger than that of the critical ice embryo, 3) they can participate in hydrogen bonding, and 4) they provide a crystallographic match to the arrangement of water molecules in ice.

Heterogeneous ice nucleation can occur via four different mechanisms or modes: immersion freezing, deposition freezing, condensation freezing, and contact freezing. These four different types of heterogeneous ice nucleation mechanisms, and the homogeneous ice nucleation mechanism are illustrated in Fig. 1.2. Immersion freezing is the mode of heterogeneous ice nucleation most relevant for mixed phase clouds (clouds containing liquid water droplets and ice crystals) (Murray et al., 2012), and occurs when an INP immersed in a supercooled liquid water droplet initiates the freezing process. This research focuses on INPs important for ice nucleation in mixed phase clouds.

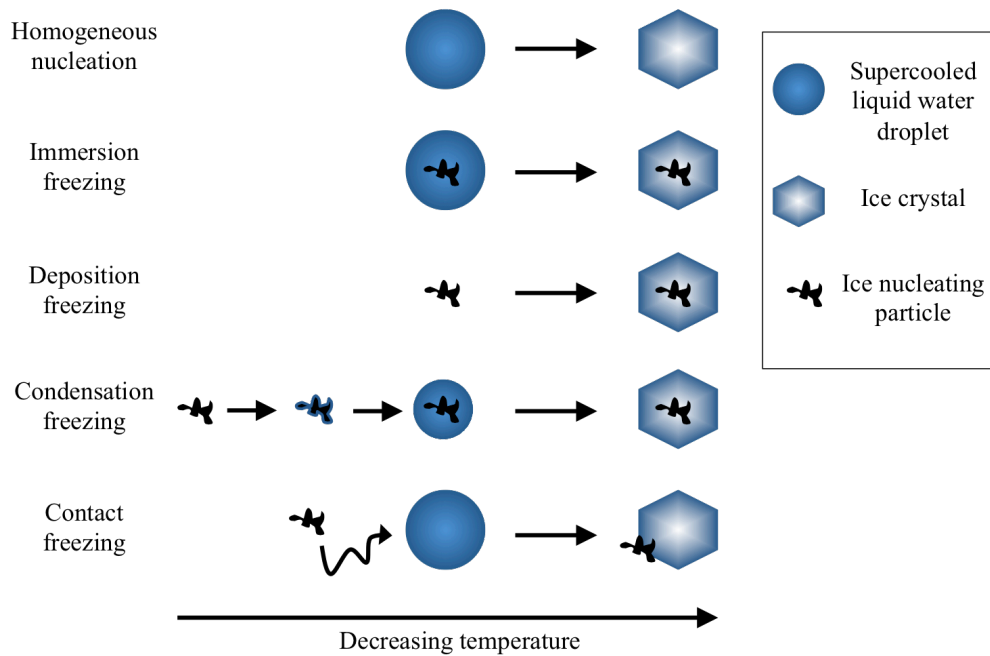
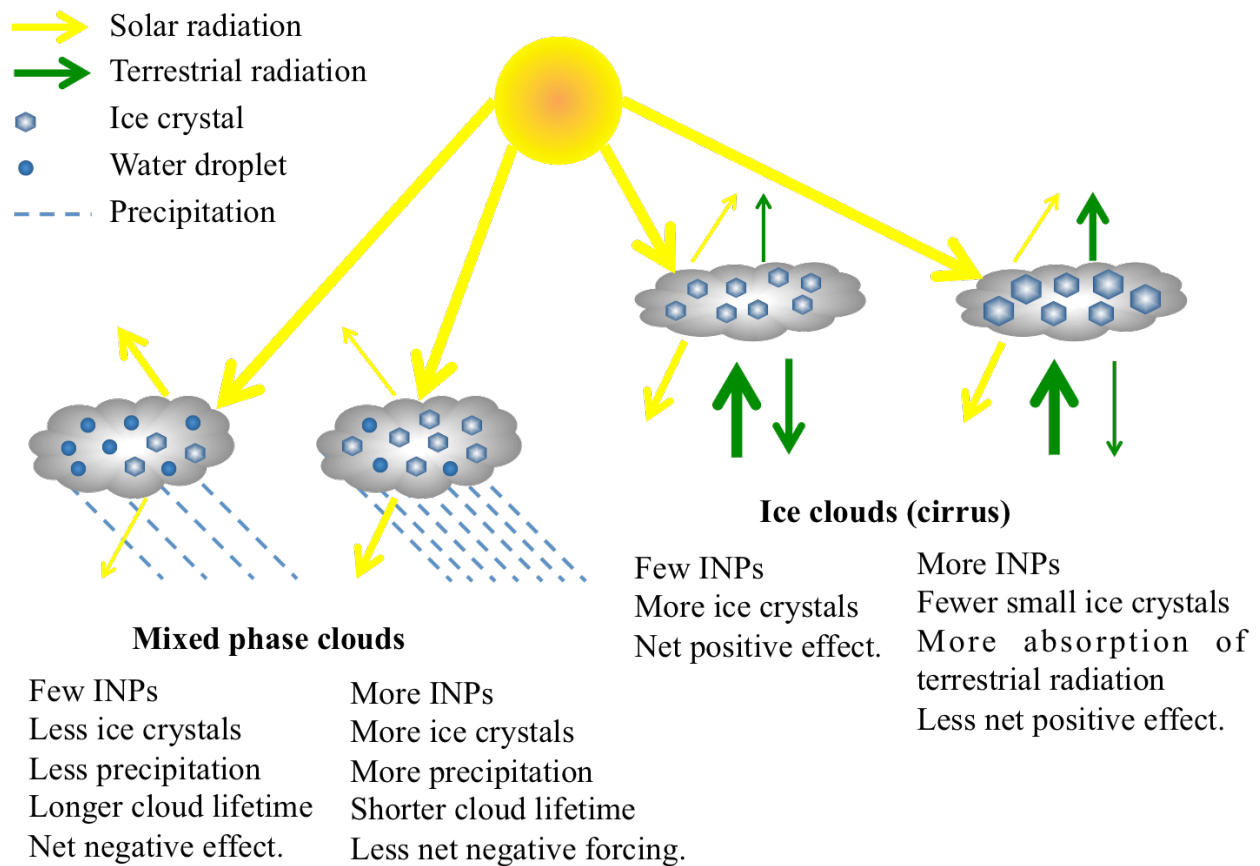


Figure 1.2: Schematic of different modes of ice nucleation (Pruppacher and Klett (1997)).

### 1.3.2 Climatic impact of INPs

INPs greatly influence the number of ice crystals in clouds, and thus can have an impact on the Earth's radiative balance and cloud precipitation (Boucher et al., 2013; Lohmann, 2002; Lohmann and Feichter, 2005; Tan et al., 2016). INPs form ice crystals in ice-clouds (e.g. cirrus clouds), and mixed phase clouds. The climatic impacts of both these particular types of clouds are discussed in the following paragraphs, and are illustrated in Fig. 1.3.



**Figure 1.3: Schematic diagram illustrating the probable effects of an increase in INPs on mixed phase clouds and ice clouds. Adapted from DeMott et al. (2010).**

In general, ice-clouds are formed at high altitudes (7-18 km) in the atmosphere (Lynch et al., 2002). However, in the Arctic it can get cold enough that ice-clouds form at lower altitudes (< 7 km). At temperatures that are low enough, ice crystals form via both homogeneous and heterogeneous nucleation (Cziczo et al., 2004; DeMott et al., 1998, 2003). Ice-clouds have a net positive forcing on the atmosphere as they absorb outgoing long wave terrestrial radiation more than they reflect incoming solar radiation. An increase in INPs may suppress homogeneous freezing, which would result in the formation of larger ice crystals in ice-clouds, and would decrease the magnitude of their net positive effect (Hendricks et al., 2011).

Mixed phase clouds form at lower altitudes (2-7 km) in the atmosphere than ice-clouds. Unlike in ice-clouds, heterogeneous ice nucleation is the only mechanism by which ice crystals are initiated in these clouds. The saturation vapour pressure over ice is lower than the saturation vapour pressure over liquid water; therefore ice crystals in mixed phase clouds will grow at the expense of water droplets. This process is termed the Wegener-Bergeron-Findeisen process (Findeisen, 1938; Pruppacher and Klett, 1997). Mixed phase clouds reflect solar radiation more than they absorb terrestrial radiation, and thus have a net negative forcing on the atmosphere (Hartmann et al., 1992). Modelling studies have shown that an increase in INPs would increase cloud precipitation, due to the Wegener-Bergeron-Findeisen process, and decrease cloud lifetime thus reducing the magnitude of net negative forcing (Lohmann, 2002; Lohmann and Feichter, 2005).

### **1.3.3 Sources of INPs**

#### **1.3.3.1 Sea spray as a source of INPs**

A potential source of INPs to the atmosphere is the ocean. Oceans dominate the Earth's surface cover, and sea spray generates a large fraction of the mass of aerosols in the atmosphere (Lewis and Schwartz, 2004). Several pieces of evidence suggest that the ocean is an important source of INPs to the atmosphere. For example, INPs have been measured in the air above the ocean (Bigg, 1973; Rosinski et al., 1986, 1987, 1988), and marine microorganisms and their by-products have been observed to catalyse ice formation (Burrows et al., 2013; Knopf et al., 2011; Rosinski et al., 1987; Wilson et al., 2015). In addition, modelling studies have suggested that sea spray aerosol can be a significant contributor to the INP population in marine environments when the source of other INPs is small (Burrows et al., 2013; Vergara-Temprado et al., 2017; Wilson et al., 2015; Yun and Penner, 2013).

As previously mentioned, sea spray aerosol is generated by the bubble bursting mechanism (Blanchard, 1964). Many studies have shown that INPs in the microlayer and bulk seawater can be emitted to the atmosphere by the bubble bursting mechanism (Alpert et al., 2011a, 2011b; Blanchard, 1964; DeMott et al., 2016; Fahlgren et al., 2015; Fall and Schnell, 1985; Knopf and Forrester, 2011; Prather et al., 2013; Rosinski et al., 1988; Schnell, 1977; Schnell and Vali, 1975, 1976; Vali et al., 1976; Wang et al., 2015; Wilson et al., 2015). However our understanding of the flux of INPs from the ocean to the atmosphere is far from complete, and more studies are needed to understand when and where INPs from the ocean are a significant source of INPs in the atmosphere.

### **1.3.3.2 Mineral dust as a source of INPs**

Another potential source of INPs to the atmosphere is wind-blown mineral dust. Although land masses do not cover the largest percentage of the Earth's surface, mineral dust has been identified as an important contributor to the atmospheric INP population in field studies and laboratory studies (Atkinson et al., 2013; Boose et al., 2016; Conen et al., 2011; Connolly et al., 2009; Eastwood et al., 2008; Klein et al., 2010; Murray et al., 2012; Niedermeier et al., 2010; Niemand et al., 2012; O'Sullivan et al., 2014; Prenni et al., 2009a, 2009b; Steinke et al., 2016; Wex et al., 2014; Wheeler et al., 2015). Modelling studies have also confirmed the importance of mineral dust acting as INPs on the global indirect aerosol effect (Burrows et al., 2013; Lohmann and Diehl, 2006). However our knowledge of the relative importance of mineral dust compared to other sources of INPs from different locations across the globe is incomplete.

### **1.3.4 The Arctic as a region of interest for climate**

In the past 30 years, warming in the Arctic has decreased sea ice and land snow by approximately 20 % and 13 %, respectively (Derksen and Brown, 2012). This may have led to an increase in sea spray particles and mineral dust from local sources in the region and, as a result, an increase in INPs. If warming in this region continues, the concentration of INPs from these local sources may continue to increase with important implications for properties of mixed phase clouds, and climate in the region. To determine if this feedback mechanism is important, studies are needed to determine the concentrations and sources of INPs in the Arctic. This is one of the main motivations behind this research.

Modelers project that we will observe an ice-free Arctic ocean before the end of the 21<sup>st</sup> century (Overland and Wang, 2013). As sea ice melts more of the ocean surface will be exposed,

increasing the potential for emission of INPs to the atmosphere. One of the aims of this research is to quantify INPs found in the microlayer and bulk seawater that could potentially be emitted into the atmosphere.

Huang et al., (2015) projected that in some parts of the Canadian Arctic there would be an increase in aridity over the next 20 years. When glaciers and permafrost in the Arctic melt erodible soil is exposed. This erodible soil can be a potential source of mineral dust in the Arctic. Ice nucleation properties of dry mineral dust from Thule, Greenland in the Arctic have been measured by Fenn and Weickmann (1959) and they found it could nucleate ice at temperatures as warm as  $-5\text{ }^{\circ}\text{C}$ , whereas most mineral dusts nucleate ice at temperatures below  $-25\text{ }^{\circ}\text{C}$  (Murray et al., 2012). Groot Zwaafink et al. (2016) also suggested, through a modelling study, that local mineral dust sources in the Arctic (mineral dust from latitudes north of  $60\text{ }^{\circ}\text{N}$ ) can dominate the total mineral dust concentrations at the surface during the summer. The research presented in this dissertation explores whether local sources of mineral dust contribute to the INP population in the Canadian Arctic.

#### **1.4 Overview of dissertation**

This research focuses on the heterogeneous ice nucleation properties of microlayer and bulk seawater samples, and atmospheric particle samples from the Canadian Arctic. Chapter 1 (this chapter) introduces aerosols, ice nucleation, sources of INPs to the atmosphere, and the significance of INPs in the atmosphere (specifically in the Arctic). Chapters 2-4 are research chapters; and Chapter 5 summarises the conclusions of this research and provides suggestions for future work.

Chapter 2 presents measurements of INPs in microlayer and bulk seawater samples from the Canadian Arctic during the summer of 2014. The properties of the INPs are probed using heating and filtration tests, and relationships between oceanic variables (e.g. salinity and bacterial abundance) are investigated. Chapter 3 presents measurements of INPs in microlayer and bulk seawater samples from the Canadian Arctic during the summer of 2016. The properties and spatial patterns of INPs are compared to results from 2014 (Chapter 2). Chapter 4 presents measurements of INPs in the marine boundary layer during the summer of 2014. Ratios of surface areas of mineral dust aerosol to sea spray aerosol are determined using computer controlled scanning electron microscopy-energy dispersive X-ray analysis (CCSEM-EDX). In addition, the source region of INPs is investigated using particle dispersion modelling.

## **Chapter 2: Ice nucleating particles in Canadian Arctic sea surface microlayer and bulk seawater**

### **2.1 Introduction**

Prior to our work, five studies had examined INPs in bulk seawater around North America and near Greenland (Fig. 2.1), but only one quantified INPs in the microlayer in the immersion mode (Wilson et al., 2015). Our work adds more measurements to the limited data on INPs in the microlayer and bulk seawater, contributing to a better understanding of how the properties and concentrations of INPs in the microlayer vary with location and time.

We investigated the concentrations and properties of INPs in the microlayer and bulk seawater samples in the immersion mode collected in the Canadian Arctic (Fig. 2.1) during the summer of 2014. The Canadian Arctic was chosen for these studies because 1) clouds in this region have been found to be especially sensitive to atmospheric concentrations of INPs (Harrington et al., 1999; Jiang et al., 2000), 2) there have not been previous studies of the freezing properties of the microlayer or bulk seawater in this region, and 3) as sea ice continues to decrease in the Arctic, the microlayer and bulk seawater may become more important sources of INPs in this region.

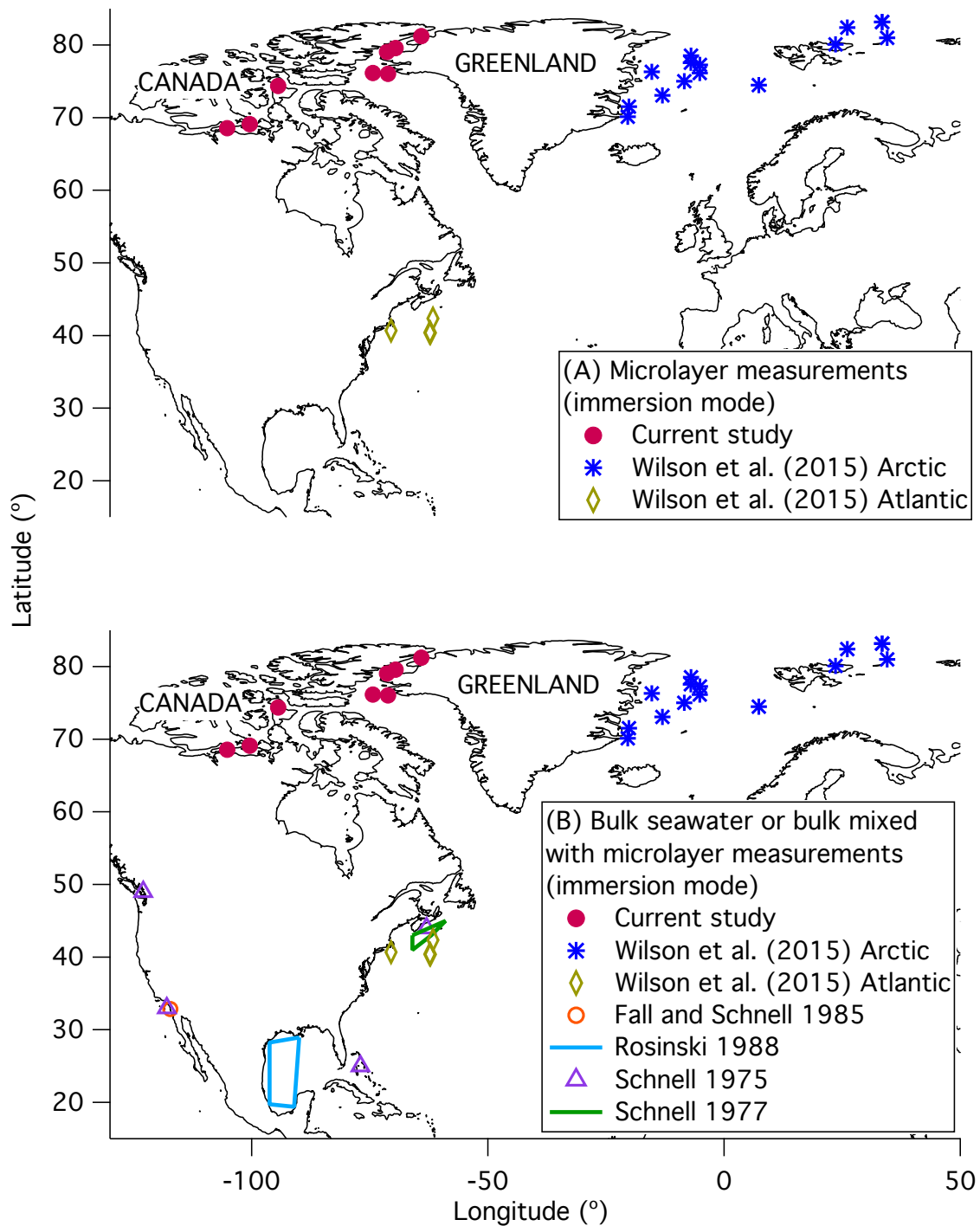


Figure 2.1: A) locations of current and previous studies of INPs (immersion mode) in the microlayer. B) Locations of current and previous studies of INPs (immersion mode) in bulk seawater or mixtures of bulk seawater and microlayer. Dates and coordinates for samples in the current study can be found in Table 2.1.

## 2.2 Experimental

### 2.2.1 Sampling locations and collection methods

All samples were collected during July and August 2014 from the eastern Canadian Arctic on board the Canadian research icebreaker CCGS *Amundsen* as part of the Network on Climate and Aerosols: addressing key uncertainties in Remote Canadian Environments (NETCARE) project. Sampling took place at the same time as the 2014 ArcticNet marine-based research program. The locations of the eight stations sampled in this study are shown in Fig. 2.1 while Table 2.1 describes sampling times and specific geographic coordinates of these stations, as well as station IDs of the geographically closest 2014 ArcticNet stations for interested readers. Supplementary details, including notes and photographs taken at each station during sampling are provided in Table B.1 (Appendix B).

**Table 2.1: Sampling times and geographic coordinates for the eight stations investigated during July-August 2014 in the Canadian Arctic.**

Station number	Sampling start time (UTC)*	Location	2014 ArcticNet Station ID
Station 2	23 <sup>rd</sup> July 2014 17:10	74°36'935N 94°43'663W	305E
Station 4	30 <sup>th</sup> July 2014 22:10	76°19'882N 071°10'329W	115
Station 5	31 <sup>st</sup> July 2014 21:00	76°16'568N 074°36'063W	108
Station 6	3 <sup>rd</sup> Aug 2014 12:20	81°21'743N 064°11'399W	KEN1
Station 7	4 <sup>th</sup> Aug 2014 18:40	79°58'672N 069°56'051W	KANE1
Station 8	5 <sup>th</sup> Aug 2014 19:20	79°04'673N 071°39'205W	KANE4
Station 9	11 <sup>th</sup> Aug 2014 20:00	69°10'009N 100°44'018W	312
Station 10	12 <sup>th</sup> Aug 2014 18:50	68°55'897N 105°19'809W	314

\*Sampling took 45-90 minutes to complete.

The microlayer samples were collected using a glass plate sampler (Harvey and Burzell, 1972; Fig. B.1 in Appendix B) from the upwind side of a small inflatable, rigid-hull boat, at least

500 m away from the CCGS *Amundsen* to avoid contamination. The glass plate was immersed vertically and withdrawn at a slow rate (between 3 to 5 cm/s) and allowed to drain for less than 5 s. The microlayer that adhered to the plate from each dip was scrapped off from one side of the glass plate with a neoprene wiper blade into a 1L high-density polyethylene (HDPE) Nalgene bottle. For each microlayer sample, approximately 500 – 1000 mL was collected, requiring 115-185 dips. Based on the amount of material collected, the number of dips and the area of the plate, the thickness of the layer collected ranged between 60 and 220  $\mu\text{m}$ . Bulk seawater samples were collected at the same times and locations as the microlayer samples using a Niskin bottle deployed from the downwind side of the zodiac. Samples were collected at 0.5 m depth within the surface mixed layer (typically the top 50 m of the Arctic ocean (Moum and Smyth, 2001; Rainville et al., 2011)) and transferred to 1L HDPE Nalgene bottles. After collection, the Nalgene bottles containing both the microlayer and bulk samples were kept cool in an insulated container. Upon returning to the ship, the samples were homogenised by gently inverting them at least ten times and then sub-sampled into smaller bottles for subsequent analyses.

The glass plate, neoprene wiper blade and all Nalgene bottles were cleaned with isopropanol and ultrapure water and rinsed with approximately 10 mL of the seawater sample before use. Isopropanol has been used in previous pre-sterilisation protocols (Csuros, 1994). The Niskin bottle was not cleaned with isopropanol before sampling, but the inside of the bottle was rinsed with a large amount of seawater by lowering and leaving it in the seawater with the top and bottom lids open for about a minute before sending down the messenger to close the lids for sample collection. Sampling with the Niskin bottle and the hand-held glass plate were done on opposite sides of the zodiac to minimize the effect of sampling with the Niskin bottle on the microlayer.

## 2.2.2 Ice nucleation properties of the samples

### 2.2.2.1 Droplet freezing technique and INP concentrations

INP concentrations as a function of temperature were determined using the droplet freezing technique (DFT; Koop et al., 1998; Vali, 1971; Whale et al., 2015; Wilson et al., 2015). Sub-samples of the microlayer and bulk seawater were stored in Nalgene bottles frozen at -80 °C for a maximum of nine months before INP analysis. A previous study suggests that freezing seawater samples does not significantly change the freezing properties of the samples (Schnell and Vali, 1975). Each microlayer and bulk seawater sample was completely thawed and homogenised by inverting at least ten times. Between 15 to 20 droplets of the sample, with volumes of 0.6 µL each, were deposited onto a hydrophobic glass slide (HR3-215; Hampton Research, Aliso Viejo, CA, USA) using a pipette. The slides were put into an airtight cell (Parsons et al., 2004), attached to a cold stage and analysed by the DFT as detailed in Wheeler et al. (2015). The droplets were cooled at a constant rate of 5 °C/min from 0 °C to -35 °C. Each experiment was repeated three times using three different slides. “Blanks” were determined by filtering the microlayer and bulk samples through a 0.02 µm Anotop 25 filter. Ultrapure water (distilled water further purified with a Millipore system, 0.22 µm filtered, 18.2 MΩcm at 25 °C) was also analysed for INPs using the DFT for comparison.

The concentration of INPs, [INP(T)], was determined from each freezing experiment by the following equation (Vali, 1971):

$$[\text{INP}(T)] = -\ln\left(\frac{N_u(T)}{N_o}\right) N_o \cdot \frac{1}{V} \quad (2.1)$$

Where  $N_u(T)$  is the number of unfrozen droplets at temperature  $T$ ,  $N_o$  is the total number of droplets used in the experiment and  $V$  is the volume of all droplets in a single experiment. This

equation applies Poisson's law to the number of freezing events observed to account for the possibility of multiple INPs contained in a single droplet. Additionally, we consider ice nucleation to be dependent on temperature and surface area of the INPs, but independent of time, but note that the time-dependent component to immersion freezing (Vali, 2014) may alter the median freezing temperature of a droplet by 0.5-2 °C per 10 °C change in cooling rate (Murray et al., 2011; Welte et al., 2012; Wheeler et al., 2015; Wright and Petters, 2013).

#### **2.2.2.2 Heating tests**

The freezing temperatures of the microlayer and bulk samples were also measured after they had been heated to 100 °C (Christner et al., 2008; Schnell and Vali, 1975; Wilson et al., 2015). This temperature was chosen because some biological materials have been shown to lose their ice nucleation activity following heating to 95 °C (Christner et al., 2008), possibly due to denaturation of the tertiary structure of ice nucleating proteins (Hill et al., 2016). Samples of microlayer and bulk seawater were put into polypropylene tubes, sealed with lids, and heated to 100 °C in a heating block (Accublock, Labnet, S/N: D1200) for an hour, then cooled to room temperature for approximately 30 minutes before freezing measurements.

#### **2.2.2.3 The size of the INPs**

Following Wilson et al. (2015), the microlayer and bulk seawater samples were passed through filters with three different pore sizes (Whatman 10 µm pore size PTFE membranes, Millex -HV 0.2 µm pore size PTFE membranes, and Anotop 25 0.02 µm pore size inorganic Anopore™ membranes). These filtered samples were subsequently used in the freezing measurements.

#### **2.2.2.4 Corrections for freezing temperature depression**

Since the microlayer and bulk seawater samples contained salts, the measured freezing temperatures were adjusted for the presence of the salts. Using measured salinities and the water activity based approach (Koop and Zobrist, 2009) hypothetical heterogeneous freezing temperatures for salt-free conditions were obtained (salinity = 0 g/kg). The freezing temperature correction was calculated using the median freezing temperature of each sample and then applied to the rest of the droplet freezing temperatures within that sample. For details see Section B.1 (Appendix B). The salinities of the microlayer and bulk seawater samples were measured within 10 minutes of sample collection using a hand-held salinity probe (SympHony; VWR, Radnor, PA, USA) which had been calibrated against discrete seawater samples analysed on a Guildline Autosal 8400B. The correction for the presence of salts based on the measured salinities ranged from 2.0 to 2.8 °C. Hypothetical heterogeneous freezing temperatures for salt-free conditions is more relevant for mixed phase clouds, where freezing typically occurs in dilute aqueous droplets with low salt concentrations (i.e., where water activity tends toward unity). The water activity corrections do not consider non-colligative effects; however, non-colligative effects have not been observed in previous immersion freezing studies with sodium chloride solutions (Alpert et al., 2011a, 2011b; Knopf et al., 2011; Zobrist et al., 2008) or seawater (Wilson et al., 2015).

#### **2.2.3 Phytoplankton and bacterial abundance**

Duplicate 5 mL sub-samples were fixed with 20 µL of 25 % Grade I glutaraldehyde (0.1 % final concentration; Sigma-Aldrich G5882), flash-frozen in liquid nitrogen, and stored at -80 °C within two hours of sampling. The samples were kept frozen at -80 °C until analysis by flow cytometry, within 7 months of collection (Marie et al., 2005). Risk of contamination was low;

gloves were worn at all times, samples were kept in sterile cryovials and fixed with glutaraldehyde using sterile tips in the dark under a fume hood at room temperature for no more than 15 mins, and the frozen samples were thawed with lids on. Cyanobacteria were identified by orange fluorescence from phycoerythrin ( $575 \pm 20$  nm). Heterotrophic bacteria samples were stained with SYBR Green I and measured at 525 nm to detect low nucleic acid (LNA) and high nucleic acid (HNA) content (Belzile et al., 2008). Archaea could not be discriminated from bacteria using this protocol; therefore, hereafter, we use the term bacteria to include both archaea and bacteria. Photosynthetic eukaryotes were identified by red fluorescence of chlorophyll ( $675 \pm 10$  nm). In each sub-sample, microspheres (1  $\mu$ m and 2  $\mu$ m, Fluoresbrite plain YG, Polysciences) were added as an internal standard as described by Tremblay et al. (2009). Analyses were performed on an Epics Altra flow cytometer (Beckman Coulter), fitted with a 488 nm laser (15 mW output; blue), using Expo32 v1.2b software (Beckman Coulter).

#### **2.2.4 Dimethyl sulfide (DMS) measurements**

Concentrations of DMS were measured on board the ship within approximately two hours of sampling. The samples were analysed by gas chromatography following purging and cryo-trapping according to protocol described in Lizotte et al. (2008).

#### **2.2.5 Statistical analysis**

Pearson correlation analysis was applied to many of the variables measured in this study to compute correlation coefficients (R). Here we use the scheme from Dancey and Reidy (2002) where correlations with R values of 0.1-0.3, 0.4-0.6 and 0.7-0.9 are classified as weak, moderate and strong, respectively. P values were also calculated to determine if the correlations were

statistically significant at the 95 % confidence level ( $p < 0.05$ ). We assumed all variables had normal distributions of errors.

## **2.3 Results and Discussion**

### **2.3.1 INPs in the microlayer and bulk seawater**

The fraction of droplets frozen in the immersion mode for both the unfiltered microlayer and bulk seawater samples are shown in Fig. 2.2. In this figure the “blanks” refer to the freezing properties of the sample after 0.02  $\mu\text{m}$  filtration. The “blanks” may still contain some INPs, since some particles  $< 0.02 \mu\text{m}$  in diameter can act as INPs (Dreischmeier et al., 2017; O’Sullivan et al., 2015). The freezing properties of the “blanks” (after correction for freezing point depression by the salts) are similar to or lower than the freezing properties of ultrapure water, which are also shown in Fig. 2.2. Note that the differences between the freezing spectra of ultrapure water and the “blanks” may be attributed to the fact that ultrapure water was filtered through a 0.22  $\mu\text{m}$  filter whereas the “blanks” were filtered through a 0.02  $\mu\text{m}$  filter pore size. The fraction-frozen curves for each station fall at warmer temperatures than their respective “blanks”, indicating that the microlayer and bulk seawater samples from all stations contained INPs. Box plots of the  $T_{10}$ -values for the “blanks”, and the microlayer and bulk seawater samples are shown in Fig. 2.3, where  $T_{10}$  represents the temperatures at which 10 % of droplets had frozen. Figure 2.3 shows that the interquartile range of freezing temperatures for the samples is higher than the interquartile range of freezing temperatures for the “blanks”, further illustrating that INPs were present in the microlayer and bulk seawater samples.

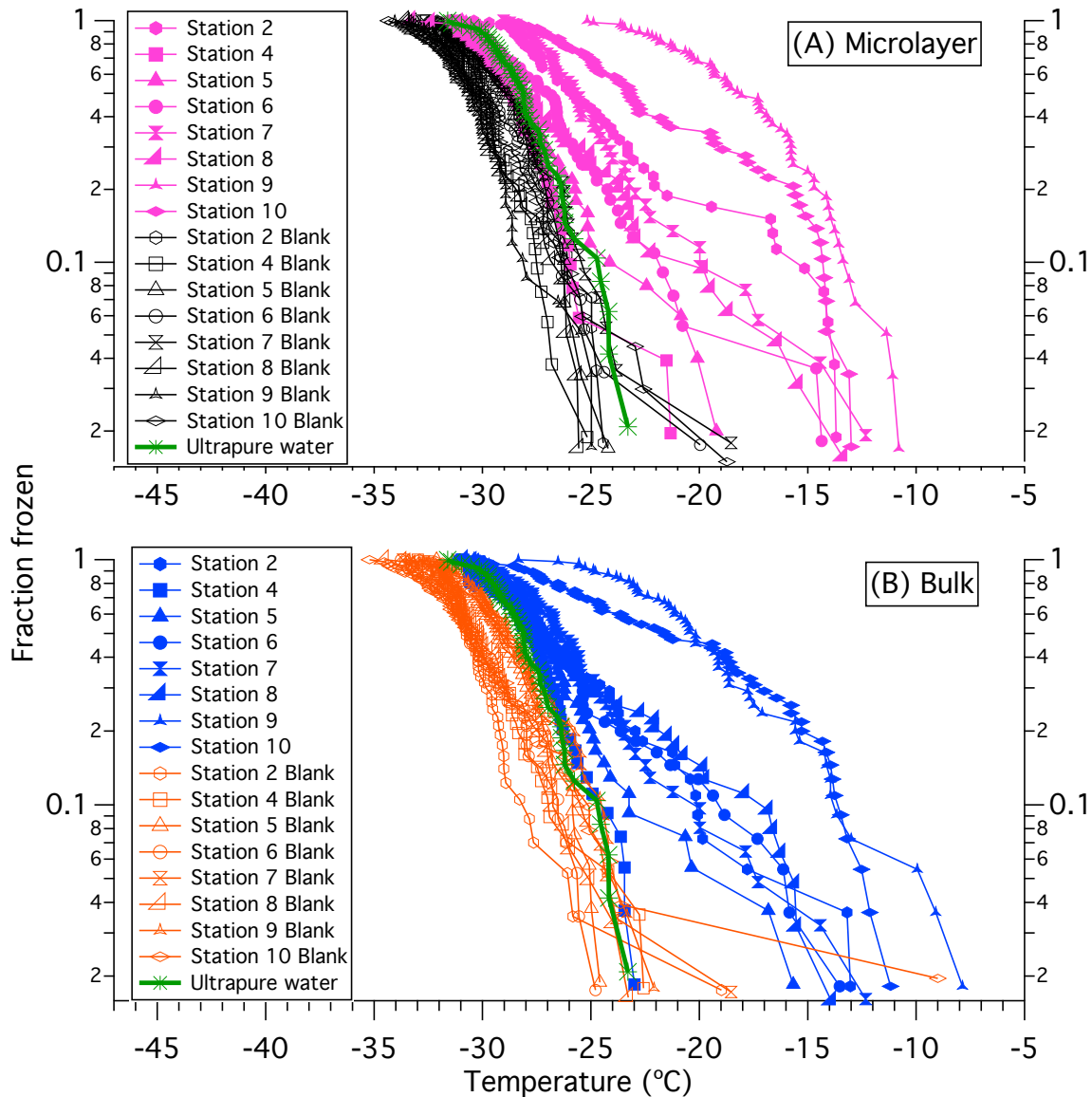
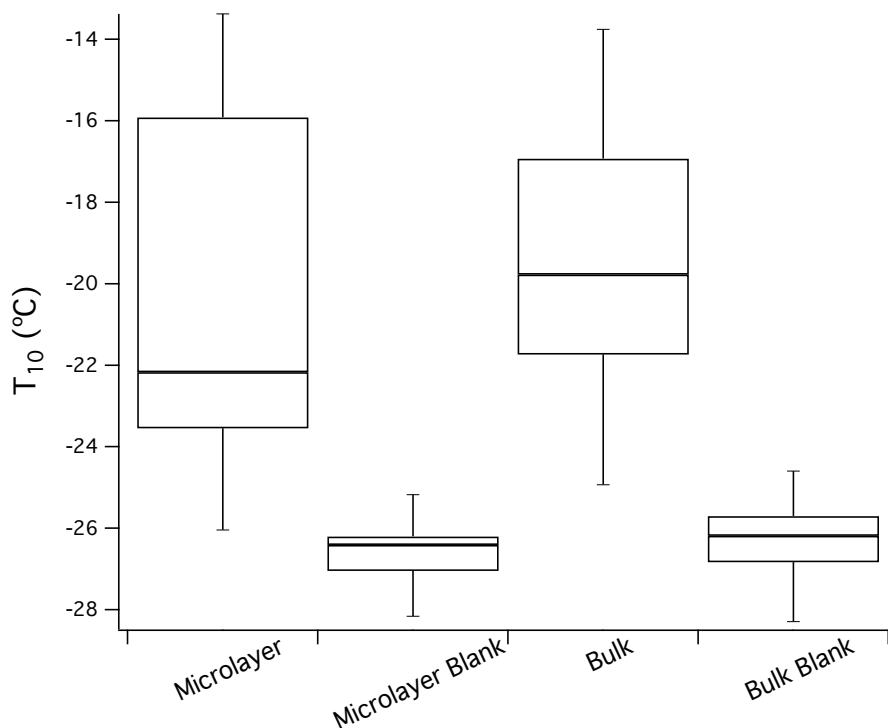


Figure 2.2: Fraction of droplets frozen (in the immersion mode) versus temperature. A) and B) correspond to the microlayer and bulk seawater, respectively. Each set of line and markers represents the results for 3 repeat experiments of a sample or “blank”, adding up to a total of between 45 to 60 freezing events in each set. Also included are the respective “blank” samples and ultrapure water. Each data point corresponds to a single freezing event in the experiments. All microlayer and bulk seawater freezing points have been corrected for freezing point depression to account for dissolved salts in seawater (Section 2.2.2.4). The uncertainty in temperature is not shown but is  $\pm 0.3$  °C.



**Figure 2.3:  $T_{10}$ -values for microlayer and bulk seawater samples. All data have been corrected for freezing point depression. Boxes represent the 25<sup>th</sup>, 50<sup>th</sup> and 75<sup>th</sup> percentiles, and whiskers represent the minima and maxima.**

The freezing curves varied significantly from sample to sample (Fig. 2.2). To understand this variability we investigated correlations between the  $T_{10}$ -values for the bulk seawater samples and the chemical and physical properties of the bulk seawater (DMS concentration, bacterial and phytoplankton abundance, seawater temperature, pH and salinity). Correlation coefficients were not statistically significant ( $p > 0.05$ ), except in the case of salinity (Table 2.2 and Fig. B.2, Appendix B). A strong negative correlation ( $R = -0.7$ ,  $p = 0.02$ ) was observed between salinity and the  $T_{10}$ -values (corrected for freezing depression by the salts). This suggests that more INPs were found in less saline waters. A similar trend was observed for  $T_{50}$ -values, where  $T_{50}$  represents the temperatures at which 50 % of droplets had frozen (Table A.2).

**Table 2.2: Correlation analyses between chemical or physical properties of bulk seawater and T<sub>10</sub>-values for the bulk seawater samples. Numbers in bold represent correlations that are statistically significant (p < 0.05).**

Chemical and physical properties	T <sub>10</sub> -value		
	R	p	n
Dimethyl sulfide concentration	0.381	8	
pH	-0.1	0.372	8
Salinity	<b>-0.7</b>	<b>0.020</b>	<b>8</b>

One possible explanation is that the INPs were associated with melting sea ice. Materials such as algal aggregates, sea ice diatoms and extracellular polymeric substances (EPS) can be released into the ocean upon sea ice melting (Assmy et al., 2013; Boetius et al., 2015; Fernández-Méndez et al., 2014) and might be potential sources of the INPs observed in this study. Also interesting, a strong positive correlation was observed between salinity and bacterial abundance (R = 0.76, p = 0.039). Consistent with these results, Galgani et al. (2016) observed a higher concentration of bacteria in the open sea (which had a higher salinity) compared to melt ponds (which had a lower salinity). Another possible explanation for the strong negative correlation between salinity and freezing temperatures is a non-colligative effect not accounted for in the corrections for freezing temperature depression discussed in Section 2.2.2.4. However, as mentioned in Section 2.2.2.4, non-colligative effects have not been observed in previous immersion freezing studies with sodium chloride solutions (Alpert et al., 2011a, 2011b; Knopf et al., 2011; Zobrist et al., 2008) or seawater (Wilson et al., 2015).

The concentration of INPs as a function of temperature, [INP(T)], for the microlayer samples analysed in this study is shown in Fig. 2.4A. Also included in Fig. 2.4A are results from Wilson et al. (2015) for the microlayer samples they collected at the locations shown in Fig. 2.1A. Concentrations of INPs in microlayer samples at stations 2, 9, and 10 overlap with the INP

concentrations observed by Wilson et al. (2015) in the Atlantic. However, the INP concentrations in the microlayer measured by Wilson et al. (2015) to the east of Greenland are higher than the concentrations measured here.

Figure 2.4B shows the concentrations of INPs as a function of temperature for the bulk seawater samples. Also included in Fig. 2.4B are results from other studies (see Fig. 2.1B for locations) that measured INPs in samples of bulk seawater or samples containing a mixture of the microlayer and bulk seawater. The range of concentrations observed in our studies agrees well with the range observed by Schnell and Vali (1975), Schnell (1977) and Wilson et al., (2015) (both Arctic and Atlantic). Note, the bulk seawater freezing data from Wilson et al., (2015) were at the detection limit of their instrument; therefore, their INP concentrations for bulk seawater should be considered upper limits.

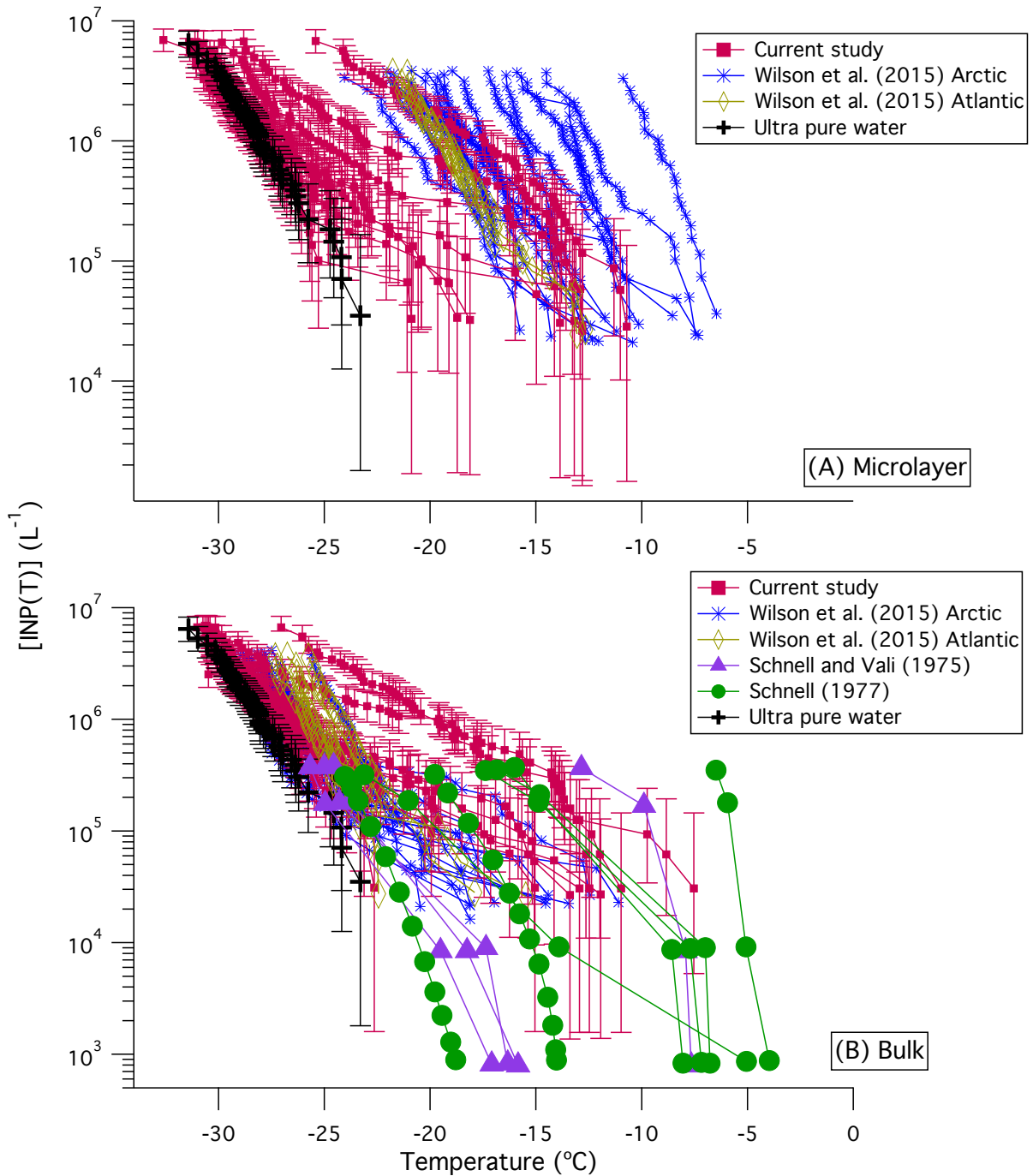
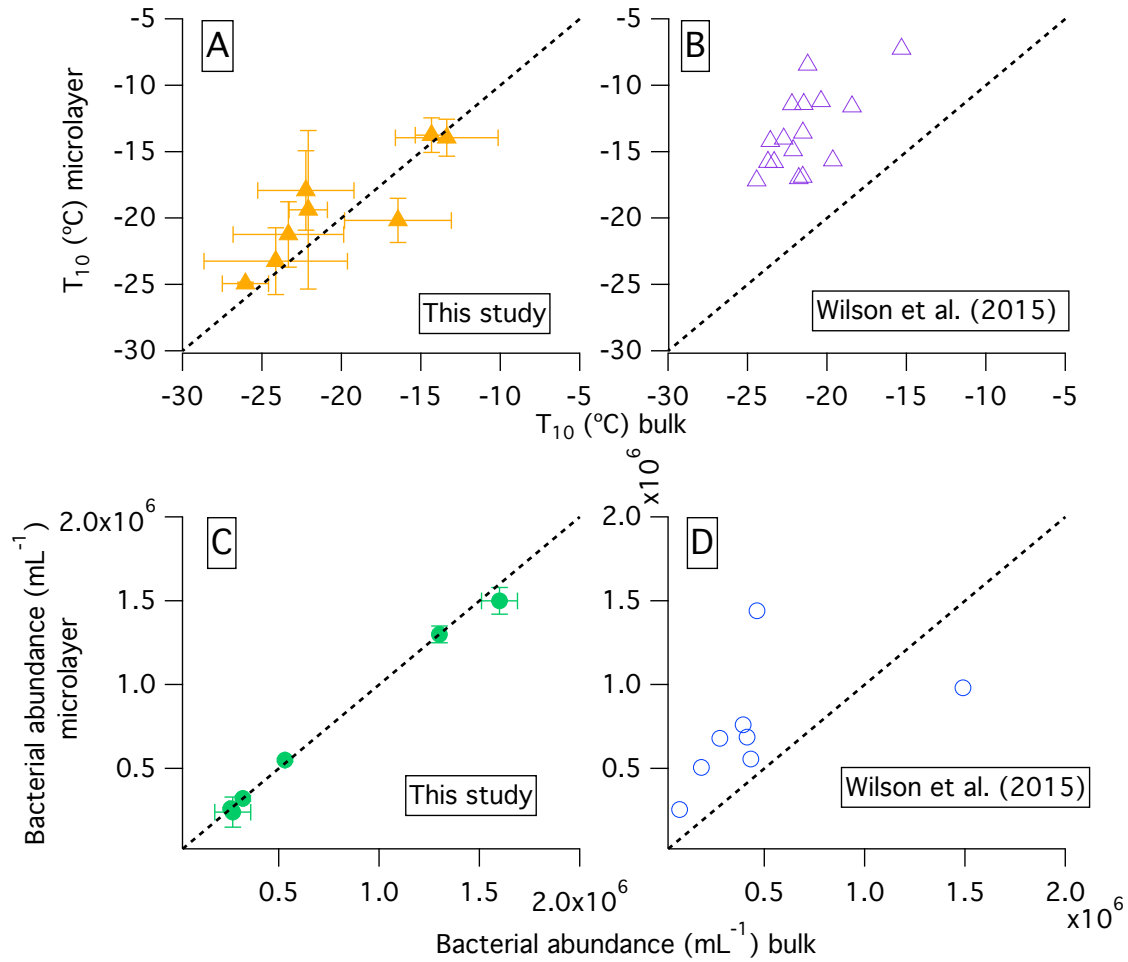


Figure 2.4: The concentrations of INPs,  $[INP(T)]$ , in A) the microlayer, and B) bulk seawater samples. All data, including those from other studies, are corrected for freezing point depression. Upper and lower limits to  $[INP(T)]$  ( $L^{-1}$ ) associated with the current study describe the statistical uncertainty due to the limited number of nucleation events observed in the freezing experiments (Koop et al. (1997)).



**Figure 2.5: Correlation plots with a 1:1 line for reference. A) Freezing temperatures for microlayer and bulk seawater samples in this study. All error bars represent the 95 % confidence intervals of the  $T_{10}$ -values from 3 replicate experiments. All data have been corrected for freezing point depression. B)  $T_{10}$ -values for microlayer and bulk seawater samples from Wilson et al. (2015). All data have been corrected for freezing point depression. C) Bacterial abundance in the microlayer and bacterial abundance in the bulk seawater in this study. There was only one reliable microlayer sample from station 7 for bacterial abundance; therefore, the percentage error for this station was assigned the maximum percentage error from the other bacterial abundance. D) Bacterial abundance in the microlayer and bacterial abundance in the bulk seawater from Wilson et al. (2015).**

A strong positive correlation ( $R = 0.9$ ,  $p = 0.002$ ) between the freezing properties of the microlayer and the freezing properties of the bulk seawater was observed in the current study.

Shown in Fig. 2.5A is a correlation plot between the  $T_{10}$ -values from the microlayer and bulk seawater samples. The data points, except for one, fall upon the 1:1 line, if the uncertainties in the measurements are considered. In contrast, Wilson et al. (2015) found significantly more INPs in the microlayer than in bulk seawater (Fig. 2.5B) in both their Arctic and Atlantic samples. Figure 2.5 also shows correlation plots for bacterial abundance in the microlayer and bulk seawater for this study (Fig. 2.5C) and from Wilson et al. (2015) (Fig. 2.5D). Similar bacterial abundances were observed in the microlayer and bulk seawater in the current study, whereas Wilson et al. (2015) found a higher bacterial abundance in the microlayer compared to the bulk seawater in most samples (Fig. 2.5D).

The differences between the results in the current study and the results from Wilson et al. (2015) may be, in part, related to sampling techniques. In the current study the glass plate technique used collected a layer that was up to 220  $\mu\text{m}$  thick, while Wilson et al. (2015) used a hydrophilic Teflon film on a rotating drum fitted to a remote-controlled sampling catamaran which collects a microlayer of thickness between 6 to 83  $\mu\text{m}$  (Knulst et al., 2003). Other studies have shown that different sampling techniques lead to different measured enrichments of the microlayer. Aller et al. (2017) compared the enrichments of the microlayer determined with the glass plate and a hydrophilic Teflon film on a rotating drum. They observed an enrichment (by a factor of approximately two) of bacteria in the microlayer when using the rotating drum, but no enrichment when using the glass plate technique. In addition, they observed an enrichment of transparent exopolymer material in the microlayer when using the rotating drum, but a smaller enrichment was observed when using the glass plate technique. Note that Aller et al. (2017) allowed seawater to stand in a 250 gallon tank for one hour before sampling the microlayer with a glass plate whereas the microlayer sampled with the rotating drum was taken directly from the

ocean. Additional studies are needed to determine if the methodology used to sample the microlayer and bulk seawater strongly influences measured INP concentrations.

The differences between the results in the current study and the results from Wilson et al. (2015) may also be related to differences in the state of the ocean at the time of sampling. To investigate this we compared monthly average chlorophyll *a* concentrations for both studies. As illustrated in Figs. B.3-B.5 (Appendix B) a clear difference between chlorophyll *a* concentrations in the current study and the Wilson et al. (2015) study was not observed.

Wind speed could also affect the stability of the microlayer and explain differences between results from the current study and the Wilson et al. (2015) study. Previous studies suggest that a microlayer may be stable up to the global average wind speed of 6.6 m/s (Wurl et al., 2011). During the current study, sampling was carried out at wind speeds ranging from 0.7 to 6.7 m/s, while Wilson et al., (2015) carried out sampling at wind speeds ranging from 1.2 to 5.9 m/s. The similar wind speeds in both studies and the fact that almost all sampling was carried out with wind speeds less than the global average suggests that the observed differences in INP concentrations is not due to wind speeds.

## 2.3.2 Properties of the INPs

### 2.3.2.1 Heat-labile biological material

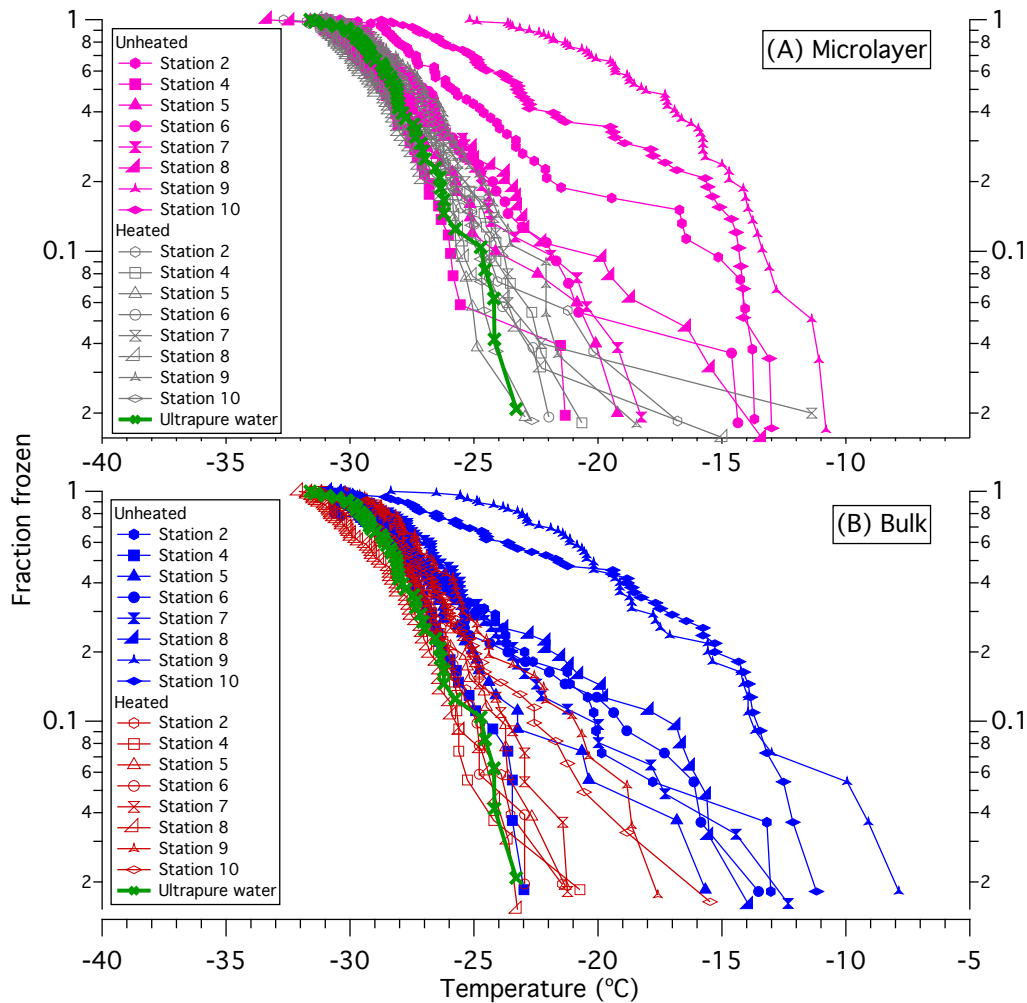


**Figure 2.6: Effect of heating on the fraction frozen for unfiltered samples from A) the microlayer, and B) bulk seawater. Each data point corresponds to one droplet freezing event, and all data have been corrected for freezing point depression. The uncertainty in temperature is not shown but is  $\pm 0.3$  °C.**

The fraction frozen curves of samples before and after heating to a temperature of 100 °C are shown in Fig. 2.6. For 7 out of 8 of the microlayer samples, and all of the bulk samples, the fraction-frozen curves are shifted to colder temperatures after heating. These results suggest that the INPs in most cases are heat-labile biological material, consistent with previous measurements

of the properties of INPs in the microlayer (Wilson et al., 2015) and bulk seawater (Schnell and Vali, 1975, 1976; Schnell, 1977).

### **2.3.2.2 Size of INPs**

The  $T_{10}$ -values as a function of filter pore size (0.02  $\mu\text{m}$ , 0.2  $\mu\text{m}$  and 10  $\mu\text{m}$ ) are shown in Fig. 2.7. For over half the samples (microlayer samples at Stations 4 and 5, bulk samples at Station 6 and bulk and microlayer samples at Stations 7, 9, and 10) the sizes of the INPs were clearly between 0.02 and 0.2  $\mu\text{m}$ , as the  $T_{10}$ -values significantly decreased when the samples were passed through a 0.02  $\mu\text{m}$  filter but not when passed through a 0.2  $\mu\text{m}$  filter. For the other samples (bulk samples at Stations 4 and 5, microlayer samples at Station 6, and microlayer and bulk samples at Stations 2 and 8), the uncertainties were too large to draw a clear conclusion about the effect of filtration. Plots of the fraction of droplets frozen versus temperature for samples filtered with a 0.02  $\mu\text{m}$ , 0.2  $\mu\text{m}$  and 10  $\mu\text{m}$  filter are shown in Fig. B.6 (Appendix B) and are consistent with the results shown in Fig. 2.7. However, it should be kept in mind that filters have been shown to retain material smaller in size than the filter pore size (Gimbert et al., 2005).

The 0.02 - 0.2  $\mu\text{m}$  size range for the INPs identified here is consistent with previous studies of INPs in the microlayer or bulk seawater. Wilson et al. (2015) concluded that INPs in the microlayer were between 0.02 and 0.2  $\mu\text{m}$  in size. Rosinski et al. (1986) found that ice freezing nuclei in aerosol of marine origin were below 0.5  $\mu\text{m}$  in size. Schnell and Vali (1975) found ocean-derived ice nuclei to be below 1  $\mu\text{m}$  in size.

The size of whole cell marine bacteria or phytoplankton (excluding femtoplankton) is typically greater than 0.2  $\mu\text{m}$  (Burrows et al., 2013; Sieburth et al., 1978), hence whole cell marine bacteria are unlikely to be the source of the INPs identified here. Furthermore,

correlations between INP concentrations and bacterial or phytoplankton abundance were not statistically significant ( $p$  values  $> 0.05$ ; see Appendix B, Table B.3). This is consistent with the suggestion that whole cells are not the source of the INPs. Potential sources of the INPs observed in this study include ultramicrobacteria, viruses, phytoplankton exudates, or bacteria exudates (Ladino et al., 2016; Wilson et al., 2015).

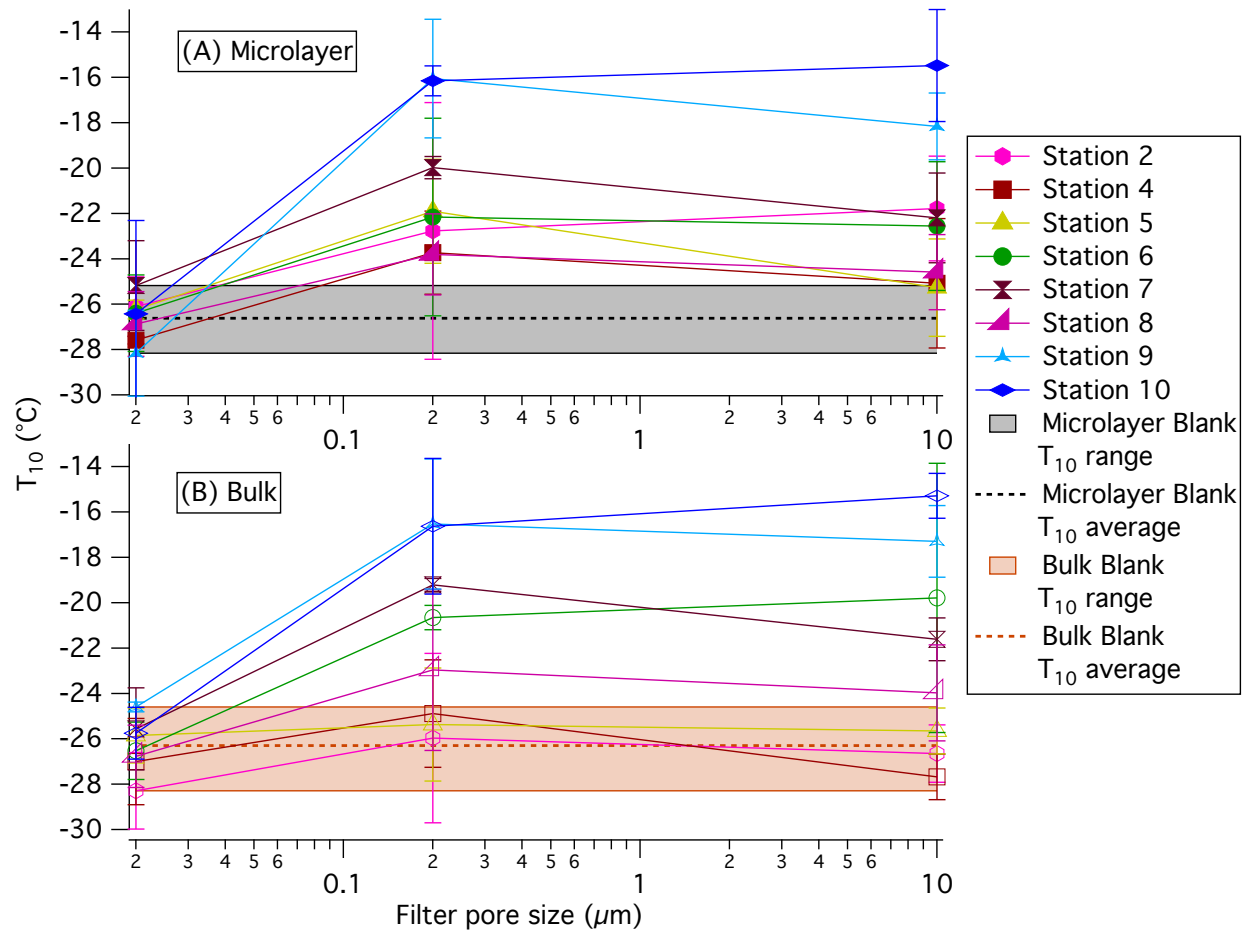


**Figure 2.7:**  $T_{10}$ -values as a function of filter pore size in A) microlayer samples, and B) bulk seawater samples. Filter pore sizes were 10, 0.2, and 0.02  $\mu\text{m}$ . Error bars are the 95 % confidence intervals of the  $T_{10}$ -values from 3 replicate experiments. All data have been corrected for freezing point depression.

## 2.4 Summary and conclusions

Concentrations of INPs in the microlayer and bulk seawaters at eight different stations in the Canadian Arctic were determined. Results showed that the INPs were ubiquitous in the microlayer and bulk seawater and that freezing temperatures as high as  $-14\text{ }^{\circ}\text{C}$  were observed in both the microlayer and bulk seawater. A strong negative correlation ( $R = -0.7$ ,  $p = 0.02$ ) was observed between salinity and freezing temperatures (after correction for freezing depression by salts). One possible explanation is that INPs were associated with melting sea ice. The concentration of INPs in the bulk seawater was in good agreement with concentrations observed in bulk seawater samples at several other locations in the Northern Hemisphere. The concentrations of INPs in the microlayer were consistent with concentrations observed by Wilson et al., (2015) off the coast of North America. Heating the samples substantially reduced the INPs' activity, suggesting that heat-labile biological materials were the likely source of that activity. Filtration of the samples showed that the INPs were between  $0.02$  and  $0.2\text{ }\mu\text{m}$ , implying that the ice-active heat-labile biological material was likely ultramicrobacteria, viruses, or extracellular material, rather than whole cells.

We conclude that the concentrations and properties of INPs in the microlayer and bulk seawater in the Canadian Arctic are similar to other locations previously studied. However, there were some important differences. On average the concentration of INPs in the microlayer in the current study was lower than the average concentration of INPs measured by Wilson et al., (2015). These differences could not be explained by chlorophyll *a* concentrations from satellite measurements. In addition, similar concentrations of INPs in the microlayer and bulk seawater were observed here, while Wilson et al., (2015) observed significant enrichment of INPs in the microlayer compared to the bulk seawater. The differences may be related to sampling

techniques, but they could also be due to the oceanic state during sampling. Further studies are needed to understand how measured concentrations of INPs in the microlayer and bulk seawater depend on sampling techniques. Further studies are also needed to understand how measured concentrations of INPs in the microlayer and bulk seawater depend on oceanic variables, particularly changing sea ice distributions.

As sea ice in the Arctic continues to decrease, the microlayer and bulk seawater could play a larger role in the overall atmospheric INP population in this region. Future modelling studies are needed to determine the magnitude of the effect this INP source has on cloud microphysics in the Arctic region and how it might change as sea ice distributions change.

## **Chapter 3: Revisiting properties and concentrations of ice nucleating particles in the sea surface microlayer and bulk seawater in the Canadian Arctic during summer**

### **3.1 Introduction**

Despite growing evidence that the ocean is an important source of INPs in the atmosphere, our understanding of the properties and concentrations of INPs in the microlayer and bulk seawater remain limited. For example, information on the spatial and temporal distributions of INPs in the microlayer and bulk seawater has not been investigated in any detail. Nevertheless, this type of information is needed to improve predictions of INPs to the atmosphere from the ocean.

Chapter 2 reported the properties and concentrations of INPs in the microlayer and bulk seawater collected in the Canadian Arctic during the summer of 2014 (Irish et al., 2017). Building on our previous studies, we returned to the Canadian Arctic during the summer of 2016 to further investigate the properties and concentrations of INPs in Arctic Ocean waters. Locations where samples were collected during both years are indicated in Fig. 3.1, and the detailed sampling dates and locations in 2016 are given in Table 3.1. By comparing results from 2016 with results from 2014, we investigate if the properties, concentrations and spatial profiles of the INPs vary from year-to-year at similar locations. This type of information is needed to understand and predict concentrations of INPs in the atmosphere.

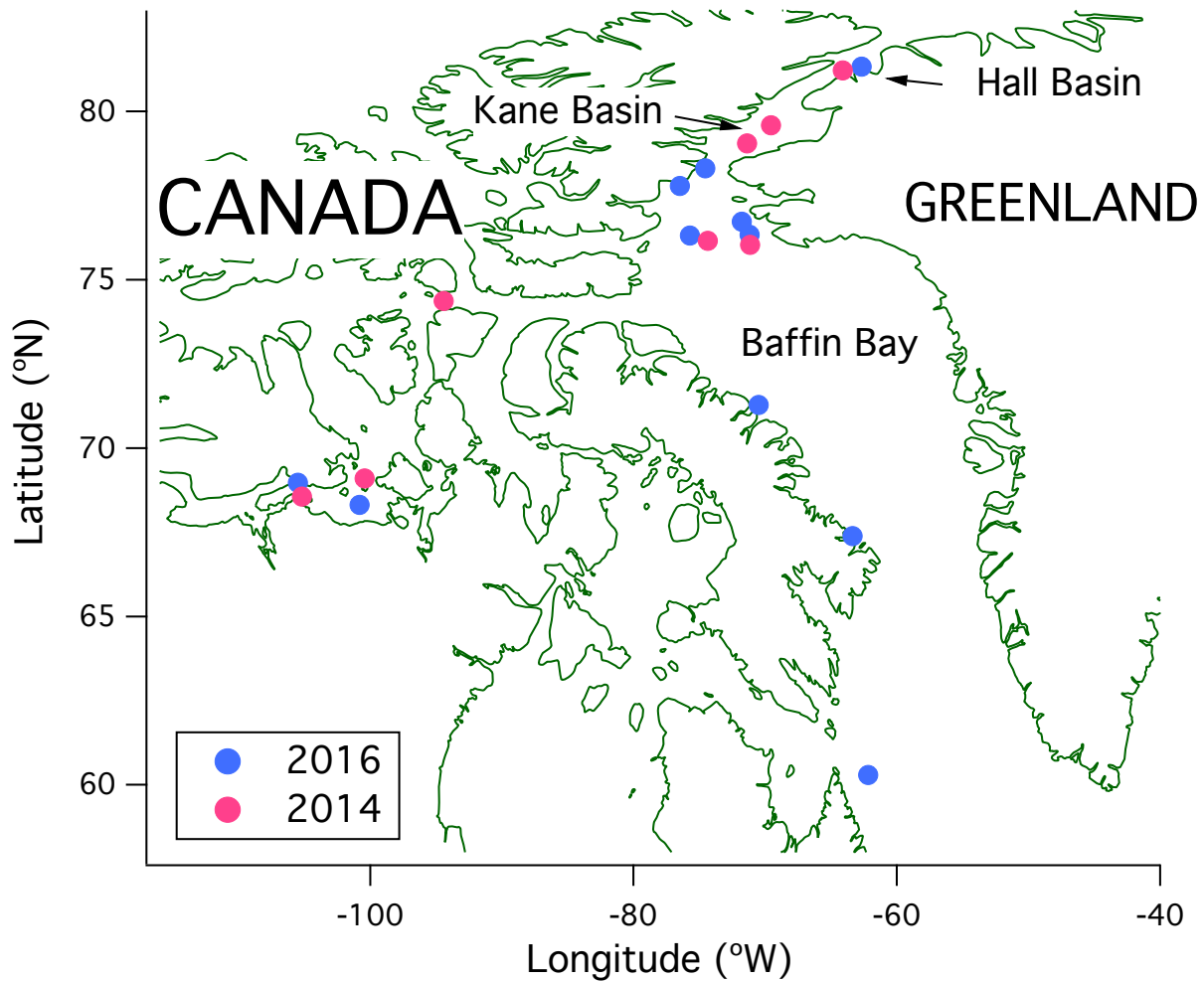


Figure 3.1: Map showing locations of microlayer and bulk seawater sampling in 2014 (pink) and 2016 (blue).

## 3.2 Experimental

### 3.2.1 Collection methods

During July and August of 2016 samples were collected from the eastern Canadian Arctic on board the CCGS *Amundsen* as part of the NETCARE project. Sampling took place at the same time as the 2016 ArcticNet marine-based research program. The locations of the eleven stations sampled in this study are shown in Fig. 3.1 while Table 3.1 describes sampling times and specific geographic coordinates of these stations, as well as station IDs of the geographically

closest 2016 ArcticNet stations for interested readers. Supplementary details, including notes and photographs taken at each sampling station, are provided in Table C.1 in Appendix C.

**Table 3.1: Sampling times and geographic coordinates for the eleven stations investigated.**

Station number	Sampling start time (UTC)	Location	2016 ArcticNet station ID
Station 1	20 <sup>th</sup> July 2016 18:30	60°17.921N 062°10.750W	ROV2
Station 2	28 <sup>th</sup> July 2016 15:30	67°23.466N 063°22.067W	PII-A-1-f
Station 3	1 <sup>st</sup> August 2016 13:30	71°17.200N 070°30.236W	169
Station 4	6 <sup>th</sup> August 2016 13:30	76°20.341N 071°11.418W	115
Station 5	8 <sup>th</sup> August 2016 11:00	76°43.777N 071°47.267W	116
Station 6	9 <sup>th</sup> August 2016 14:30	76°18.789N 075°42.963W	105
Station 7	11 <sup>th</sup> August 2016 17:00	77°47.213N 076°29.841W	TS233
Station 8	13 <sup>th</sup> August 2016 10:30	81°20.041N 062°40.774W	139
Station 9	15 <sup>th</sup> August 2016 14:00	78°18.659N 074°33.757W	127
Station 10	21 <sup>st</sup> August 2016 10:00	68°19.199N 100°49.010W	QMG2
Station 11	23 <sup>rd</sup> August 2016 10:30	68°58.699N 105°30.022W	314

### 3.2.1.1 Automated sampler method

In contrast to 2014, when we collected microlayer samples manually using a glass plate sampler (Irish et al., 2017), in 2016, microlayer samples were collected using rotating glass plates attached to an automated sampling catamaran (Fig C.1, Appendix C; Shinki et al., 2012). At station 1, the automated sampling catamaran was deployed from a small inflatable, rigid-hull boat at least 500 m away from the CCGS *Amundsen*. The automated sampling catamaran was remotely driven at least 20 m away from the small inflatable, rigid-hull boat before the rotating glass plates were activated. A rotation rate of 10 revolutions per minute was used. From station 2 onwards, the automated rotating glass plates on the sampling catamaran experienced technical problems. Subsequently, the automated sampling catamaran was kept on the upwind side of the

small inflatable, rigid-hull boat with its engine turned off, at least 500 m away from the CCGS *Amundsen* to avoid contamination, and the glass plates were rotated manually between 11 to 18 revolutions per minute. Even though manual rotation was used, for convenience, we will refer to the method as “automated sampling”, and the instrument as an “automated sampler” in all cases. The microlayer that adhered to the plates from each rotation was scrapped off with fixed Teflon wiper blades into a manifold and then pumped through Teflon tubing into HDPE Nalgene bottles (ranging from 250 mL to 2 L in size). The thickness of the microlayer collected was approximately 80  $\mu\text{m}$  based on the rotation rate (between 11 - 18 revolutions per minute), the average volume collected (3000 mL), and an average collection time (18 minutes). Bulk seawater samples were collected at the same times and locations as the microlayer samples through Teflon tubing suspended 0.2 m below the automated sampler. The bulk seawater was pumped, using peristaltic pumps, into HDPE Nalgene bottles (ranging from 250 mL to 2 L in size). After collection, the Nalgene bottles containing the microlayer and bulk seawater samples were kept cool in an insulated container. Upon returning to the ship, the samples were homogenised by gently (so as to not break up cells that may be present in the samples) inverting them at least ten times and then sub-sampled into smaller bottles for subsequent analyses.

The glass plates, aluminium manifold, Teflon tubing and all Nalgene bottles were sterilised first with bleach, then cleaned with isopropanol and finally rinsed with ultrapure water. After cleaning, the sampler was further rinsed by collecting then discarding microlayer and bulk seawater for approximately 2 minutes, before samples were retained. Procedural blanks were prepared by running approximately 1 L of ultrapure water through the sample tubing on the automated sampler for approximately 10 minutes.

## **3.2.2 Ice nucleation properties of the samples**

### **3.2.2.1 Droplet freezing technique and INP concentrations**

INP concentrations as a function of temperature were determined using the droplet freezing technique (DFT; Koop et al., 1998; Vali, 1971; Whale et al., 2015; Wilson et al., 2015). Sub-samples of the microlayer and bulk seawater were kept in 15 mL polypropylene tubes between 1 to 4 °C for a maximum of 4 hours before INP analysis.

In the freezing experiments three hydrophobic glass slides (Hampton Research, Aliso Viejo, CA, USA) were placed directly on a cold stage (Whale et al., 2015) and between 15 to 30 droplets of the sample, with volumes of 1 µL each, were deposited onto each of the glass slides using a pipette. A chamber with a webcam attached to the top of it was placed over the slides to isolate them from ambient air, and a flow of ultrapure N<sub>2</sub> was passed through the chamber as described by Whale et al. (2015). The droplets were cooled at a constant rate of 10 °C/min from 0 °C to -35 °C and the webcam recorded videos of the droplets during cooling. All videos were analysed by the DFT to determine the freezing temperature of each droplet. For comparison, ultrapure water, as well as the procedural blanks, were analysed for INPs using the DFT.

The concentration of INPs, [INP(T)] (L<sup>-1</sup>), was determined from each freezing experiment using Eq. 2.1 from Chapter 2 (Vali, 1971).

### **3.2.2.2 Heating and filtration tests**

The freezing temperatures of the microlayer and bulk seawater samples were also measured after they had been passed through syringe filters with three different pore sizes (Whatman 10 µm pore size PTFE membranes, Millex–HV 0.2 µm pore size PTFE membranes, and Anotop 25 0.02 µm pore size inorganic Anopore™ membranes) (Irish et al., 2017; Wilson et

al., 2015). The sub-samples of the microlayer and bulk seawater were left for a maximum of 4 hours before filtration and INP analysis.

The freezing temperatures of the microlayer and bulk seawater samples were also measured after they had been heated to 100 °C (Christner et al., 2008; Irish et al., 2017; Schnell and Vali, 1975; Wilson et al., 2015). In this case, samples were stored at -80 °C for less than 6 months and analysed in the laboratory at the University of British Columbia. Before heating the stored samples, they were completely thawed and homogenised by inverting at least ten times. Then the freezing temperatures were determined after heating the samples at 100 °C for approximately an hour.

Separate experiments show that storage of the samples at -80 °C for a maximum of six months does not affect the INP concentration in microlayer and bulk seawater samples (see Fig. C.2, Appendix C).

### **3.2.2.3 Corrections for freezing temperature depression**

The measured freezing temperatures were adjusted for the depression of the freezing temperature by the presence of salts to generate freezing temperatures applicable to salt-free conditions (salinity = 0 g/kg), which is relevant for mixed phase clouds. The adjusted freezing temperatures were calculated as in Section 2.2.2.4.

The salinities of the microlayer and bulk seawater samples were measured within 10 minutes of sample collection using a hand-held salinity probe (SympHony; VWR, Radnor, PA, USA). The salinities (measured in practical salinity units (psu)) were corrected after collection using a linear fit to salinometer readings. The correction for freezing point depression by the presence of salts based on the measured salinities ranged from 1.2 to 2.6 °C.

### **3.2.3 Bacterial and phytoplankton abundance**

The abundances of heterotrophic bacteria and phytoplankton < 20 µm (i.e., phycoerythrin-containing cyanobacteria, phycocyanin-containing cyanobacteria and autotrophic eukaryotes) were measured by flow cytometry. Duplicate 4 mL subsamples were fixed with glutaraldehyde (Grade I; 0.12 % final concentration; Sigma-Aldrich G5882) in the dark at room temperature for 15 min, flash-frozen in liquid nitrogen and then stored at -80 °C until analysis. Samples for heterotrophic bacteria enumeration were stained with SYBR Green I (Invitrogen) following Belzile et al. (2008). Bacteria were counted with a BD Accuri C6 flow cytometer using the blue laser (488 nm). The green fluorescence of nucleic acid-bound SYBR Green I was measured at 525 nm. Archaea could not be discriminated from Bacteria using this protocol; therefore, hereafter, we use the term bacteria to include both Archaea and Bacteria with HNA and LNA content. Samples for < 20 µm phytoplankton abundances were analysed using a CytoFLEX flow cytometer (Beckman Coulter) fitted with a blue (488 nm) and red laser (638 nm), using CytoExpert v2 software. Using the blue laser, forward scatter, side scatter, orange fluorescence from phycoerythrin (582/42 nm BP) and red fluorescence from chlorophyll (690/50 nm BP) were measured. The red laser was used to measure the red fluorescence of phycocyanin (660/20 nm BP). Polystyrene microspheres of 2 µm diameter (Fluoresbrite YG, Polysciences) were added to each sample as an internal standard (Marie et al., 2005; Tremblay et al., 2009).

### **3.2.4 Fraction of meteoric water from stable oxygen isotope data**

The fraction of meteoric water (terrestrial run-off plus precipitation) was determined by analysing the stable oxygen isotope ( $\delta^{18}\text{O}$ ) ratio of water in each bulk seawater sample. The  $\delta^{18}\text{O}$  is defined as a per mil deviation of  $\text{H}_2^{18}\text{O}/\text{H}_2^{16}\text{O}$  ratio of the bulk seawater sample from that of

the Vienna Standard Mean Ocean Water. Stable oxygen isotope samples were collected at the same times and locations as the microlayer and bulk seawater samples. The samples were analysed for the determination of  $\delta^{18}\text{O}$  using the method outlined by Burgers et al. (2017). Assuming each sample is a mixture of meteoric water, sea ice melt, and a seawater end-member, the fraction of meteoric water was calculated using the following conservation equations (Yamamoto-Kawai et al., 2005):

$$f_{SIM}S_{SIM} + f_{MW}S_{MW} + f_{SW}S_{SW} = S_{obs} \quad (3.1)$$

$$f_{SIM}\delta_{SIM} + f_{MW}\delta_{MW} + f_{SW}\delta_{SW} = \delta_{obs} \quad (3.2)$$

$$f_{SIM} + f_{MW} + f_{SW} = 1 \quad (3.3)$$

Where  $f$ ,  $S$ , and  $\delta$  represent fraction, salinity, and  $\delta^{18}\text{O}$ , respectively, and the subscripts *obs*, *SIM*, *MW*, and *SW* represent observed, sea ice melt, meteoric water, and seawater end-members, respectively. Note that a negative meteoric water fraction ( $f_{MW} < 0$ ) can be generated depending on how the seawater end-member is defined. Seawater end-member values were defined using arctic outflow water values as outlined by Burgers et al. (2017) because most of our sampling stations were influenced by this water mass assembly within our study area.

### 3.2.5 Chlorophyll *a* satellite data

Chlorophyll *a* concentrations for case 1 waters (waters dominated by phytoplankton) were retrieved from the GlobColour project website (<http://globcolour.info>, *ACRI-ST, France*). The GlobColour project provides a high resolution, long time-series of global ocean colour information by merging data from several satellite systems. For the data used here, these include either or both of: the Moderate Imaging Spectrometer (MODIS) on the Aqua Earth Observing System (EOS) mission, and the Visible/Infrared Imager Radiometer Suite (VIIRS) aboard the

Suomi National Polar-orbiting Partnership satellite. The GlobColour project merges data from multiple satellite systems in several different ways. For this work we used data merged with weighted averaging, where weightings are based on the sensor and/or product. For more information regarding the weighted averaging based on the sensors refer to the GlobColour Product User Guide ([http://www.globcolour.info/CDR\\_Docs/GlobCOLOUR\\_PUG.pdf](http://www.globcolour.info/CDR_Docs/GlobCOLOUR_PUG.pdf)). Data are available at daily, 8-day, and monthly resolutions. In this study 8-day data were used to achieve the best balance between complete spatial coverage and high time resolution. Spatial resolution is  $1/24^\circ$  ( $\sim 4$  km). To determine the chlorophyll *a* concentration at a given sampling location, we used the grid cell corresponding to the location of that station.

### **3.2.6 Statistical analysis**

Pearson correlation analysis was applied to many of the variables measured in this study to compute correlation coefficients (*R*). *P* values were also calculated to determine the significance of the correlations at the 95 % confidence level ( $p < 0.05$ ).

## **3.3 Results and Discussion**

### **3.3.1 Concentrations of INPs**

The frozen fraction curves for all microlayer and bulk seawater samples are shown in Fig. C.3 (Appendix C). Also shown for comparison are the fraction frozen curves for ultrapure water and ultrapure water passed through the tubing in the automated sampler (the procedural blanks). In addition, the frozen fraction curves of the samples after passing through a  $0.02 \mu\text{m}$  Anotop 25 syringe filter are shown.

For the bulk seawater, all untreated samples froze at temperatures warmer than ultrapure water. Freezing temperatures as warm as  $-6\text{ }^{\circ}\text{C}$  were observed. In addition, the bulk seawater samples also froze at warmer temperatures than the procedural blanks. These results indicate the presence of ice-active material in all bulk seawater samples.

For the microlayer samples, all samples froze at temperatures warmer than ultrapure water. These results also suggest that all microlayer samples contained ice-active material. For some microlayer samples, some of the freezing temperatures were lower than the freezing temperatures of the procedural blanks. However, the freezing temperatures of the procedural blanks should be viewed as an upper limit to the background freezing temperatures, since prior to collecting the blanks, the sampler had not been rinsed as thoroughly as before collecting the microlayer samples.

The 95% confidence interval of the median temperatures at which 50 % of the droplets froze in the microlayer and bulk seawater samples were  $-18.6 \pm 3.0\text{ }^{\circ}\text{C}$  and  $-21.1 \pm 3.0\text{ }^{\circ}\text{C}$ , respectively, in 2016. In contrast, in 2014, the median temperatures at which 50 % of the droplets froze in the microlayer and bulk seawater samples were lower at  $-27.2 \pm 2.3\text{ }^{\circ}\text{C}$  and  $-26.8 \pm 2.0\text{ }^{\circ}\text{C}$ , respectively.

In Fig. 3.2, the concentrations of INPs,  $[\text{INP}(\text{T})]$ , measured in 2016 are compared with concentrations measured in 2014. In both 2016 and 2014 the concentrations of INPs vary by at least 2 orders of magnitude at one temperature, but on average concentrations measured in 2016 were higher than the concentrations measured in 2014. The presence of peaks or bumps in the freezing spectra indicates the presence of specific groups of INPs in the samples (Bigg and Hopwood, 1963; Vali, 1971; Welti et al., 2018). Fig. 3.2 shows that a few samples from both

2014 and 2016 show bumps on their freezing spectra, suggesting the presence of more than one specific group of INPs in these samples.

Shown in Fig. 3.3 is the correlation between  $T_{10}$ -values in the microlayer and bulk seawater samples from 2016. A strong positive correlation ( $R = 0.89$  and  $p < 0.001$ ) was observed between the freezing properties of the microlayer and the freezing properties of the bulk seawater, consistent with our previous observations (Irish et al., 2017). In 2016, 5 out of 11 samples had warmer  $T_{10}$ -values in the microlayer compared to bulk seawater. However, in the 2014 samples, only 1 out of 8 samples had warmer  $T_{10}$ -values in the microlayer compared to bulk seawater (Irish et al., 2017). The difference between 2016 and 2014 may simply be due to year-to-year variations in the properties of the microlayer relative to the bulk seawater related to variations in oceanic conditions. For example, Collins et al. (2017) documented differences in the activity of marine microbial communities between 2016 and 2014 in the Canadian Arctic. In addition, the differences between 2016 and 2014 may be related to sampling techniques. In 2014 the glass plate technique collected a layer that was up to 220  $\mu\text{m}$  thick. In contrast, in 2016 a thinner layer (approximately 80  $\mu\text{m}$  thick) was collected. In the thicker layers collected in 2014, the microlayer INPs would have been diluted by bulk waters. Preliminary studies show that results collected with the glass plate method and automated sampler method are comparable (see Fig. C.4 (Appendix C)). However, additional studies of how INP activity varies as a function of microlayer sample thickness are necessary to further resolve this issue.

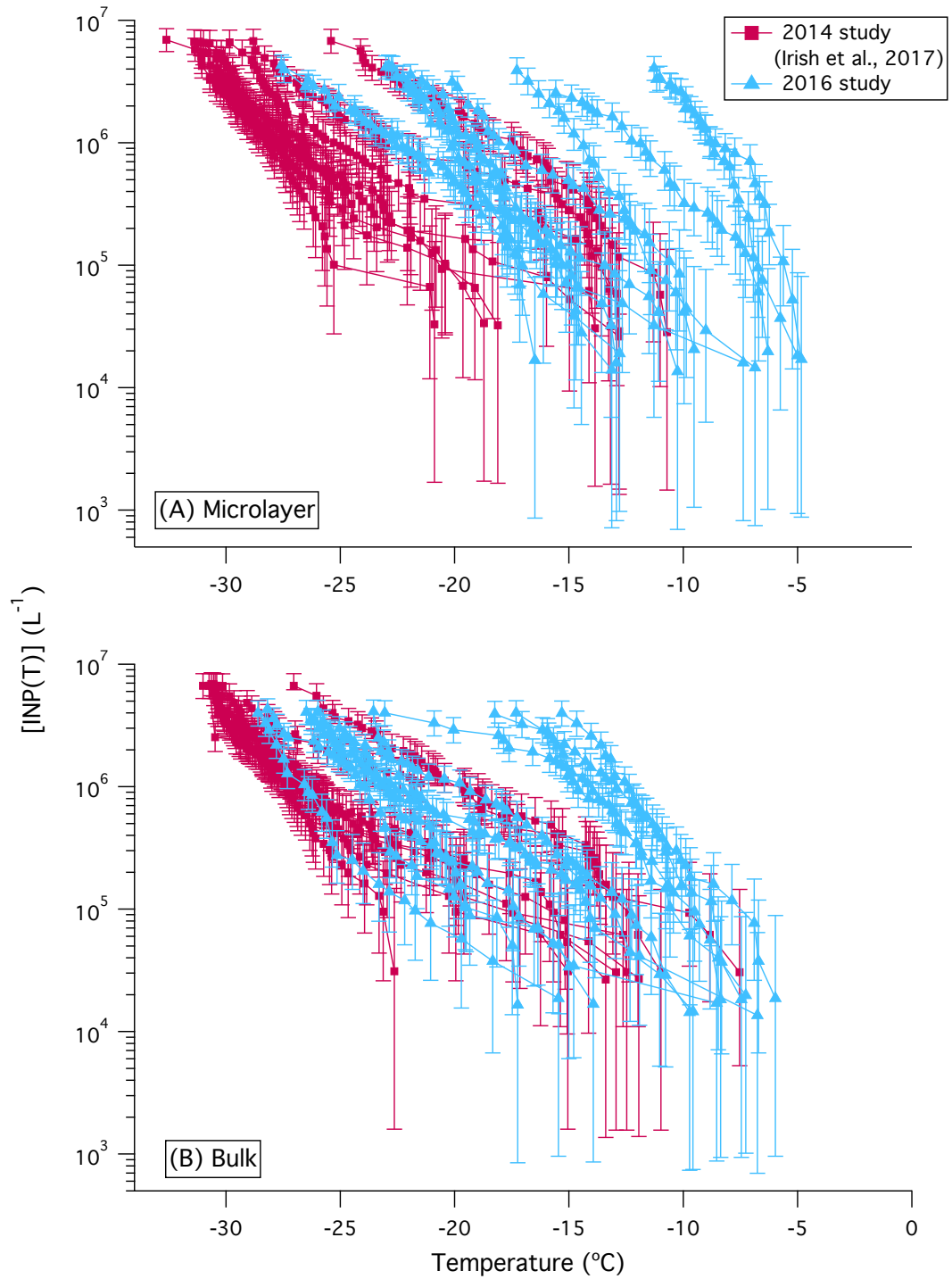


**Figure 3.2: Comparison of the concentrations of INPs,  $[INP(T)]$ , in A) the microlayer, and B) bulk seawater samples from the 2014 study (dark pink squares) and the 2016 study (blue triangles). All data are corrected for freezing point depression. Error bars represent the statistical uncertainty due to the limited number of nucleation events observed in the freezing experiments (Koop et al., 1997).**

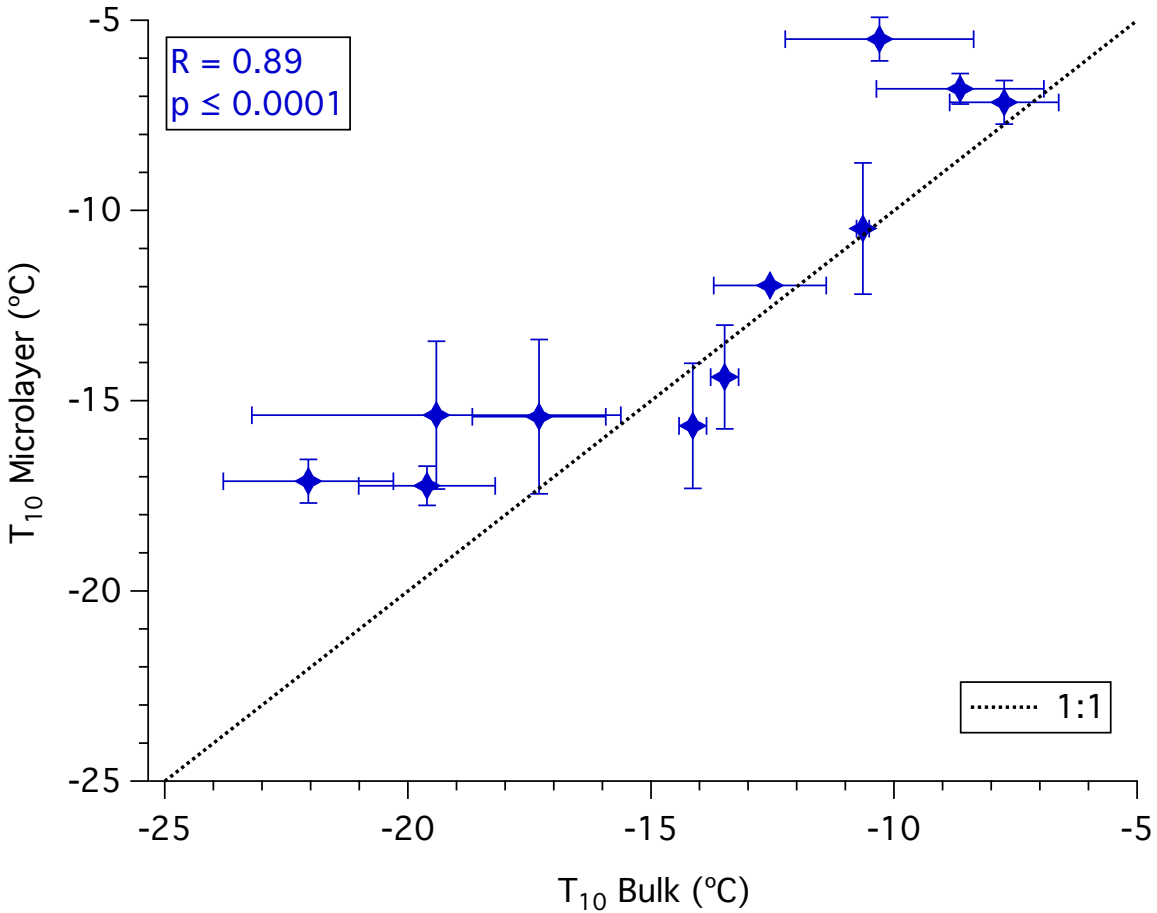


**Figure 3.3: Relationship between  $T_{10}$ -values for microlayer and bulk seawater samples with a 1:1 line for reference. Data points are the average  $T_{10}$ -values from three repeat experiments. Error bars are the 95 % confidence interval for three repeat experiments.**

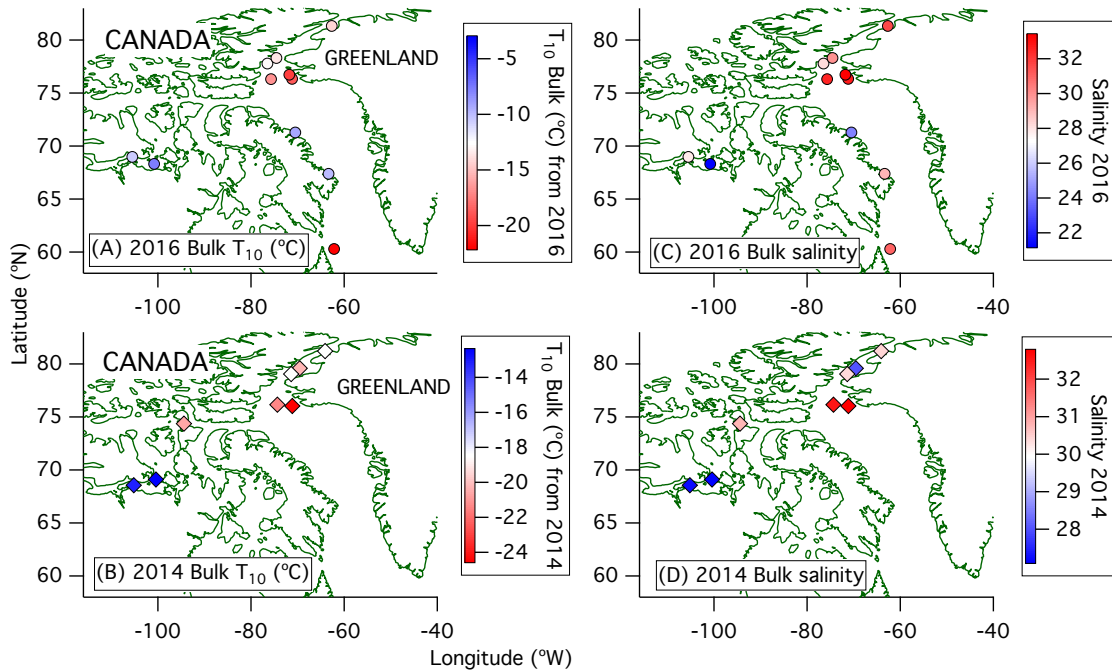
### 3.3.2 Effect of heating and filtering the samples

Figure C.5 (Appendix C) shows that the frozen fraction curves were shifted to colder temperatures after the microlayer and bulk seawater samples were heated to 100 °C. These results are similar to what we observed for the 2014 samples (Irish et al., 2017). This suggests that the ice-active material we found in the microlayer and bulk seawater samples was likely heat-labile biological material (Christner et al., 2008).

Figure C.6 (Appendix C) shows that the temperature at which droplets had frozen in microlayer and bulk seawater samples significantly decreased after the samples were filtered with a 0.02  $\mu\text{m}$  filter, but not with 10 or 0.2  $\mu\text{m}$  filters. A similar result was observed in the 2014 samples (Irish et al., 2017), suggesting that the INPs in the microlayer and bulk seawater were between 0.2 and 0.02  $\mu\text{m}$  in size.

### **3.3.3 Spatial patterns of INPs in the Canadian Arctic**

The spatial patterns of  $T_{10}$ -values and salinities for bulk seawater samples in both 2016 and 2014 are shown in Fig. 3.4. The same spatial patterns, but for microlayer samples, are shown in Fig. C.7 (Appendix C). Spatial patterns of salinities, in addition to the  $T_{10}$ -values, are shown since salinities were the strongest predictor of freezing in the samples (see Section 3.3.4). In each panel the colour scales have been adjusted to easily compare the general pattern of  $T_{10}$ -values and salinities between years. For both 2014 and 2016, the  $T_{10}$ -values for samples taken from northern Baffin Bay and Nares Strait between Greenland and Canada, above 75 °N, are generally lower than the  $T_{10}$ -values elsewhere. On the other hand, for the same samples, the salinities are generally higher than salinities we observed elsewhere.



**Figure 3.4: Spatial patterns of (A, B)  $T_{10}$ -values, and (C, D) salinities in (A, C) 2016 and (B, D) 2014 for bulk seawater.**

To further investigate the similarities in spatial patterns between 2014 and 2016, a comparison was made of  $T_{10}$ -values and salinities for sampling sites in close proximity for the two years. Labelled in Fig. 3.5A are sampling sites in 2014 and 2016 identified as being in close proximity. A strong positive correlation ( $R = 0.9$ ,  $p < 0.001$ ) was found between the  $T_{10}$ -values measured in 2014 and  $T_{10}$ -values measured in 2016 when comparing locations in close proximity (Fig. 3.5B), suggesting that the spatial patterns of  $T_{10}$ -values measured in 2014 and 2016 were similar even though on average  $T_{10}$ -values were higher in 2016.

Water masses are identifiable from physical properties such as salinity and temperature. A strong positive correlation ( $R = 0.78$ ,  $p \leq 0.001$ ) was found between the salinities measured in 2014 and salinities measured in 2016 when comparing locations in close proximity (Fig. 3.5C), which suggests that we sampled similar water masses in both years at those locations. However,

no statistically significant correlation ( $R = 0.4$ ,  $p > 0.05$ ) was observed between the temperatures of the bulk seawater measured in 2014 and the temperatures of bulk seawater measured in 2014.

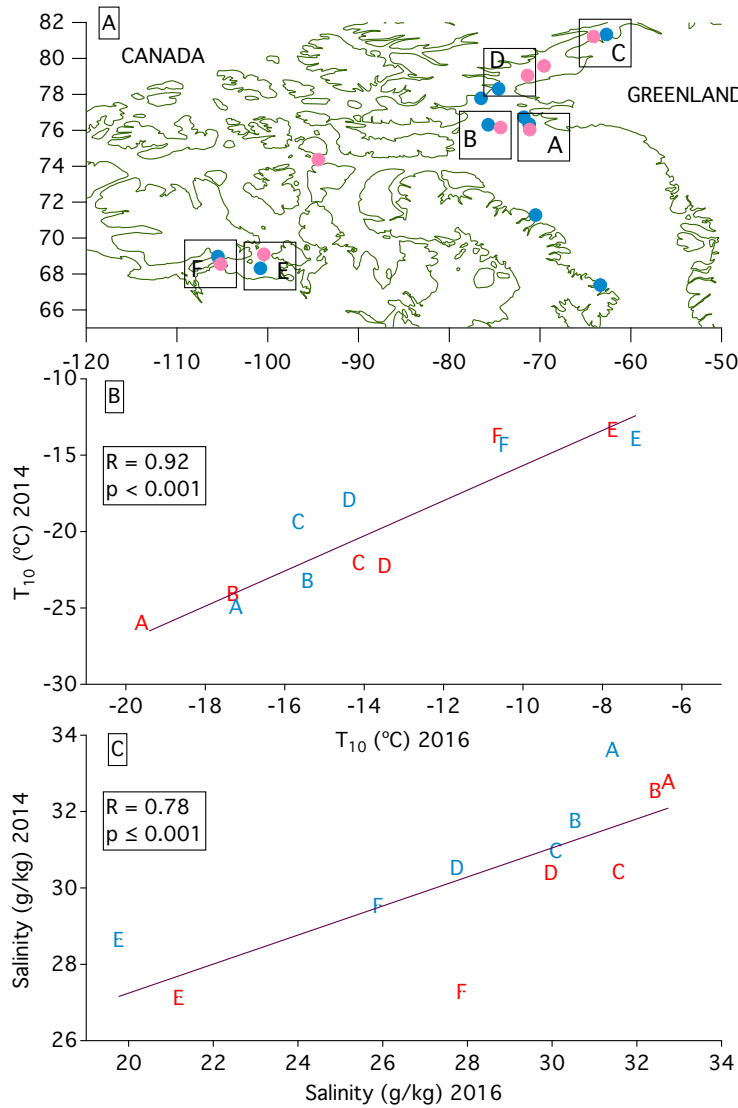


**Figure 3.5: A) Map showing regions of similar sampling locations in 2014 (pink) and in 2016 (blue). Sampling sites in 2014 that were near sampling sites in 2016 were paired together (indicated with boxes in the figure) and assigned letters A-F. Although there are two stations in box A for 2016, we only used data for the station that was closest to the one in 2014. Relationships between B)  $T_{10}$ -values, and C) salinities for microlayer and bulk seawater samples in 2014 and 2016 for similar sampling locations. The letters plotted in B) and C) indicate the locations in A). Red letters represent bulk seawater data and blue letters represent microlayer data.**

### **3.3.4 Correlations with biological and physical properties of the microlayer and bulk seawater**

In Fig. 3.6 and Table 3.2, we present correlations between  $T_{10}$ -values from bulk seawater and heterotrophic bacterial abundance, phytoplankton (including 0.2-20  $\mu\text{m}$  photosynthetic eukaryotes and cyanobacteria) abundance, salinity and temperature for the 2016 data. The strongest relationships with  $T_{10}$ -values for both the bulk seawater and microlayer samples were with salinity (bulk:  $R = -0.83$ ,  $p \leq 0.001$ ; microlayer:  $R = -0.74$ ,  $p < 0.01$ ). As discussed by Irish et al. (2017), a possible explanation for the negative correlation between salinity and freezing temperature is that the INPs are associated with sea ice melt. Melting sea ice not only decreases surface ocean salinity, but can also release sea ice microorganisms, such as sea ice diatoms and bacteria, and their exudates that may serve as effective INPs (Assmy et al., 2013; Boetius et al., 2015; Ewert and Deming, 2013; Fernández-Méndez et al., 2014). Also interesting, a strong negative correlation was observed between  $T_{10}$ -values in bulk seawater and bacterial abundance ( $R = -0.77$ ,  $p < 0.01$ ). A higher concentration of bacteria has been observed in the open sea compared to melt ponds, and bacteria produce copious amounts of exopolymers when they are stressed during melting processes (Galgani et al., 2016). Although there may be fewer bacteria in melting sea ice, these bacteria may be stressed by the melting process and produce exopolymers that could act as INPs.

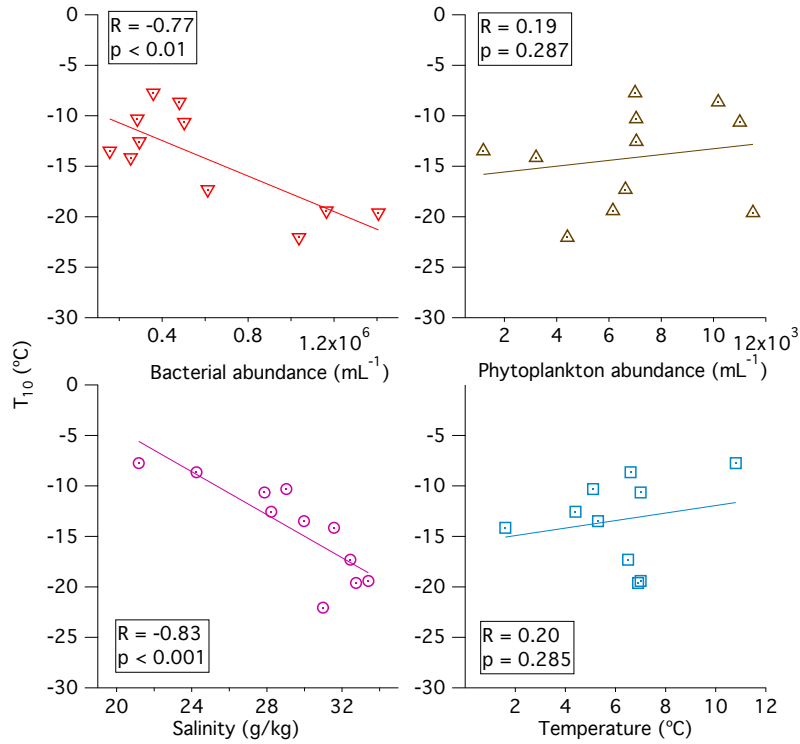


**Figure 3.6: Relationships between biological and physical properties of bulk seawater and  $T_{10}$ -values for the 2016 study.**

**Table 3.2: Correlations between biological and physical properties of microlayer and bulk seawater and  $T_{10}$ -values for 2016. Values in bold indicate results that are statistically significant. The symbol n/a represents correlations for which there were no data.**

	Microlayer $T_{10}$ -value			Bulk $T_{10}$ -value		
	R	p	n	R	p	n
Heterotrophic bacterial abundance	-0.42	0.100	11	<b>-0.77</b>	<b>0.003</b>	<b>11</b>
Total phytoplankton abundance (0.2 - 20 $\mu\text{m}$ )	-0.06	0.436	11	0.19	0.287	11
Salinity	<b>-0.74</b>	<b>0.005</b>	<b>11</b>	<b>-0.83</b>	<b>0.001</b>	<b>11</b>
Temperature	n/a	n/a	n/a	0.20	0.285	10

In addition to melting sea ice, terrestrial run-off (including that from melting glaciers and permafrost) also decreases salinity, and could be a source of ice nucleating material to the surface ocean (Christner et al., 2008). An analysis of  $\delta^{18}\text{O}$  in our study area showed that our

samples could be influenced by non-sea ice fresh water, particularly in Hall Basin and Kane Basin within Nares Strait (Burgers et al., 2017). As shown in Fig. 3.7 a strong positive correlation was observed between  $T_{10}$ -values ( $R = 0.91$ ,  $p < 0.001$ ) and  $T_{50}$ -values ( $R = 0.72$ ,  $p < 0.05$ ) of bulk seawater samples, and the fraction of meteoric water in bulk seawater. This result suggests that terrestrial run-off, instead of sea ice melt, may be a more important source of INPs in this study. This is consistent with previous studies that have measured an abundance of INPs in freshwater sources such as rivers and lakes (Knackstedt et al., 2018; Moffett et al., 2018; Moffett, 2016).

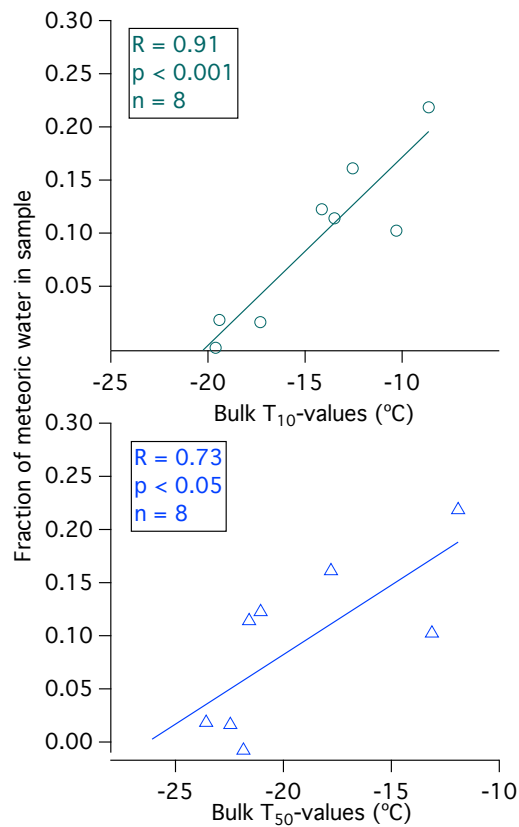


**Figure 3.7: Relationships between the fraction of meteoric water in each sample, and the  $T_{10}$ -values and  $T_{50}$ -values for bulk seawater for the 2016 study. Note that a negative  $f_{MW}$  was generated for one station (station 4) due to the definition of our seawater end-member.**

Another possible explanation for the negative correlation between salinity and INPs is a non-colligative effect of sea salt on the freezing temperature. Solutes can impact freezing temperature by blocking INP active sites (Kumar et al., 2018). To test this hypothesis, we varied the salinity in one of the microlayer samples (station 4) by adding commercial sea salt (Instant Ocean™), while keeping the concentration of ice nucleating material in the samples constant (see Section C.1, Appendix C for more details). The  $T_{10}$ -values for these salinity-enhanced samples (after correcting for freezing point depression) varied by less than the uncertainty in the measurements as the salinity of the sample was increased from 29 to 55 g/kg (Fig. C.9, Appendix C). These results suggest that sea salt does not have a non-colligative effect on the freezing temperature of the samples, at least not for the microlayer sample tested (station 4). Consistent with these results, non-colligative effects have not been observed in previous studies of immersion freezing with seawater and salt solutions (Alpert et al., 2011a, 2011b; Knopf et al., 2011; Wilson et al., 2015; Zobrist et al., 2008).

### 3.3.4.1 Chlorophyll *a* satellite data correlations

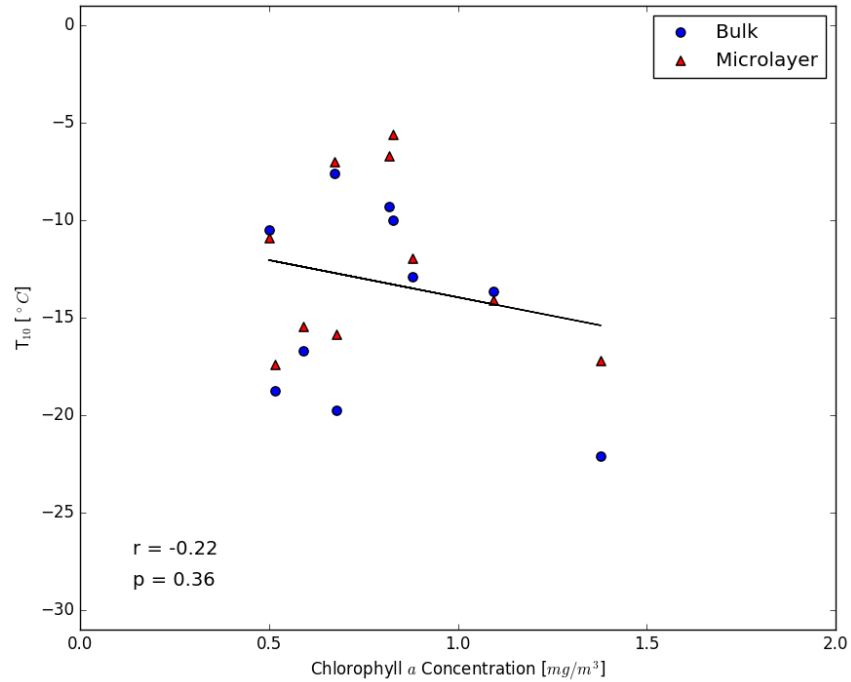


**Figure 3.8: Correlation plot between chlorophyll *a* concentrations derived from satellite imagery from the GlobColour project and the T<sub>10</sub>-values of microlayer and bulk seawater for 2016.**

Figure 3.8 shows correlations between the chlorophyll data retrieved from GlobColour and the T<sub>10</sub>-values for the microlayer and bulk seawater. The results indicate that correlations between T<sub>10</sub>-values in the microlayer or bulk seawater and chlorophyll *a* are not statistically significant. These observations are consistent with recent work by Wang et al. (2015), who showed that INP concentrations in sea spray aerosol emitted during a mesocosm tank experiment were not simply coupled to chlorophyll *a* concentrations.

## 3.4 Conclusions

The INP concentrations of microlayer and bulk seawater were determined at eleven stations in the Canadian Arctic during the summer of 2016, and compared to measurements

made in 2014 (Irish et al., 2017). Some samples had freezing temperatures as high as  $-5\text{ }^{\circ}\text{C}$ . Filtration reduced the freezing temperatures of all samples, suggesting ice-active particulate material was universally present in the microlayer and bulk seawaters we studied. Freezing temperatures also decreased after heat treatment indicating that the ice-active material was likely heat-labile biological material, consistent with previous measurements of INPs in the microlayer (Wilson et al., 2015) and bulk seawater (Schnell, 1977; Schnell and Vali, 1975, 1976). The ice-active material we observed in seawater was between  $0.2$  and  $0.02\text{ }\mu\text{m}$  in size, also consistent with previous studies of INPs in the microlayer (Wilson et al., 2015) and bulk seawater (Rosinski et al., 1986; Schnell and Vali, 1975).

We found a strong negative correlation between salinity and freezing temperatures, and a strong positive correlation between the fraction of meteoric water in the samples and freezing temperatures leading to the hypothesis that the INPs are associated with freshwater microorganisms from terrestrial run-off. Chlorophyll *a* concentrations from satellite measurements did not correlate with INP concentrations in seawater, consistent with recent work by Wang et al. (2015) in a mesocosm tank experiment. A possible explanation for these observations is that INP concentrations are not sensitive to the instantaneous photosynthetic productivity of a biological community, but rather to the nature of that community, and its life stage, including potential stresses experienced by sympagic communities during sea ice melt.

When comparing the INP concentrations in regions of close proximity between 2014 and 2016, we found little variability in the spatial pattern of INPs or salinity. In 2016, we observed higher concentrations of INPs nucleating ice at higher temperatures, particularly in the microlayer samples, than we did in 2014.

## **Chapter 4: Ice nucleating particles in the marine boundary layer in the Canadian Arctic during summer 2014**

### **4.1 Introduction**

Chapter 1 listed examples of atmospherically relevant INPs that include, but are not limited to, sea spray aerosol and mineral dusts (DeMott et al., 2016; Després et al., 2012; Hoose and Möhler, 2012; Murray et al., 2012; Niemand et al., 2012; Szyrmer and Zawadzki, 1997). Sea spray aerosol is generated by wave breaking and the bubble bursting mechanism at the ocean surface (Blanchard, 1964). Chapters 2 and 3, and other recent work have shown that the ocean contains INPs, and that sea spray aerosol can be a significant contributor to the INP population when the source of other INPs is small (Burrows et al., 2013; Irish et al., 2017; Rosinski et al., 1986; Schnell, 1977; Schnell and Vali, 1975, 1976; Vergara-Temprado et al., 2017; Wilson et al., 2015). However our understanding of the flux of INPs from the ocean to the atmosphere is far from complete.

Mineral dust is transported to the atmosphere by wind erosion, which is sensitive to factors like soil composition, soil moisture, and wind velocity (Ginoux et al., 2001). As mentioned in Chapter 1, mineral dust has been identified as an important contributor to the atmospheric INP population in many field and laboratory studies (Atkinson et al., 2013; Boose et al., 2016; Chen et al., 2018; Conen et al., 2011; Connolly et al., 2009; Creamean et al., 2013; DeMott et al., 2015; Eastwood et al., 2008; Hill et al., 2016; Kaufmann et al., 2016; Klein et al., 2010; Murray et al., 2012; Niedermeier et al., 2010; Niemand et al., 2012; O’Sullivan et al., 2014; Rangel-Alvarado et al., 2015; Steinke et al., 2016; Wang et al., 2015; Wex et al., 2014;

Wheeler et al., 2015). Modelling studies have also confirmed that mineral dust particles are important atmospheric INPs (Alizadeh-Choobari et al., 2015; Atkinson et al., 2013; Burrows et al., 2013; Hendricks et al., 2011; Hoose et al., 2010; Lohmann and Diehl, 2006; Prenni et al., 2009b; Vergara-Temprado et al., 2017). However in remote regions, such as the Arctic, the relative contribution of mineral dust to the INP population compared to sea spray is unknown.

Chapter 1 described how warming in the Arctic has decreased sea ice and land snow (Derksen and Brown, 2012), and how warming may impact INP concentrations in this region. To determine if increases in INP concentrations in the atmosphere may occur in future as a result of a decrease in sea ice and land snow, studies are needed to determine the concentrations and sources of INPs in the Arctic at present. If warming in this region continues, the concentration of INPs from local sources may continue to increase, influencing the properties of mixed phase clouds, and climate in the region.

To help address the issues raised above we 1) determined concentrations of INPs in the Canadian Arctic marine boundary layer during summer 2014, 2) measured the ratio of surface areas of mineral dust particles to sea spray particles, and 3) investigated the source region of the INPs using a particle dispersion model. The specific goals of this study were to quantify the concentrations of INPs in the Canadian Arctic marine boundary layer during the summer of 2014 and to provide insights into the source of INPs in this region.

## **4.2 Experimental**

### **4.2.1 Sampling locations**

All measurements and sample collections were performed on board the CCGS *Amundsen* as part of the NETCARE project. The 28 sampling locations are shown in Fig. 4.1, and the

sampling dates, times, and coordinates are detailed in Table D.1 (Appendix D). The air temperature, relative humidity (RH), and wind speed during sampling are shown in Fig. D.1 (Appendix D). INP concentrations from a subset of the locations (indicated with blue rings around the red symbols in Fig. 4.1) were previously reported in DeMott et al. (2016) but are also included here as they were collected during the same expedition and with the same methodology. The data reported in DeMott et al. (2016) only included sites in Baffin Bay, days where it did not rain and conditions when the apparent wind direction measured on the ship was between 0-90 degrees or 270-360 degrees, where 0/360 corresponds to the bow of ship (where the apparent wind direction is defined as the wind direction experienced by an observer on the moving ship as opposed to the true wind direction, which is defined as the wind direction experienced by an observer when the ship is stationary).

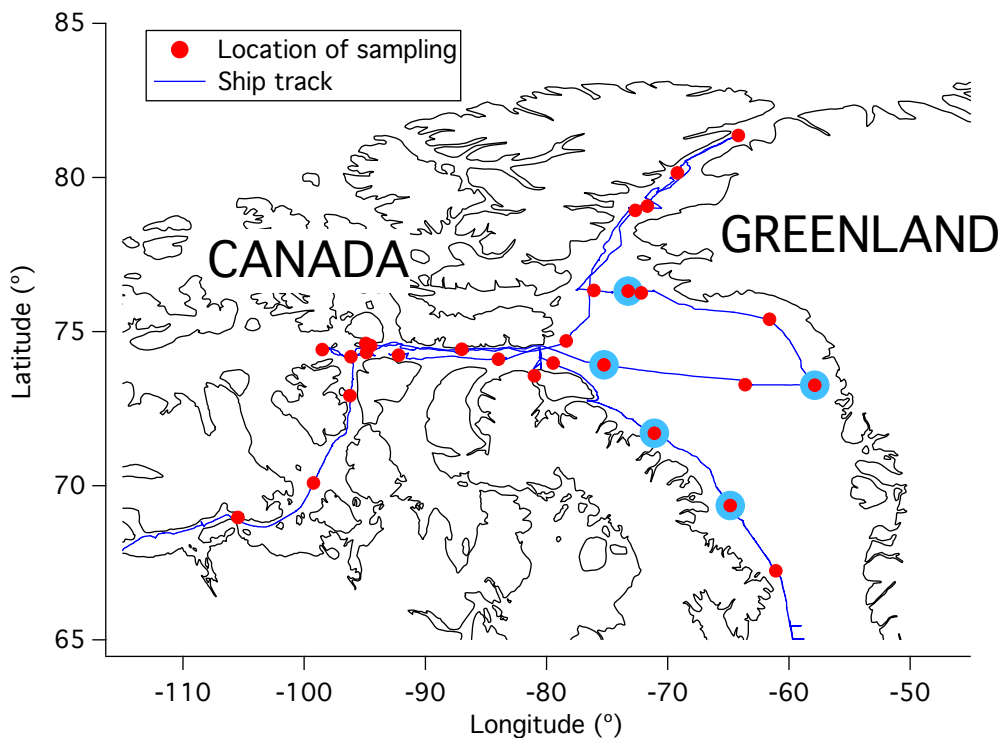


**Figure 4.1: Locations of sampling. Blue circles around the red dots indicate the locations of samples used in DeMott et al. (2016). Information on specific geographical coordinates is given in Table D.1 (Appendix D).**

## **4.2.2 Quantification of INPs**

To determine the concentration of INPs, atmospheric particles were collected on hydrophobic glass slides using a micro-orifice single stage impactor (MOSSI; MSP corp., Shoreview, MN, USA; Fig. D.2, Appendix D). The freezing properties of the collected particles were then determined with the droplet freezing technique (DFT). The combination (MOSSI-DFT) is similar to the micro-orifice uniform deposit impactor droplet freezing technique (MOUDI-DFT) recently used to determine the size resolved concentrations of INPs (Mason et al., 2015b, 2015a, 2016). The main difference between the MOSSI-DFT technique and the MOUDI-DFT technique is the use of a single stage impactor compared to a multistage impactor. The use of a single stage impactor simplifies the analysis and reduces collection time but sacrifices size information. The MOSSI-DFT technique is also similar to the technique used by others to measure deposition freezing (Knopf et al., 2010, 2014, Wang et al., 2012a, 2012b).

### **4.2.2.1 Micro-orifice single stage impactor**

The MOSSI was located on the port side of the bridge on the ship, approximately 10 m in front of the ship's smokestack. During sampling the flow rate through the MOSSI was 10 L/min, resulting in particles with aerodynamic diameters  $> 0.18 \mu\text{m}$  being collected on the hydrophobic glass slides placed within the MOSSI. The collection time of samples with the MOSSI for INP analysis was approximately 20 minutes. The MOSSI sampled air through a louvered total suspended particulate (TSP) inlet, which was approximately 15 m above sea level. The nozzle plate within the MOSSI contained 300 micro-orifices. As a result, particles collected on the hydrophobic glass slides beneath the nozzle plate were concentrated into 300 spots. After

collection the hydrophobic glass slides containing the particles were stored at 4 °C for no longer than 3 months prior to analysis.

Particle rebound can be an issue with an inertial impactor such as the MOSSI. Particle rebound occurs when particles impact the collection substrate but are not retained. Rebound has been shown to be reduced at RH values above 70 %, although this depends on the chemical composition of the particles (Bateman et al., 2013; Chen et al., 2011; Fang et al., 1991; Lawson, 1980; Saukko et al., 2012; Vasiliou et al., 1999; Winkler, 1974). During collection with the MOSSI the RH was always well above 70 % (Fig. D.1, Appendix D), with an average of 93 %. Furthermore, field measurements of INP concentrations using the MOUDI-DFT (a method similar to the MOSSI-DFT) have shown good agreement with INP concentrations measured with an instrument that is not susceptible to particle rebound (a continuous flow diffusion chamber; CFDC) when the RH of the sampled aerosol was as low as 40 % (DeMott et al., 2017; Mason et al., 2016). Nevertheless, particle rebound cannot be ruled out, and therefore the INP concentrations reported here should be considered as lower limits.

#### **4.2.2.2 Droplet freezing technique**

The DFT (Koop et al., 1998; Mason et al., 2015b) was used to determine the concentration of INPs in the immersion mode collected on hydrophobic glass slides using the MOSSI. Briefly, the hydrophobic glass slides containing the collected particles were located in a temperature and relative humidity controlled flow cell, coupled to an optical microscope with a charged-coupled device camera and a 1.25x objective (Axiolab; Zeiss, Oberkochen, Germany). Typically between 15-25 spots of particles (out of the 300 spots generated by the micro-orifices in the nozzle plate) could be monitored in the CCD field of view, which was approximately

12.25 mm<sup>2</sup> in area). Water was then condensed on the hydrophobic glass slides by decreasing the temperature to 2 °C and flowing a gas (pure Helium) with a dew point of greater than 2 °C over the hydrophobic glass slides. This resulted in water droplets (with diameters between 100 to 500 μm) condensing on the spots (referred to here as spot droplets) as well as water droplets condensing on other areas of the slides (referred to here as non-spot droplets). After the droplets were condensed, the temperature of the flow cell was decreased at a rate of 10 °C/min. From videos recorded while the temperature was decreased, the freezing temperature of each droplet was manually determined by observing the change in the droplet's optical properties. The droplets that contained spots of deposited particles were also identified from these videos. For comparison purposes, hydrophobic glass slides that were not exposed to atmospheric particles were also processed in the same way as described above and labelled as blanks.

The number of INPs as a function of temperature,  $\#INP(T)$ , was calculated for each experiment using the following equation:

$$\#INP(T) = \left( -\ln \left( \frac{N_u(T)}{N_s} \right) \right) N_s \quad (4.1)$$

Where  $N_u$  is the number of unfrozen droplets covering the spots, and  $N_s$  is the number of spots in the field of view. Equation 4.1 accounts for the possibility that each droplet covering a spot can contain multiple INPs (Vali, 1971).

Equation 4.1 assumes that each spot was covered by only one droplet. For cases when more than one droplet formed on a spot, the first droplet that froze was considered in Eq. 4.1. This was expected to give an equivalent result to the case of only one droplet condensing on the spot. For cases when one droplet contained two spots (this occurred for 2 % of the total number of spots in all experiments), an upper limit to the number of INPs was calculated by assuming

two droplets covered the two spots and both droplets froze at the observed freezing temperature. A lower limit was calculated by assuming the two spots were covered by two droplets with one droplet freezing at the observed freezing temperature and the other droplet freezing at  $-37\text{ }^{\circ}\text{C}$  (approximately the homogeneous freezing temperature). If one droplet contained 3 or more spots a similar procedure to the above was used to calculate the upper and lower limits to  $\#INP(T)$ .

Freezing of droplets that did not cover spots was a relatively rare occurrence at the temperature range we focus on in this manuscript ( $\geq -25\text{ }^{\circ}\text{C}$ ; see Section 4.3.1). For example the ratio of frozen non-spot droplets to frozen spot droplets was 0.02 and 0.07 at  $-25\text{ }^{\circ}\text{C}$  and  $-20\text{ }^{\circ}\text{C}$ , respectively. We assumed these relatively rare occurrences were due to particles  $< 0.18\text{ }\mu\text{m}$  in diameter that were not focused into spots, or due to rebound of a small fraction of the particles off the hydrophobic glass slides. To take into account the INPs not concentrated into the spots, we added the number of frozen non-spot droplets at each temperature to Eq. 4.1. Since the freezing of non-spot droplets was a relatively rare occurrence, we did not apply the Vali correction (Vali, 1971) to these freezing events.

Approximately 2 % of the freezing events in our experiments occurred by contact freezing between  $-16.2$  and  $-34.8\text{ }^{\circ}\text{C}$ . Contact freezing occurred when a frozen droplet grew in size, due to the Wegener-Bergeron-Findeisen process (Findeisen, 1938), and caused the freezing of a neighbouring unfrozen droplet. When calculating concentrations of INPs, contact freezing events were excluded.

The atmospheric concentration of INPs as a function of temperature,  $[INP(T)]$ , was calculated with the following equation:

$$[INP(T)] = \#INP(T) \cdot \frac{300}{N_s} \cdot \frac{1}{V} \quad (4.2)$$

Where  $V$  is the volume of air sampled and the ratio of  $300/N_s$  takes into account that only a fraction of the total number of spots in the sample were observed in a freezing experiment.

#### **4.2.3 Effect of ship emissions on measured INP**

To determine if particles from the ship's smokestack affected the measured INP concentrations, we first investigated the relationship between INP concentrations measured on the ship and the gas-phase HONO concentrations, a product of the reaction between  $\text{NO}_x$  from the ship smokestack and water (Von Glasow et al., 2003). HONO was measured by a chemical ionisation mass spectrometer located on the bridge of the ship about 5 m in front of the smokestack. No correlation was observed between HONO and INP concentrations at  $-25\text{ }^\circ\text{C}$  ( $R = 0.05$ ,  $p = 0.403$ ).

Second we separated our INP results into samples that were not exposed to smokestack emissions based on measured wind direction and wind speed, and samples that may have been exposed to smokestack emissions based on measured wind direction and wind speed. When the apparent wind direction measured on the ship was between  $0\text{-}90^\circ$  and  $270\text{-}360^\circ$  (where  $0^\circ/360^\circ =$  bow of ship) and when the apparent wind speed (minute average) was higher than 2.5 m/s for the entire collection time, we assumed that the samples were not exposed to smokestack emissions. Within the uncertainty of the measurements, the INP concentrations measured when samples were not exposed to smokestack emissions (based on the apparent wind direction and speed) are the same as INP concentrations measured when samples may have been exposed to smokestack emissions (Fig. D.3, Appendix D). Since the criteria discussed above and the results from the HONO analysis do not suggest measured INP concentrations were influenced by the smoke stack emissions, all samples that were collected have been included in this study.

#### 4.2.4 Particle dispersion modelling

FLEXPART-WRF (Brioude et al., 2013), a version of the Lagrangian particle dispersion model FLEXPART (Stohl et al., 2005), was used to investigate the potential emission source regions of the INPs. FLEXPART-WRF is driven by meteorology from the Weather Research and Forecasting (WRF) model (Skamarock et al., 2008), and was run in backward mode. The simulation domain for FLEXPART-WRF is shown in Fig. D.4 (Appendix D).

WRF 3.5.1 was run for the 2014 Amundsen campaign using initial and boundary conditions from the European Centre for Medium-Range Weather Forecasts (ECMWF) operational analysis (a grid resolution on  $0.25^\circ$ ). The ECMWF wind, temperature, and RH were used to nudge the WRF run every 6 hours above the atmospheric boundary layer. A full list of the parameterizations and options used for the WRF simulations is given in Table 1 of Wentworth et al. (2016).

FLEXPART-WRF was run in backward mode at 20-minute intervals along the ship track. For each run 100,000 particles were released from the ship's location in a volume  $100 \times 100$  m in the horizontal and from 0 to 60 m above mean sea level in the vertical. The particles were followed backward for seven days with output generated hourly.

As mentioned above, each INP sample was collected over a period of approximately 20 minutes. As a result, one FLEXPART-WRF run overlapped with each INP sampling period. The FLEXPART-WRF runs that overlapped in time with the INP sampling periods were used to produce potential emission sensitivity (PES) plots for the INP samples. A PES plot was produced by integrating the FLEXPART-WRF output over the 7 days prior to the release of particles. The value of the PES in a particular grid cell is proportional to the particles' residence time in that cell. Since this study is concerned with INP sources from the surface, only particles within the

footprint layer (0 to 300 m altitude) are considered when calculating PES values, and we report PES values for the footprint layer.

#### **4.2.5 Statistical analyses**

Pearson correlation analysis was used to compute correlation coefficients (R). P values were also calculated to determine if the correlations were statistically significant at the 95 % confidence level ( $p < 0.05$ ).

#### **4.2.6 Computer controlled scanning electron microscopy with energy dispersive X-ray spectroscopy (CCSEM-EDX)**

Immediately following the collection of each sample for INP analysis, additional particle samples were collected to determine the ratio of mineral dust surface area to sea salt surface area by computer controlled scanning electron microscopy with energy dispersive X-ray spectroscopy (CCSEM-EDX). Particles were collected on transmission electron microscopy (TEM) grids (carbon 200 mesh; Ted Pella) using the same MOSSI used to collect INP samples. Collection time of samples for CCSEM-EDX was 20 minutes. The samples were kept at room temperature for a maximum of 38 months before analysis. Since a long collection time was used (approximately 20 min), particles in the spots directly below the micro-orifices of the nozzle plate in the MOSSI were too close together to identify individual mineral dust and sea salt surface particles using CCSEM-EDX. To overcome this issue, we only analysed particles on the edge of the spots directly below the micro-orifices of the nozzle plate with the CCSEM-EDX.

Due to time constraints, only three samples (two with a high [INP(T)] and one with a low [INP(T)]) were analysed by CCSEM-EDX to determine the ratios of mineral dust surface area to

sea salt surface area. The method of using CCSEM-EDX to study atmospheric particles is described by Laskin et al. (2006). Particles with sizes between 0.15 to 5  $\mu\text{m}$  (area equivalent diameters) were analysed. First, the atomic percentages of each particle were determined from EDX spectra. Then, based on the atomic percentages of each particle, particles were classified as sea salt, mineral dust, or other using the scheme shown in Fig. D.5 (Appendix D), which is based on the work by Laskin et al. (2012). After each particle was classified, the surface areas of mineral dust particles and sea salt particles were determined using 2D projected images recorded by SEM. Note that actual surface area of mineral dust is underestimated using this method due to surface irregularities and complex topology. The ratio of mineral dust surface area to sea salt surface area was then determined by dividing the surface area of mineral dust for each sample by the surface area of sea salt for the same sample.

### **4.3 Results and Discussion**

#### **4.3.1 Measured INP concentrations**

The measured concentrations of INPs,  $[\text{INP}(T)]$ , sampled in the Arctic are shown in Figs. 4.2B and 4.2C. The measured  $[\text{INP}(T)]$  on hydrophobic glass slides that were not exposed to atmospheric particles, referred to as “blanks”, are shown in red in Figs. 4.2A and 4.2C. Freezing of the blanks occurred over the range of  $-25.9$  to  $-38.4$   $^{\circ}\text{C}$ . For the droplet sizes and cooling rates used here homogeneous freezing occurs at approximately  $-37$   $^{\circ}\text{C}$ . Therefore the freezing that occurred in the blanks at temperatures above approximately  $-37$   $^{\circ}\text{C}$  was due to heterogeneous freezing likely caused by the hydrophobic glass slides. In the following we will focus on  $[\text{INP}(T)]$  at temperatures of  $-25$   $^{\circ}\text{C}$  and warmer since no freezing from the blanks was observed

in this temperature range. A full time series of  $[\text{INP}(T)]$  at  $-15$ ,  $-20$ , and  $-25$  °C are reported in Fig D.6 (Appendix D).

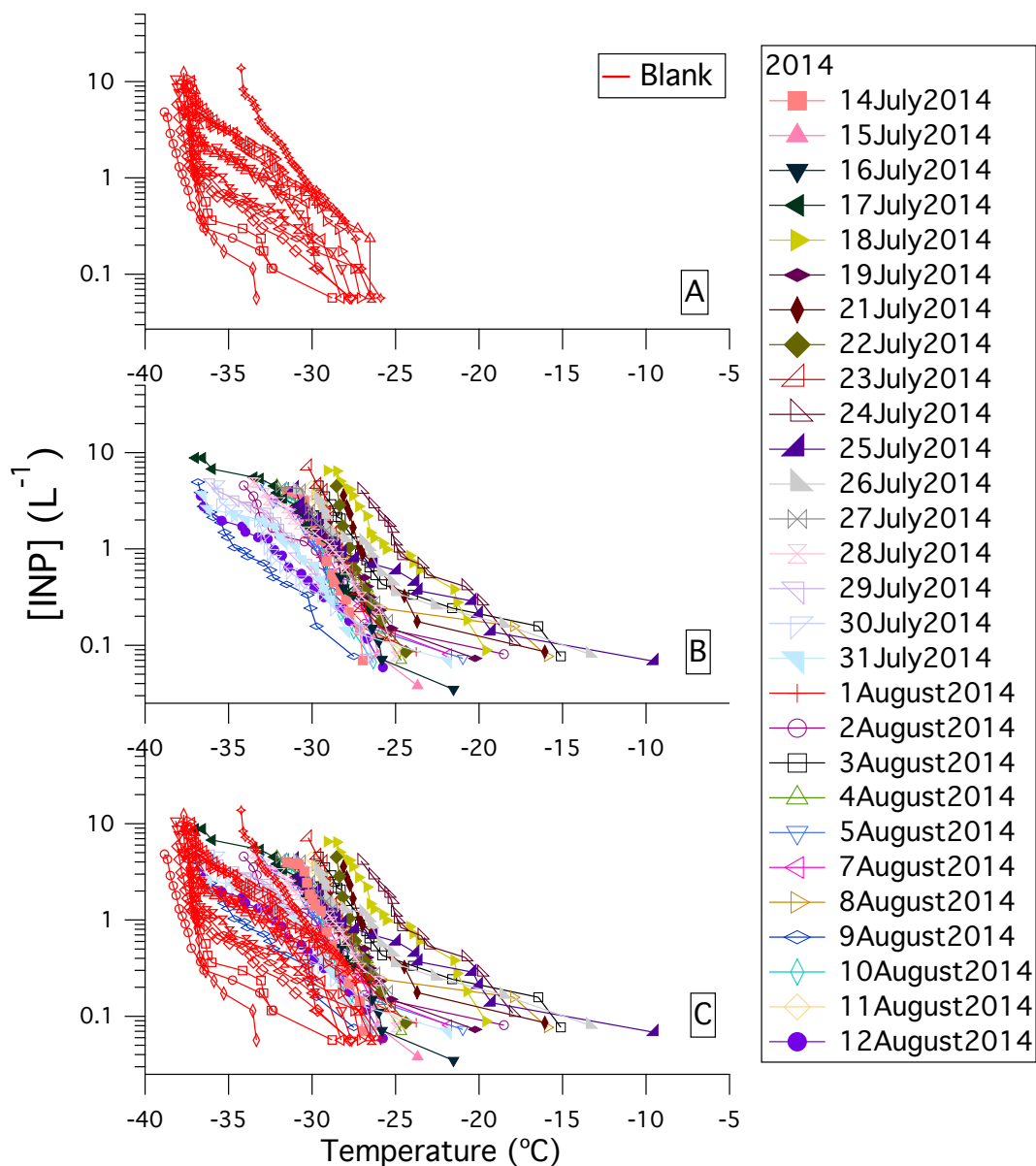


**Figure 4.2:** Plot of  $[\text{INP}]$  ( $\text{L}^{-1}$ ) as a function of temperature ( $^{\circ}\text{C}$ ) for A) the blanks, B) the samples, and C) the blanks and samples. The  $[\text{INP}]$  ( $\text{L}^{-1}$ ) of 11 blanks are shown in A and C. Each blank was performed on a separate hydrophobic glass substrate. Error bars are not shown to improve the visibility of the data in the plot. Error bars in the x direction are  $\pm 0.3$   $^{\circ}\text{C}$  for each data point. Error bars in the y direction were calculated using nucleation statistics following Koop et al. (1997); the errors for our measured  $[\text{INP}]$  ( $\text{L}^{-1}$ ) are reported in Fig. D.6 (Appendix D).

In Fig. 4.3 we compare recent measurements of  $[\text{INP}(T)]$  from several field campaigns in marine environments with the average concentrations measured in the current study. Figure 4.3 illustrates that the average INP concentrations measured in the current study fall within the range of INP concentrations measured in other marine environments. This observation, however, does not confirm that sea spray aerosol was the major source of INPs during the studies reported here.

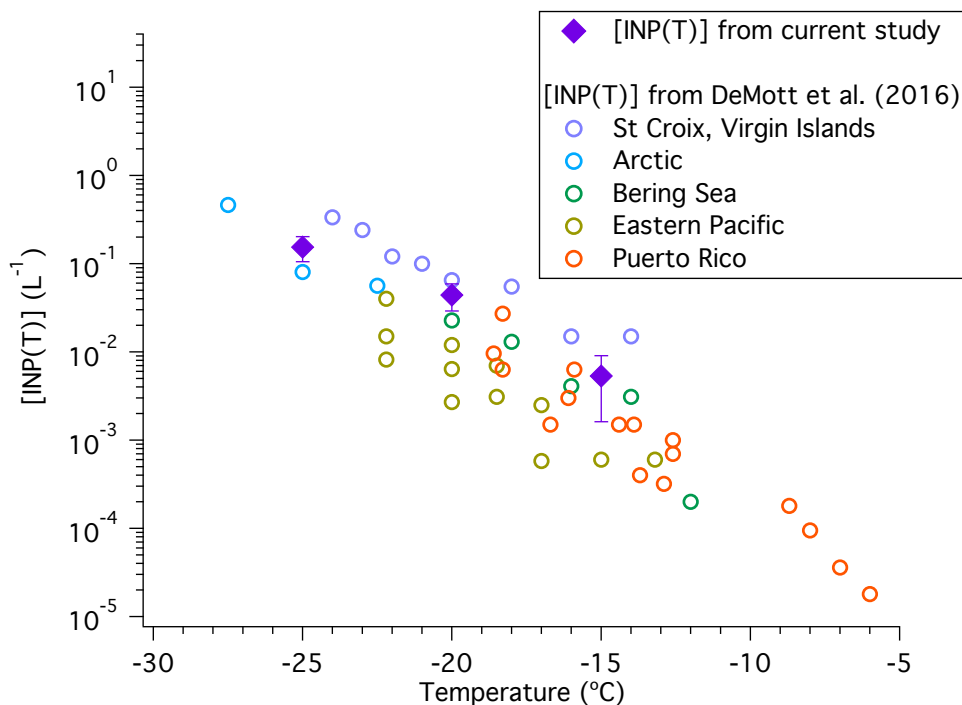


**Figure 4.3:** Plot of  $[\text{INP}]$  ( $\text{L}^{-1}$ ) as a function of temperature including a comparison to field results from several recent field studies in marine environments reported in DeMott et al. (2016). The purple diamonds represent averages of the data reported in this study at  $-15$ ,  $-20$ , and  $-25$   $^{\circ}\text{C}$ . Error bars are the standard error of the mean. Other coloured circles represent INP measurements from field studies in marine environments reported in DeMott et al., (2016), with the locations indicated in the legend.

#### 4.3.2 Measured ratios of mineral dust surface area to sea salt surface area

For three samples (two with high  $[\text{INP}(T)]$  and one with low  $[\text{INP}(T)]$ ), we calculated the ratios of mineral dust surface area to sea salt surface area using CCSEM-EDX. The two samples

corresponding to high [INP(T)] were collected on July 21<sup>st</sup> and 25<sup>th</sup>. The sample corresponding to a low [INP(T)] was collected on July 29<sup>th</sup>. In Table D.2 (Appendix D) we report the total number of particles analysed by CCSEM-EDX for each sample and the fraction of particles classified as mineral dust and sea salt particles. Shown in Fig. 4.4A are the calculated ratios of mineral dust surface area to sea salt surface area using surface area measurements from CCSEM-EDX. For the three samples, this ratio ranged from 0.03 to 0.09. Using this ratio we estimated the ratio of [INP(T)] from mineral dust, [INP(T)]<sub>MD</sub>, to [INP(T)] from sea spray, [INP(T)]<sub>SS</sub>, using the following equation:

$$\frac{[INP(T)]_{MD}}{[INP(T)]_{SS}} = \frac{n_s(MD) \cdot S_{MD}}{n_s(SS) \cdot S_{SS}} \quad (4.3)$$

Where  $n_s(SS)$  is the ice active surface site density for sea spray aerosol,  $n_s(MD)$  is the ice active surface site density for mineral dust, and  $S_{SS}$  and  $S_{MD}$  are the total surface areas measured by CCSEM-EDX for sea salt and mineral dust, respectively. The  $n_s(SS)$  were determined using laboratory data from DeMott et al. (2016). The  $n_s(MD)$  were calculated using the exponential function reported by Niemand et al. (2012) that was determined from freezing data of Asian dust, Saharan dust, Canary Island dust, and Israel dust. For details see Section D.1 (Appendix D).

The ratios of INP concentrations based on Eq. 4.3 for freezing temperatures of -25, -20, and -15 °C, are shown in Figs. 4.4B, 4.4C, and 4.4D respectively. These ratios suggest that for the three samples when CCSEM-EDX measurements were performed, the [INP(T)]<sub>MD</sub> are higher than the [INP(T)]<sub>SS</sub> (ratios were between 10 to 10<sup>3</sup>, inclusive of errors, at -15, -20, and -25 °C), assuming the  $n_s$ -values used are applicable for the field studies reported here. These results also suggest that mineral dust is a more important contributor to the INP population than sea spray aerosol for the times and locations corresponding to the CCSEM-EDX measurements.

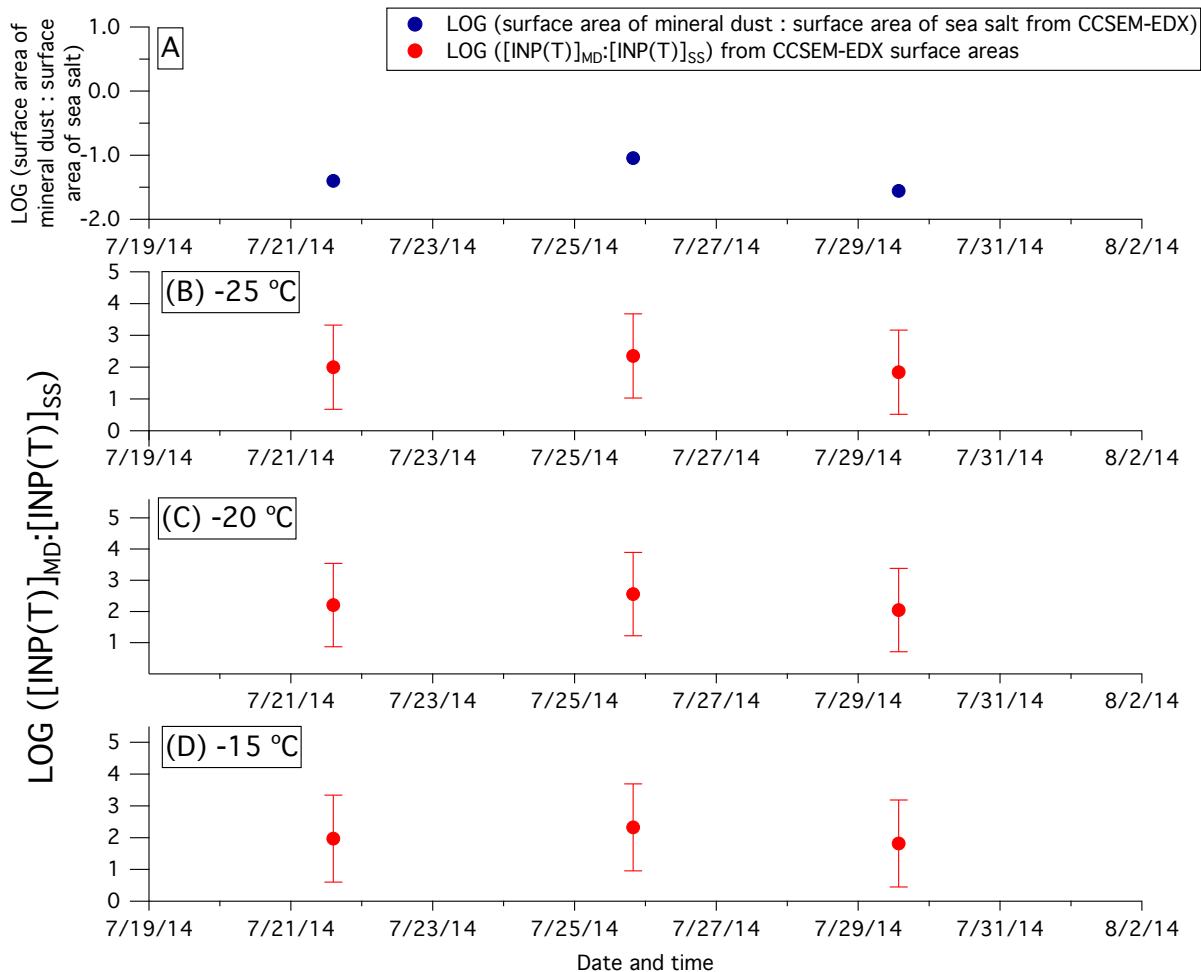


**Figure 4.4:** A) Ratios of the surface area of mineral dust to the surface area of sea salt measured by CCSEM-EDX (blue circles). Ratios of predicted  $[INP(T)]_{MD}$  to the predicted  $[INP(T)]_{SS}$  calculated using CCSEM-EDX measurements (red circles) at B) -25 °C, C) -20 °C, and D) -15 °C.

### 4.3.3 Particle dispersion modelling

Figure 4.5A shows the averaged PES for the footprint layer for all samples combined and suggests that the source of INPs sampled during the campaign was local (i.e. the Canadian Arctic Archipelago, Baffin Bay, and Eastern Greenland).

Figure 4.5B shows the averaged PES for the footprint layer for samples that had the highest INP concentrations (top 36 % of the samples) at -25 °C. Figure 4.5C shows the average

PES for the footprint layer for samples that had the lowest INP concentrations (bottom 36 % of the samples) at -25 °C. A cut-off of 36 % was selected since no freezing was observed in 36 % of the samples at -25 °C. Figure 4.5D shows the ratio of the average PES for the highest INP concentrations to the average PES for all samples. Figure 4.5E shows the ratio of the average PES for the lowest INP concentrations to the average PES for all samples. Previous work has shown that ratios of average PES are useful for identifying likely sources (Hirdman et al., 2010). Considering all figures together, the highest INP concentrations are associated with lower latitude regions such as the Hudson Bay area, eastern Greenland, or northwestern continental Canada. On the other hand, the lowest concentrations (below the detection limit at -25 °C) were often associated with regions further north and over Baffin Bay.

Figures 4.5F and 4.5G show maps of surface cover type (i.e. bare land, open water, sea ice, and snow cover) from the first and last days of the campaign, respectively, based on data from the National Snow and Ice Data Centre (NSIDC, 2008). The maps of surface coverage were combined with the PES values in the footprint layer from FLEXPART to determine the total residence time over each surface type for a given INP sample. Specifically, surface coverage data from the NSIDC was downloaded in GEOTiff format and converted to vector shapefiles. The fraction of each FLEXPART grid cell that was over each surface type category (e.g. bare land, open water) was then calculated using these vector shapefiles. The residence time in a grid cell was then multiplied by the fraction of the cell in each surface type category, and then the results were summed over all grid cells to determine the relative time spent over each surface type.

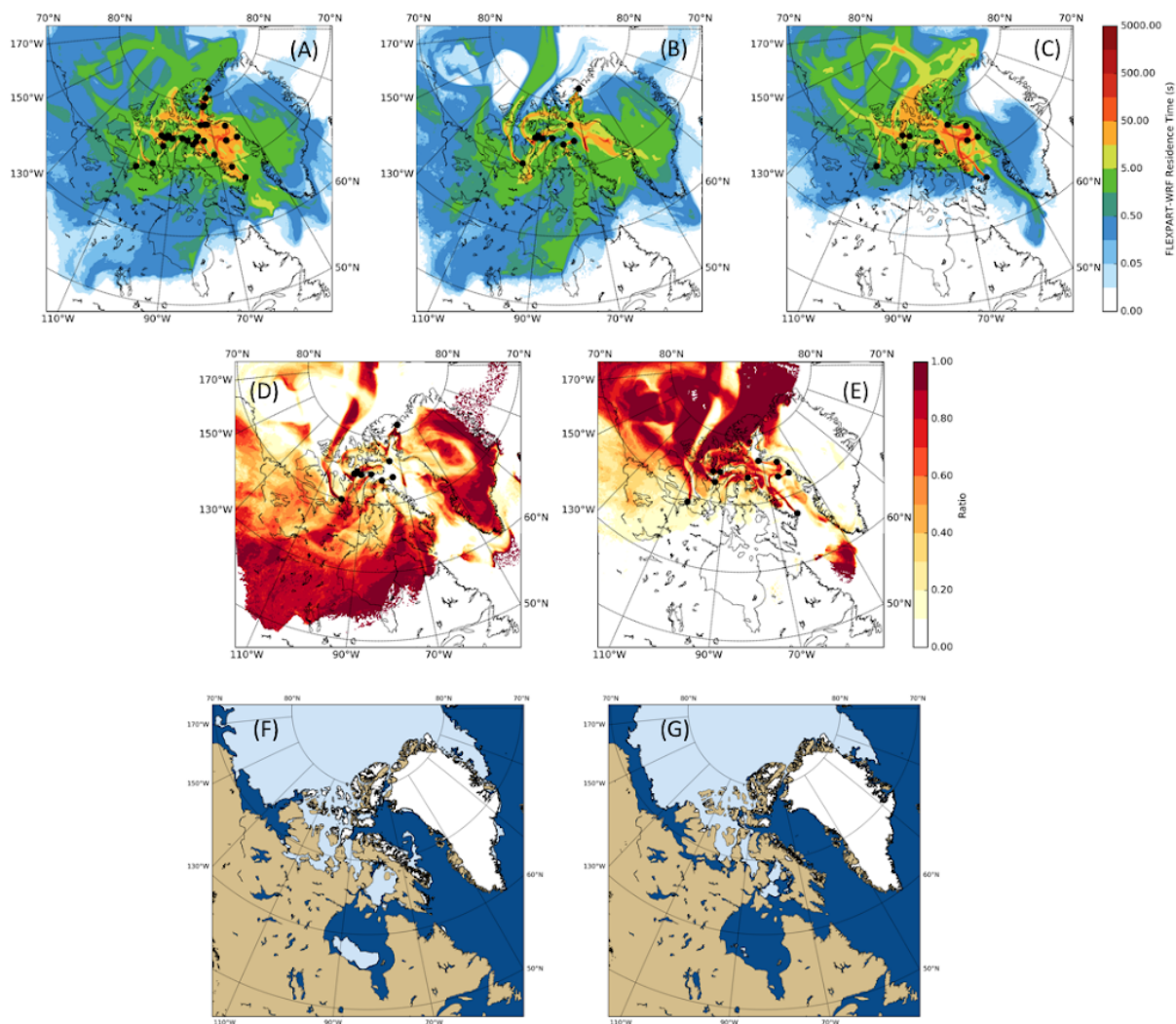


Figure 4.5: Top row: Average FLEXPART-WRF footprint potential emission sensitivities (PES) plots for A) all sampling days, B) the 36 % of samples with the highest  $[\text{INP}(\text{T})]$  ( $\text{L}^{-1}$ ), and C) the 36 % of samples with the lowest  $[\text{INP}(\text{T})]$  ( $\text{L}^{-1}$ ). Black circles indicate the ship's position at the sampling mid-time. Middle row: Maps showing the ratios of D) plot B to plot A, and E) plot C to plot A. Bottom row: Maps showing the surface cover type on F) the first day of sampling (14<sup>th</sup> July), and G) the last day of sampling (12<sup>th</sup> August). Bare land, open water, sea ice, and snow cover are shown as beige, dark blue, light blue, and white, respectively. The NSIDC data classifies each 4 x 4 km grid cell as one covered by sea, land without snow, sea ice, or snow-covered land. In these plots, white represents snow-covered land, light blue represents sea ice, dark blue represents open water, and beige represents bare land. Note that for this study, lakes are included in the bare land category.

Correlations between the total residence time over each surface type and the concentration of INPs for each sample at -15, -20, and -25 °C were then investigated (Table 4.1 and Fig D.7, Appendix D). This correlation analysis showed statistically significant ( $p < 0.05$ ) positive correlations between the total residence time over bare land in the footprint layer, and both [INP(T)] at -15 °C ( $R = 0.5$ ) and -25 °C ( $R = 0.4$ ). On the other hand, a statistically significant negative correlation was observed between the total residence time in the footprint layer over sea ice and both [INP(T)] at -20 °C ( $R = -0.4$ ) and -25 °C ( $R = -0.3$ ). Furthermore, a statistically significant negative correlation was observed between the total residence time in the footprint layer over open water and [INP(T)] at -20 °C ( $R = -0.4$ ). These negative correlations can be explained by a stronger source of INPs from bare land compared to sea ice or open water. Related, Bigg (1996) observed a correlation between INP concentrations measured in the high Arctic and the time since the sampled air mass was last in contact with open ocean ( $R = -0.54$ ,  $p < 10^{-4}$ ). In contrast Bigg and Leck (2001) observed no correlation between INP concentrations and the time since the sampled air mass was last in contact with open ocean.

**Table 4.1: Correlation coefficients (R), p and n values for correlation analysis between [INP] ( $L^{-1}$ ) at -15, -20, and -25 °C and the time the air mass spent over different surface types within 0-300 m of the surface. Numbers in bold indicate correlations that are statistically significant ( $p < 0.05$ ).**

	-15 °C			-20 °C			-25 °C		
	<b>R</b>	<b>p</b>	<b>n</b>	<b>R</b>	<b>p</b>	<b>n</b>	<b>R</b>	<b>p</b>	<b>n</b>
<b>Bare land residence time</b>	<b>0.5</b>	<b>0.008</b>	<b>27</b>	0.3	0.058	27	<b>0.4</b>	<b>0.033</b>	<b>27</b>
<b>Open water residence time</b>	-0.1	0.240	27	<b>-0.4</b>	<b>0.023</b>	<b>27</b>	-0.3	0.054	27
<b>Sea ice residence time</b>	-0.2	0.180	27	<b>-0.4</b>	<b>0.028</b>	<b>27</b>	<b>-0.3</b>	<b>0.041</b>	<b>27</b>
<b>Snow cover residence time</b>	-0.2	0.162	27	0.2	0.183	27	0.0	0.449	27

#### 4.4 Conclusions

Concentrations of INPs in the marine boundary layer were measured at 28 different locations in the Canadian Arctic. Results showed that the concentrations of INPs are similar to concentrations measured in other marine environments.

For three collected samples the ratio of mineral dust surface area to sea spray surface area ranged from 0.03 to 0.09. Based on these ratios and the ice active surface site densities of mineral dust and sea spray aerosol determined in previous laboratory studies, mineral dust is a more important contributor to the INP population than sea spray aerosol for the samples analysed (ratios were between 10 to  $10^3$  at -15, -20, and -25 °C), assuming the ice active surface site densities of mineral dust and sea spray aerosol determined in laboratory studies are applicable to these field studies. This result suggests that INPs from mineral dust are more important contributors to the INP population than sea spray aerosol for the times and locations during sampling. Previous studies have shown that INPs are ubiquitous in Arctic seawater (Irish et al., 2017; Wilson et al., 2015). However, whether these INPs are transported into the atmosphere is determined by wind speed. Wind speeds above approximately 10-15 m/s are required for a breaking wave regime where bubbles will burst at the surface of the ocean (Sarmiento and Gruber, 2006). The average wind speed during sampling in this study was 5 m/s. This suggests that any INPs in the ocean may not have been transported into the atmosphere.

Particle dispersion modelling suggested that the INPs sampled in this study were likely not from long-range transport. For the days where the [INP(T)] was high, a likely source was Hudson Bay area, eastern Greenland, or northwestern continental Canada. For days where the [INP(T)] was low, the air mass spent more time over regions further north and over Baffin Bay.

Correlation analyses showed that there were statistically significant positive correlations between [INP(T)] at -15 and -25 °C and the time the air mass spent over land. Statistically significant negative correlations were observed between [INP(T)] at -20 and -25 °C and the time the air mass spent over sea ice, and [INP(T)] at -20 °C and the time the air mass spent over open water. This correlation analysis together with the particle dispersion modelling provides further evidence that sea spray aerosol was likely not the major source of INPs during sampling.

As warming increases in the Arctic, more erodible soil will be exposed for longer periods of time (Huang et al., 2015). These results, together with our freezing results suggest that warming in the Arctic will increase concentrations of INPs from mineral dust in the region, with possible implications for cloud properties and climate. Additional studies, including modelling and field studies are needed to quantify the importance of this feedback process for climate in the region.

## **Chapter 5: Conclusions and future work**

### **5.1 Concentrations and properties of INPs in the microlayer and bulk seawater in the Canadian Arctic**

Chapters 2 and 3 reported the concentrations and properties of INPs measured in microlayer and bulk seawater samples during two field campaigns in the Canadian Arctic. Chapter 2 focused on identifying the concentrations and properties of INPs measured during the summer of 2014, and Chapter 3 focused on comparing concentrations and properties of INPs measured during the summer of 2016 with those measured in 2014. During both field campaigns we observed that 1) INPs were found to be ubiquitous in microlayer and bulk seawaters, 2) the INPs were likely heat-labile biological materials and between 0.2 and 0.02  $\mu\text{m}$  in size, 3) there was a strong negative correlation between salinity and freezing temperatures, and a strong positive correlation between the fraction of meteoric water in each sample and freezing temperatures, possibly due to INPs associated with biological material from terrestrial run-off, and 4) concentrations of INPs could not be explained by satellite-derived chlorophyll *a* concentrations.

The relationship between the fraction of meteoric water in the samples and freezing temperatures suggest that the INPs are associated with freshwater microorganisms from terrestrial run-off. Warming in the Arctic will lead to a decrease in land ice and snow coverage. The melt from land ice and snow may contain many materials that could act as INPs, for example glacial mineral deposits, or terrestrial biological material. Recent chemical analysis of particles found in snow suggested they were made up of biological materials, as well as inorganic compounds with similar characteristics to mineral dust (Rangel-Alvarado et al., 2015).

Schnell and Vali (1976) were the first to suggest that an increase in the primary production of phytoplankton may cause an increase of INP concentrations in seawater. This suggests that biological processes may influence concentrations of INPs in seawater. INP concentrations have been observed to peak during a time of high biological activity (i.e. a bloom) (Wang et al., 2015) which is sometimes accompanied by an increase in concentrations of chlorophyll *a* (Bird and Kalff, 1984; McCluskey et al., 2017; Schnell and Vali, 1976). Therefore it is natural to assume that regions of high chlorophyll *a* concentrations may be associated with INP sources in seawater. Indeed, some studies have shown that an increase in ambient INP concentrations from sea spray coincides with an increase of chlorophyll *a* concentrations in seawater (DeMott et al., 2016). However, our results did not find a simple relationship between INP concentrations measured in seawater and chlorophyll *a* concentrations. This is consistent with studies that found chlorophyll *a* is not always an appropriate metric for biological productivity, and marine sources of INPs outside of biologically active environments should be considered (Prather et al., 2013; Wang et al., 2015). The complex relationship between ocean biology and sources of INPs needs further exploration in different ocean environments and seasons to make estimates of ambient INP concentrations emitted by sea spray for climate models (DeMott et al., 2016; McCluskey et al., 2017).

Although the spatial patterns of INPs and salinities were similar in 2014 and 2016, we observed some differences between the years; notably the concentrations of INPs were higher on average in 2016 compared to 2014, and INP concentrations were enhanced in the microlayer compared to bulk seawater in several samples collected in 2016, unlike in 2014.

The results from Chapters 2 and 3 may have important implications; warming in the Arctic will melt more land snow and ice, which will increase terrestrial run-off and thus may

increase concentrations of INPs in seawater. Additionally, warming in the Arctic will melt more sea ice, which will expose more of the ocean surface to the atmosphere. However, the emission of INPs identified in the ocean to the atmosphere has not yet been investigated and future work regarding this is discussed in Section 5.3.

## **5.2 Measurements of INPs in the marine boundary layer in the Canadian Arctic**

Chapter 4 reported ambient concentrations of INPs measured in the Canadian Arctic marine boundary layer during the summer of 2014. The concentrations of INPs measured here fell within the range of INPs measured in other marine environments (DeMott et al., 2016). This observation, however, did not confirm that sea spray aerosol was the major source of INPs during this campaign.

The surface areas of mineral dust and sea spray aerosol were determined from the campaign using CCSEM-EDX. From calculated ratios of mineral dust surface area to sea spray surface area, and the ice active surface site densities of mineral dust and sea spray aerosol determined in previous laboratory studies, we estimated the ratio of the concentration of INPs from mineral dust to the concentration of INPs from sea spray. This estimate suggested that mineral dust was a more important contributor to the INP population than sea spray aerosol for the samples analysed. Although Chapters 2 and 3 showed that INPs are ubiquitous in Arctic seawater (Irish et al., 2017; Wilson et al., 2015), whether these INPs are transported into the atmosphere will be determined by wind speed. The average wind speed during sampling in this study was 5 m/s. However, wind speeds above approximately 10-15 m/s are required for a breaking wave regime where bubbles will burst at the surface of the ocean (Sarmiento and

Gruber, 2006). This suggests that any INPs we observed in the ocean may not have been transported into the atmosphere during this study.

Particle dispersion modelling was used to further investigate the sources of INPs. The highest concentrations of INPs were associated with regions such as the Hudson Bay area, eastern Greenland, or northwestern continental Canada. The lowest concentrations of INPs observed were associated with regions further north of the sampling sites and over Baffin Bay. A weak positive correlation was also observed between INP concentrations and the time the air mass spent over bare land. These combined results suggested that mineral dust from regional continental areas was an important contributor to the INP population in the Canadian Arctic marine boundary layer during the summer of 2014.

The Canadian Arctic Archipelago is a unique environment where both the ocean and land are partially covered in ice and snow. When warming occurs in the Arctic, more ocean and land will be exposed due to the melting of sea and land ice and snow. Since local mineral dust is an important contributor to the population of INPs in this region, melting land ice and snow would expose more erodible soil. Subsequently, more INPs from erodible soil could be transferred to the atmosphere. This would have implications on cloud properties and lifetime, and the climate in the region.

### **5.3 Avenues for future research**

In Chapters 2 and 3 we found INPs were ubiquitous in the microlayer and bulk seawater, and that an important source of INPs was from meteoric water, which includes terrestrial run-off from glacial and snow melt. Warming in the Arctic will melt more land ice and snow, so it will

be important to investigate the types of INPs found in land ice and snow that may be released into the Arctic Ocean.

An inter-comparison study is necessary to compare results from the different microlayer and bulk seawater collection methods used for this research: the hand held glass plate, and the automated sampler. Chapter 3 highlighted the issue that both methods collect different thicknesses of microlayer. Therefore it would be useful to further investigate the INP activity as a function of microlayer thickness.

Following results from Chapter 4, sea spray aerosol may not be an important contributor to the INP population in marine boundary layer in the Canadian Arctic at present. However, future climate may alter the quantity of sea spray aerosol released into the atmosphere, which might influence cloud properties and lifetime in the Arctic. Whether or not INPs will be emitted into the atmosphere after they have been released into the ocean will depend largely on wind speed. More modelling studies would help determine whether warming in the Canadian Arctic would increase sea spray aerosol emissions in the region as a result of an increase in wind speed (Cheng et al., 2014; Cohen et al., 2018). In addition, when land ice and snow coverage decreases due to warming, the population of INPs in seawater might change.

Throughout Chapters 2 and 3 INP concentrations were measured in the microlayer and bulk seawater, but the transfer of INPs from microlayer and bulk seawater to the atmosphere was not investigated. In the 2016 field campaign the Dalhousie Aerosol Water Tank (DAWT) was used on board the *CCGS Amundsen* to generate sea spray aerosol from seawater that was collected in the Canadian Arctic. The DAWT experiment is similar to other laboratory microcosm experiments such as the Marine Aerosol Reference Tank experiment (McCluskey et al., 2017; Prather et al., 2013; Stokes et al., 2013; Wang et al., 2015). As sea spray was generated

particles were collected from the DAWT using the MOSSI. The INP concentration data from these experiments are yet to be analysed and it would be useful to compare the concentrations of INPs collected from microlayer and bulk seawater to the concentrations of INPs collected from the DAWT. Additional experiments to determine the flux of INPs from seawater to the atmosphere would also be valuable.

As previously mentioned, studies have reported that sea spray aerosol can be an important contributor to the INP population in marine environments when the source of other INPs is small (Burrows et al., 2013; Vergara-Temprado et al., 2017; Wilson et al., 2015). Chapter 4 reported that mineral dust was a more important contributor to the atmospheric INP population than sea spray aerosol. Measurements of ambient INP concentrations in the marine boundary layer in regions not likely to be influenced by air masses from land such as the Southern Ocean would be necessary to compare to measurements of ambient INP concentrations in the Arctic.

In Chapter 4 a new technique was used to collect INPs, therefore it would be useful to carry out inter-comparisons between the MOSSI and instruments already well-established in the field such as the CFDC (Rogers et al., 2001). In addition in Chapter 4, the issue of potential particle rebound in the MOSSI was highlighted. Future studies should focus on the extent to which particle rebound occurs at different atmospheric conditions, and how much it influences measurements of INP concentrations.

The composition of INPs measured in the field has often been inferred using correlation statistics. For example in Chapters 2 and 3 the concentrations of INPs were correlated with a number of oceanic parameters. This type of analysis, however, can never be conclusive. In Chapter 4 the composition of INPs collected in the marine boundary layer was probed using

CCSEM-EDX. While this technique is a lengthy process as it involves only looking at one particle at a time, it provides evidence for the source of the INPs. This technique should be used more when investigating INPs collected in the field.

## References

- Albrecht, B. A.: Aerosols, cloud microphysics, and fractional cloudiness, *Science*, 245, 1227–1230, 1989.
- Alizadeh-Choobari, O., Sturman, A. and Zawar-Reza, P.: Global distribution of mineral dust and its impact on radiative fluxes as simulated by WRF-Chem, *Meteorol. Atmos. Phys.*, 127, 635–648, doi:10.1007/s00703-015-0390-4, 2015.
- Aller, J. Y., Radway, J. C., Kilhau, W. P., Bothe, D. W., Wilson, T. W., Vaillancourt, R. D., Quinn, P. K., Coffman, D. J., Murray, B. J. and Knopf, D. A.: Size-resolved characterization of the polysaccharidic and proteinaceous components of sea spray aerosol, *Atmos. Environ.*, 154, 331–347, doi:10.1016/j.atmosenv.2017.01.053, 2017.
- Alpert, P. A., Aller, J. Y. and Knopf, D. A.: Ice nucleation from aqueous NaCl droplets with and without marine diatoms, *Atmos. Chem. Phys.*, 11, 5539–5555, doi:10.5194/acpd-11-8291-2011, 2011a.
- Alpert, P. A., Aller, J. Y. and Knopf, D. A.: Initiation of the ice phase by marine biogenic surfaces in supersaturated gas and supercooled aqueous phases, *Phys. Chem. Chem. Phys.*, 13, 19882–19894, doi:10.1039/c1cp21844a, 2011b.
- Andreae, M. O. and Rosenfeld, D.: Aerosol-cloud-precipitation interactions. Part 1. The nature and sources of cloud-active aerosols, *Earth-Science Rev.*, 89, 13–41, doi:10.1016/j.earscirev.2008.03.001, 2008.
- Assmy, P., Ehn, J. K., Fernández-Méndez, M., Hop, H., Katlein, C., Sundfjord, A., Bluhm, K., Daase, M., Engel, A., Fransson, A., Granskog, M. A., Hudson, S. R., Kristiansen, S., Nicolaus, M., Peeken, I., Renner, A. H. H., Spreen, G., Tatarek, A. and Wiktor, J.: Floating Ice-Algal Aggregates below Melting Arctic Sea Ice, *PLoS One*, 8, e76599–e76612, doi:10.1371/journal.pone.0076599, 2013.
- Atkinson, J. D., Murray, B. J., Woodhouse, M. T., Whale, T. F., Baustian, K. J., Carslaw, K. S., Dobbie, S., O’Sullivan, D., Malkin, T. L. and O’Sullivan, D.: The importance of feldspar for ice nucleation by mineral dust in mixed-phase clouds, *Nature*, 498, 355–358, doi:10.1038/nature12278, 2013.
- Atkinson, M. J. and Bingman, C.: Elemental composition of commercial seasalts, *J. Aquaric.*

Aquat. Sci., 8, 39–43 [online] Available from: <http://www.rudyv.be/Aquarium/sels.pdf>, 1997.

Ault, A. P., Moffet, R. C., Baltrusaitis, J., Collins, D. B., Ruppel, M. J., Cuadra-Rodriguez, L. A., Zhao, D., Guasco, T. L., Ebben, C. J., Geiger, F. M., Bertram, T. H., Prather, K. A. and Grassian, V. H.: Size-dependent changes in sea spray aerosol composition and properties with different seawater conditions, *Environ. Sci. Technol.*, 47, 5603–5612, doi:10.1021/es400416g, 2013.

Bateman, A. P., Belassein, H. and Martin, S. T.: Impactor Apparatus for the Study of Particle Rebound: Relative Humidity and Capillary Forces, *Aerosol Sci. Technol.*, 6826, 131017104109009, doi:10.1080/02786826.2013.853866, 2013.

Belzile, C., Brugel, S., Nozais, C., Gratton, Y. and Demers, S.: Variations of the abundance and nucleic acid content of heterotrophic bacteria in Beaufort Shelf waters during winter and spring, *J. Mar. Syst.*, 74, 946–956, doi:10.1016/j.jmarsys.2007.12.010, 2008.

Bigg, E. K.: Ice Nucleus Concentrations in Remote Areas, *J. Atmos. Sci.*, 30, 1153–1157, doi:10.1175/1520-0469(1973)030<1153:INCIRA>2.0.CO;2, 1973.

Bigg, E. K.: Ice forming nuclei in the high Arctic, *Tellus, Ser. B Chem. Phys. Meteorol.*, 48, 223–233, doi:10.1034/j.1600-0889.1996.t01-1-00007.x, 1996.

Bigg, E. K. and Hopwood, S. C.: Ice Nuclei in the Antarctic, *J. Atmos. Sci.*, 20, 185–188, doi:Ice Nuclei in the Antarctic, 1963.

Bigg, E. K. and Leck, C.: Cloud-active particles over the central Arctic Ocean, *J. Geophys. Res.*, 106, 32,155-32,166, 2001.

Bird, D. F. and Kalff, J.: Empirical Relationships between Bacterial Abundance and Chlorophyll Concentration in Fresh and Marine Waters, *Can. J. Fish. Aquat. Sci.*, 41, 1015–1023, doi:10.1139/f84-118, 1984.

Blanchard, D. C.: Sea-to-Air Transport of Surface Active Material, *Science*, 146, 396–397, 1964.

Blanchard, D. C. and Keith, C.: The Electrification of the Atmosphere by Particles from Bubbles in the Sea, *Prog. Oceanogr.*, 1, 73–202, doi:10.1016/0079-6611(63)90004-1, 1963.

Blanchard, D. C. and Woodcock, A. H.: Bubble Formation and Modification in the Sea and its Meteorological Significance, *Tellus*, 9, 145–158, doi:10.1111/j.2153-3490.1957.tb01867.x, 1957.

Boetius, A., Anesio, A. M., Deming, J. W., Mikucki, J. and Rapp, J. Z.: Microbial ecology of the

cryosphere: sea ice and glacial habitats, *Nat. Rev. Microbiol.*, 13, 677–690, doi:10.1038/nrmicro3522, 2015.

Boose, Y., Welti, A., Atkinson, J., Ramelli, F., Danielczok, A., Bingemer, H. G., Plötze, M., Sierau, B., Kanji, Z. A. and Lohmann, U.: Heterogeneous ice nucleation on dust particles sourced from nine deserts worldwide - Part 1: Immersion freezing, *Atmos. Chem. Phys.*, 16, 15075–15095, doi:10.5194/acp-16-15075-2016, 2016.

Boucher, O., Randall, D., Artaxo, P., Bretherton, C., Feingold, G., Forster, P., Kerminen, V.-M., Kondo, Y., Liao, H., Lohmann, U., Rasch, P., Satheesh, S. K., Sherwood, S., Stevens, B. and Zhang, X. Y.: Clouds and aerosols, *Clim. Chang. 2013 Phys. Sci. Basis Work. Gr. I Contrib. to Fifth Assess. Rep. Intergov. Panel Clim. Chang.*, 9781107057, 571–658, doi:10.1017/CBO9781107415324.016, 2013.

Brioude, J., Arnold, D., Stohl, A., Cassiani, M., Morton, D., Seibert, P., Angevine, W., Evan, S., Dingwell, A., Fast, J. D., Easter, R. C., Pisso, I., Burkhardt, J. and Wotawa, G.: The Lagrangian particle dispersion model FLEXPART-WRF version 3.1, *Geosci. Model Dev.*, 6, 1889–1904, doi:10.5194/gmd-6-1889-2013, 2013.

Burgers, T. M., Miller, L. A., Thomas, H., Else, B. G. T., Gosselin, M. and Papakyriakou, T.: Surface Water  $p\text{CO}_2$  Variations and Sea-Air  $\text{CO}_2$  Fluxes During Summer in the Eastern Canadian Arctic, *J. Geophys. Res. Ocean.*, 122, 9663–9678, doi:10.1002/2017JC013250, 2017.

Burrows, S. M., Hoose, C., Pöschl, U. and Lawrence, M. G.: Ice nuclei in marine air: Biogenic particles or dust?, *Atmos. Chem. Phys.*, 13, 245–267, doi:10.5194/acp-13-245-2013, 2013.

Chen, J., Wu, Z., Augustin-Bauditz, S., Grawe, S., Hartmann, M., Pei, X., Liu, Z., Ji, D. and Wex, H.: Ice-nucleating particle concentrations unaffected by urban air pollution in Beijing, China, *Atmos. Chem. Phys.*, 18, 3523–3539, doi:10.5194/acp-18-3523-2018, 2018.

Chen, S.-C., Tsai, C.-J., Chen, H.-D., Huang, C.-Y. and Roam, G.-D.: The Influence of Relative Humidity on Nanoparticle Concentration and Particle Mass Distribution Measurements by the MOUDI, *Aerosol Sci. Technol.*, 45, 596–603, doi:10.1080/02786826.2010.551557, 2011.

Cheng, C. S., Lopes, E., Fu, C. and Huang, Z.: Possible impacts of climate change on wind gusts under downscaled future climate conditions: Updated for Canada, *J. Clim.*, 27, 1255–1270, doi:10.1175/JCLI-D-13-00020.1, 2014.

Christner, B. C., Cai, R., Morris, C. E., McCarter, K. S., Foreman, C. M., Skidmore, M. L.,

Montross, S. N. and Sands, D. C.: Geographic, seasonal, and precipitation chemistry influence on the abundance and activity of biological ice nucleators in rain and snow., *Proc. Natl. Acad. Sci. U. S. A.*, 105, 18854–18859, doi:10.1073/pnas.0809816105, 2008.

Cochran, R. E., Ryder, O. S., Grassian, V. H. and Prather, K. A.: Sea spray aerosol: The chemical link between the oceans, atmosphere, and climate, *Acc. Chem. Res.*, 50, 599–604, doi:10.1021/acs.accounts.6b00603, 2017.

Cohen, J., Pfeiffer, K. and Francis, J. A.: Warm Arctic episodes linked with increased frequency of extreme winter weather in the United States, *Nat. Commun.*, 9, 1–12, doi:10.1038/s41467-018-02992-9, 2018.

Collins, D. B., Ault, A. P., Moffet, R. C., Ruppel, M. J., Cuadra-Rodriguez, L. A., Guasco, T. L., Corrigan, C. E., Pedler, B. E., Azam, F., Aluwihare, L. I., Bertram, T. H., Roberts, G. C., Grassian, V. H. and Prather, K. A.: Impact of marine biogeochemistry on the chemical mixing state and cloud forming ability of nascent sea spray aerosol, *J. Geophys. Res. Atmos.*, 118, 8553–8565, doi:10.1002/jgrd.50598, 2013.

Collins, D. B., Burkart, J., Chang, R. Y. W., Lizotte, M., Boivin-Rioux, A., Blais, M., Mungall, E. L., Boyer, M., Irish, V. E., Massé, G., Kunkel, D., Tremblay, J. É., Papakyriakou, T., Bertram, A. K., Bozem, H., Gosselin, M., Levasseur, M. and Abbatt, J. P. D.: Frequent ultrafine particle formation and growth in Canadian Arctic marine and coastal environments, *Atmos. Chem. Phys.*, 17, 13119–13138, doi:10.5194/acp-17-13119-2017, 2017.

Conen, F., Morris, C. E., Leifeld, J., Yakutin, M. V. and Alewell, C.: Biological residues define the ice nucleation properties of soil dust, *Atmos. Chem. Phys.*, 11, 9643–9648, doi:10.5194/acp-11-9643-2011, 2011.

Connolly, P. J., Möhler, O., Field, P. R., Saathoff, H., Burgess, R., Choularton, T. W. and Gallagher, M. W.: Studies of heterogeneous freezing by three different desert dust samples, *Atmos. Chem. Phys.*, 9, 2805–2824, doi:10.5194/acp-13-10079-2013, 2009.

Creamean, J. M., Suski, K. J., Rosenfeld, D., Cazorla, A., DeMott, P. J., Sullivan, R. C., White, A. B., Ralph, F. M., Minnis, P., Comstock, J. M., Tomlinson, J. M. and Prather, K. A.: Dust and biological aerosols from the Sahara and Asia influence precipitation in the western U.S., *Science*, 339, 1572–8, doi:10.1126/science.1227279, 2013.

Csuros, M.: *Environmental Sampling and Analysis for Technicians*, Lewis Publisher, New

York., 1994.

Cziczo, D. J., DeMott, P. J., Brooks, S. D., Prenni, A. J., Thomson, D. S., Baumgardner, D., Wilson, J. C., Kreidenweis, S. M. and Murphy, D. M.: Observations of organic species and atmospheric ice formation, *Geophys. Res. Lett.*, 31, 2–5, doi:10.1029/2004GL019822, 2004.

Dancey, C. P. and Reidy, J.: *Statistics Without Maths for Psychology*, 2nd ed., Pearson Education Limited, Harlow, England., 2002.

DeMott, P. J., Rogers, D. C., Kreidenweis, S. M., Chen, Y., Twohy, C. H., Baumgardner, D., Heymsfield, A. J. and Chan, K. R.: The role of heterogeneous freezing nucleation in upper tropospheric clouds: Inferences from SUCCESS, *Geophys. Res. Lett.*, 25, 1387–1390, doi:10.1029/97GL03779, 1998.

DeMott, P. J., Cziczo, D. J., Prenni, A. J., Murphy, D. M., Kreidenweis, S. M., Thomson, D. S., Borys, R. and Rogers, D. C.: Measurements of the concentration and composition of nuclei for cirrus formation, *Proc. Natl. Acad. Sci.*, 100, 14655–14660, doi:10.1073/pnas.2532677100, 2003.

DeMott, P. J., Prenni, A. J., Liu, X., Kreidenweis, S. M., Petters, M. D., Twohy, C. H., Richardson, M. S., Eidhammer, T. and Rogers, D. C.: Predicting global atmospheric ice nuclei distributions and their impacts on climate., *Proc. Natl. Acad. Sci. U. S. A.*, 107, 11217–11222, doi:10.1073/pnas.0910818107, 2010.

DeMott, P. J., Prenni, A. J., McMeeking, G. R., Sullivan, R. C., Petters, M. D., Tobo, Y., Niemand, M., Möhler, O., Snider, J. R., Wang, Z. and Kreidenweis, S. M.: Integrating laboratory and field data to quantify the immersion freezing ice nucleation activity of mineral dust particles, *Atmos. Chem. Phys.*, 15, 393–409, doi:10.5194/acp-15-393-2015, 2015.

DeMott, P. J., Hill, T. C. J., McCluskey, C. S., Prather, K. A., Collins, D. B., Sullivan, R. C., Ruppel, M. J., Mason, R. H., Irish, V. E., Lee, T., Hwang, C. Y., Rhee, T. S., Snider, J. R., McMeeking, G. R., Dhaniyala, S., Lewis, E. R., Wentzell, J. J. B., Abbatt, J., Lee, C., Sultana, C. M., Ault, A. P., Axson, J. L., Diaz Martinez, M., Venero, I., Santos-Figueroa, G., Stokes, M. D., Deane, G. B., Mayol-Bracero, O. L., Grassian, V. H., Bertram, T. H., Bertram, A. K., Moffett, B. F. and Franc, G. D.: Sea spray aerosol as a unique source of ice nucleating particles, *Proc. Natl. Acad. Sci.*, 113, 5797–5803, doi:10.1073/pnas.1514034112, 2016.

DeMott, P. J., Hill, T. C. J., Petters, M. D., Bertram, A. K., Tobo, Y., Mason, R. H., Suski, K. J.,

McCluskey, C. S., Levin, E. J. T., Schill, G. P., Boose, Y., Rauker, A. M., Miller, A. J., Zaragoza, J., Rocci, K., Rothfuss, N. E., Taylor, H. P., Hader, J. D., Chou, C., Huffman, J. A., Pöschl, U., Prenni, A. J. and Kreidenweis, S. M.: Comparative measurements of ambient atmospheric concentrations of ice nucleating particles using multiple immersion freezing methods and a continuous flow diffusion chamber, *Atmos. Chem. Phys.*, 17, 11227–11245, doi:10.5194/acp-2017-417, 2017.

Derksen, C. and Brown, R.: Spring snow cover extent reductions in the 2008-2012 period exceeding climate model projections, *Geophys. Res. Lett.*, 39, 1–6, doi:10.1029/2012GL053387, 2012.

Després, V. R., Alex Huffman, J., Burrows, S. M., Hoose, C., Safatov, A. S., Buryak, G., Fröhlich-Nowoisky, J., Elbert, W., Andreae, M. O., Pöschl, U. and Jaenicke, R.: Primary biological aerosol particles in the atmosphere: a review, *Tellus, Ser. B Chem. Phys. Meteorol.*, 64, doi:10.3402/tellusb.v64i0.15598, 2012.

Dreichmeier, K., Budke, C., Wiehemeier, L., Kottke, T. and Koop, T.: Boreal pollen contain ice-nucleating as well as ice-binding ‘antifreeze’ polysaccharides, *Sci. Rep.*, 7, 41890–41903, doi:10.1038/srep41890, 2017.

Eastwood, M. L., Cremel, S., Gehrke, C., Girard, E. and Bertram, A. K.: Ice nucleation on mineral dust particles: Onset conditions, nucleation rates and contact angles, *J. Geophys. Res. Atmos.*, 113, 1–9, doi:10.1029/2008JD010639, 2008.

Ewert, M. and Deming, J. W.: Sea Ice Microorganisms: Environmental Constraints and Extracellular Responses, *Biology (Basel)*, 2, 603–628, doi:10.3390/biology2020603, 2013.

Fahlgren, C., Gómez-Consarnau, L., Zábori, J., Lindh, M. V., Krejci, R., Mårtensson, E. M., Nilsson, D. and Pinhassi, J.: Seawater mesocosm experiments in the Arctic uncover differential transfer of marine bacteria to aerosols, *Environ. Microbiol. Rep.*, 7, 460–470, doi:10.1111/1758-2229.12273, 2015.

Fall, R. and Schnell, R. C.: Association of an ice-nucleating pseudomonad with cultures of the marine dinoflagellate, *heterocapsa niei*, *J. Mar. Res.*, 43, 257–265, 1985.

Fang, C. P., McMurry, P. H., Marple, V. A. and Rubow, K. L.: Effect of flow-induced relative humidity changes on size cuts for sulfuric acid droplets in the Microorifice Uniform Deposit Impactor (MOUDI), *Aerosol Sci. Technol.*, 14, 266–277, doi:10.1080/02786829108959489,

1991.

Fenn, R. W. and Weickmann, H. K.: Some results of aerosol measurements, *Geofis. pura e Appl.*, 42, 53–61, 1959.

Fernández-Méndez, M., Wenzhöfer, F., Peeken, I., Sørensen, H. L., Glud, R. N. and Boetius, A.: Composition, buoyancy regulation and fate of ice algal aggregates in the Central Arctic Ocean, *PLoS One*, 9, e107452–e107465, doi:10.1371/journal.pone.0107452, 2014.

Findeisen: Colloidal meteorological processes in the formation of precipitation, *Meteorol. Zeitschrift*, 55, 121–133, doi:10.1127/metz/2015/0675, 1938.

Finlayson-Pitts, B. J. and Pitts Jr.: *Chemistry of the upper and lower atmosphere: Theory, experiments and applications*, Academic Press, San Diego, CA., 2000.

Friese, E. and Ebel, A.: Temperature dependent thermodynamic model of the system  $\text{H}^+$ - $\text{NH}_4^+$ - $\text{Na}^+$ - $\text{SO}_4^{2-}$ - $\text{NO}_3^-$ - $\text{Cl}^-$ - $\text{H}_2\text{O}$ ., 2010.

Galgani, L., Piontek, J. and Engel, A.: Biopolymers form a gelatinous microlayer at the air-sea interface when Arctic sea ice melts, *Sci. Rep.*, 6, 29465–29475, doi:10.1038/srep29465, 2016.

Gieré, R. and Querol, X.: Solid particulate matter in the atmosphere, *Elements*, 6, 215–222, doi:10.2113/gselements.6.4.215, 2010.

Gimbert, L. J., Haygarth, P. M., Beckett, R. and Worsfold, P. J.: Comparison of centrifugation and filtration techniques for the size fractionation of colloidal material in soil suspensions using sedimentation field-flow fractionation, *Environ. Sci. Technol.*, 39, 1731–1735, doi:10.1021/es049230u, 2005.

Ginoux, P., Chin, M., Tegen, I., Prospero, J. M., Holben, B., Dubovik, O. and Lin, S.-J.: Sources and distributions of dust aerosols simulated with the GOCART model, *J. Geophys. Res.*, 106, 20255–20273, 2001.

Von Glasow, R., Lawrence, M. G., Sander, R. and Crutzen, P. J.: Modeling the chemical effects of ship exhaust in the cloud-free marine boundary layer, *Atmos. Chem. Phys.*, 3, 233–250, doi:10.5194/acp-3-233-2003, 2003.

Groot Zwaaftink, C. D., Grythe, H., Skov, H. and Stohl, A.: Substantial contribution of northern high-latitude sources to mineral dust in the Arctic, *J. Geophys. Res. Atmos.*, 121, 13,678–13,697, doi:10.1002/2016JD025482, 2016.

Harrington, J. Y., Reisin, T., Cotton, W. R. and Kreidenweis, S. M.: Cloud resolving simulations

of Arctic stratus part II: Transition-season clouds, *Atmos. Res.*, 51, 45–75, doi:10.1016/S0169-8095(98)00098-2, 1999.

Hartmann, D. L., Ockert-Bell, M. E. and Michelsen, M. L.: The effect of cloud type on Earth's energy balance: results for selected regions, *J. Clim.*, 5, 1157–1171, doi:10.1175/1520-0442(1992)005<1157:TEOCTO>2.0.CO;2, 1992.

Harvey, G. W. and Burzell, L. A.: A Simple Microlayer Method for Small Samples, *Limnol. Oceanogr. Methods*, 17, 156–157, 1972.

Hendricks, J., Kärcher, B. and Lohmann, U.: Effects of ice nuclei on cirrus clouds in a global climate model, *J. Geophys. Res. Atmos.*, 116, 1–24, doi:10.1029/2010JD015302, 2011.

Herbert, R. J., Murray, B. J., Dobbie, S. J. and Koop, T.: Sensitivity of liquid clouds to homogeneous freezing parameterizations, *Geophys. Res. Lett.*, 42, 1599–1605, doi:10.1002/2014GL062729. Received, 2015.

Hill, T. C. J., DeMott, P. J., Tobo, Y., Fröhlich-Nowoisky, J., Moffett, B. F., Franc, G. D. and Kreidenweis, S. M.: Sources of organic ice nucleating particles in soils, *Atmos. Chem. Phys.*, 16, 7195–7211, doi:10.5194/acp-16-7195-2016, 2016.

Hirdman, D., Burkhardt, J. F., Sodemann, H., Eckhardt, S., Jefferson, A., Quinn, P. K., Sharma, S., Ström, J. and Stohl, A.: Long-term trends of black carbon and sulphate aerosol in the Arctic: Changes in atmospheric transport and source region emissions, *Atmos. Chem. Phys.*, 10, 9351–9368, doi:10.5194/acp-10-9351-2010, 2010.

Hoose, C. and Möhler, O.: Heterogeneous ice nucleation on atmospheric aerosols: A review of results from laboratory experiments, *Atmos. Chem. Phys.*, 12, 9817–9854, doi:10.5194/acp-12-9817-2012, 2012.

Hoose, C., Kristjánsson, J. E., Chen, J.-P. and Hazra, A.: A Classical-Theory-Based Parameterization of Heterogeneous Ice Nucleation by Mineral Dust, Soot, and Biological Particles in a Global Climate Model, *J. Atmos. Sci.*, 67, 2483–2503, doi:10.1175/2010JAS3425.1, 2010.

Huang, J., Yu, H., Guan, X., Wang, G. and Guo, R.: Accelerated dryland expansion under climate change, *Nat. Clim. Chang.*, 6, 166–171, doi:10.1038/nclimate2837, 2015.

IPCC: Working Group I Contribution to the IPCC Fifth Assessment Report, *Climate Change 2013: The Physical Science Basis*, edited by D. L. Hartmann, A. M. G. K. Tank, and M.

Rusticucci, Cambridge University Press., 2014.

Irish, V. E., Elizondo, P., Chen, J., Choul, C., Charette, J., Lizotte, M., Ladino, L. A., Wilson, T. W., Gosselin, M., Murray, B. J., Polishchuk, E., Abbatt, J. P. D., Miller, L. A. and Bertram, A. K.: Ice-nucleating particles in Canadian Arctic sea-surface microlayer and bulk seawater, *Atmos. Chem. Phys.*, 17, 10583–10595, doi:10.5194/acp-17-10583-2017, 2017.

Jiang, H., Cotton, W. R., Pinto, J. O., Curry, J. A. and Weissbluth, M. J.: Cloud Resolving Simulations of Mixed-Phase Arctic Stratus Observed during BASE: Sensitivity to Concentration of Ice Crystals and Large-Scale Heat and Moisture Advection, *J. Atmos. Sci.*, 57, 2105–2117, doi:10.1175/1520-0469(2000)057<2105:CRSOMP>2.0.CO;2, 2000.

Kaufmann, L., Marcolli, C., Hofer, J., Pinti, V., Hoyle, C. R. and Peter, T.: Ice nucleation efficiency of natural dust samples in the immersion mode, *Atmos. Chem. Phys.*, 16, 11177–11206, doi:10.5194/acp-16-11177-2016, 2016.

Klein, H., Nickovic, S., Haunold, W., Bundke, U., Nillius, B., Ebert, M., Weinbruch, S., Schuetz, L., Levin, Z., Barrie, L. A. and Bingemer, H.: Saharan dust and ice nuclei over Central Europe, *Atmos. Chem. Phys.*, 10, 10211–10221, doi:10.5194/acp-10-10211-2010, 2010.

Knackstedt, K., Moffett, B. F., Hartmann, S., Wex, H., Hill, T. C. J., Glasgo, E., Reitz, L., Augustin-Bauditz, S., Beall, B., Bullerjahn, G. S., Fröhlich-Nowoisky, J., Grawe, S., Lubitz, J., Stratmann, F. and McKay, R. M.: A terrestrial origin for abundant riverine nanoscale ice-nucleating particles, *Environ. Sci. Technol.*, acs.est.8b03881, doi:10.1021/acs.est.8b03881, 2018.

Knopf, D. A. and Forrester, S. M.: Freezing of water and aqueous NaCl droplets coated by organic monolayers as a function of surfactant properties and water activity, *J. Phys. Chem. A*, 115, 5579–5591, doi:10.1021/jp2014644, 2011.

Knopf, D. A., Wang, B., Laskin, A., Moffet, R. C. and Gilles, M. K.: Heterogeneous nucleation of ice on anthropogenic organic particles collected in Mexico City, *Geophys. Res. Lett.*, 37, L11803–L11808, doi:10.1029/2010GL043362, 2010.

Knopf, D. A., Alpert, P. A., Wang, B. and Aller, J. Y.: Stimulation of ice nucleation by marine diatoms, *Nat. Geosci.*, 4, 88–90, doi:10.1038/ngeo1037, 2011.

Knopf, D. A., Alpert, P. A., Wang, B., Brien, R. E. O., Kelly, S. T., Laskin, A., Gilles, M. K. and Moffet, R. C.: Microspectroscopic imaging and characterization of individually identified ice nucleating particles from a case field study, *J. Geophys. Res. Atmos.*, 119, 365–381,

doi:10.1002/2014JD021866.Received, 2014.

Knulst, J. C., Rosenberger, D., Thompson, B. and Paatero, J.: Intensive Sea Surface Microlayer Investigations of Open Leads in the Pack Ice during Arctic Ocean 2001 Expedition, *Langmuir*, 19, 10194–10199, doi:10.1021/la035069+, 2003.

Koop, T. and Murray, B. J.: A physically constrained classical description of the homogeneous nucleation of ice in water, *J. Chem. Phys.*, 145, 211915, doi:10.1063/1.4962355, 2016.

Koop, T. and Zobrist, B.: Parameterizations for ice nucleation in biological and atmospheric systems., *Phys. Chem. Chem. Phys.*, 11, 10839–10850, doi:10.1039/b914289d, 2009.

Koop, T., Luo, B., Biermann, U. M., Crutzen, P. J. and Peter, T.: Freezing of HNO<sub>3</sub>/H<sub>2</sub>SO<sub>4</sub>/H<sub>2</sub>O Solutions at Stratospheric Temperatures: Nucleation Statistics and Experiments, *J. Phys. Chem. A*, 101, 1117–1133, doi:10.1021/jp9626531, 1997.

Koop, T., Ng, H. P., Molina, L. T. and Molina, M. J.: A New Optical Technique to Study Aerosol Phase Transitions: The Nucleation of Ice from H<sub>2</sub>SO<sub>4</sub> Aerosols, *J. Phys. Chem. A*, 102, 8924–8931, doi:10.1021/jp9828078, 1998.

Kumar, A., Marcolli, C., Luo, B. and Peter, T.: Ice nucleation activity of silicates and aluminosilicates in pure water and aqueous solutions – Part 1: The K-feldspar microcline, *Atmos. Chem. Phys.*, 18, 7057–7079, 2018.

Ladino, L. A., Yakobi-Hancock, J. D., Kilitau, W. P., Mason, R. H., Si, M., Li, J., Miller, L. A., Schiller, C. L., Huffman, J. A., Aller, J. Y., Knopf, D. A., Bertram, A. K. and Abbatt, J. P. D.: Addressing the ice nucleating abilities of marine aerosol: A combination of deposition mode laboratory and field measurements, *Atmos. Environ.*, 132, 1–10, doi:10.1016/j.atmosenv.2016.02.028, 2016.

Laskin, A., Cowin, J. P. and Iedema, M. J.: Analysis of individual environmental particles using modern methods of electron microscopy and X-ray microanalysis, *J. Electron Spectros. Relat. Phenomena*, 150, 260–274, doi:10.1016/j.elspec.2005.06.008, 2006.

Laskin, A., Moffet, R. C., Gilles, M. K., Fast, J. D., Zaveri, R. A., Wang, B., Nigge, P. and Shutthanandan, J.: Tropospheric chemistry of internally mixed sea salt and organic particles: Surprising reactivity of NaCl with weak organic acids, *J. Geophys. Res. Atmos.*, 117, 1–12, doi:10.1029/2012JD017743, 2012.

Lawson, D. R.: Impaction surface coatings intercomparison and measurements with cascade

impactors, *Atmos. Environ.*, 14, 195–199, doi:10.1016/0004-6981(80)90278-4, 1980.

Lewis, E. R. and Schwartz, S. E.: Sea salt aerosol production: mechanisms, methods, measurements and models - a critical review, American Geophysical Union, Washington, DC., 2004.

Liss, P. S. and Duce, R. A.: *The Sea Surface and Global Change*, Cambridge University Press, Cambridge., 1997.

Lizotte, M., Levasseur, M., Scarratt, M. G., Michaud, S., Merzouk, A., Gosselin, M. and Pommier, J.: Fate of dimethylsulfoniopropionate (DMSP) during the decline of the northwest Atlantic Ocean spring diatom bloom, *Aquat. Microb. Ecol.*, 52, 159–173, doi:10.3354/ame01232, 2008.

Lohmann, U.: A glaciation indirect aerosol effect caused by soot aerosols, *Geophys. Res. Lett.*, 29, 1052, doi:10.1029/2001gl014357, 2002.

Lohmann, U. and Diehl, K.: Sensitivity Studies of the Importance of Dust Ice Nuclei for the Indirect Aerosol Effect on Stratiform Mixed-Phase Clouds, *J. Atmos. Sci.*, 63, 968–982, doi:10.1175/JAS3662.1, 2006.

Lohmann, U. and Feichter, J.: Global indirect aerosol effects: a review, *Atmos. Chem. Phys.*, 5, 715–737, doi:10.5194/acpd-4-7561-2004, 2005.

Lynch, D. K., Sassen, K., Starr, D. C. and Stephens, G.: *Cirrus*, Oxford University Press, New York, NY, USA., 2002.

Marie, D., Simon, N. and Vaultot, D.: Phytoplankton cell counting by flow cytometry, in *Algal Culturing Techniques*, pp. 253–267, Academic Press, London., 2005.

Mason, R. H., Si, M., Li, J., Chou, C., Dickie, R., Toom-Sauntry, D., Pöhlker, C., Yakobi-Hancock, J. D., Ladino, L. A., Jones, K., Leaitch, W. R., Schiller, C. L., Abbatt, J. P. D., Huffman, J. A. and Bertram, A. K.: Ice nucleating particles at a coastal marine boundary layer site: correlations with aerosol type and meteorological conditions, *Atmos. Chem. Phys. Discuss.*, 15, 16273–16323, doi:10.5194/acpd-15-16273-2015, 2015a.

Mason, R. H., Chou, C., McCluskey, C. S., Levin, E. J. T., Schiller, C. L., Hill, T. C. J., Huffman, J. A., DeMott, P. J. and Bertram, A. K.: The micro-orifice uniform deposit impactor–droplet freezing technique (MOUDI-DFT) for measuring concentrations of ice nucleating particles as a function of size: improvements and initial validation, *Atmos. Meas. Tech.*, 8, 2449–

2462, doi:10.5194/amt-8-2449-2015, 2015b.

Mason, R. H., Si, M., Chou, C., Irish, V. E., Dickie, R., Elizondo, P., Wong, R., Brintnell, M., Elsasser, M., Lassar, W. M., Pierce, K. M., Leaitch, W. R., MacDonald, A. M., Platt, A., Toom-Sauntry, D., Sarda-Estève, R., Schiller, C. L., Suski, K. J., Hill, T. C. J., Abbatt, J. P. D., Huffman, J. A., DeMott, P. J. and Bertram, A. K.: Size-resolved measurements of ice nucleating particles at six locations in North America and one in Europe, *Atmos. Chem. Phys.*, 16, 1637–1651, doi:10.5194/acpd-15-20521-2015, 2016.

McCluskey, C. S., Hill, T. C. J., Malfatti, F., Sultana, C. M., Lee, C., Santander, M. V., Beall, C. M., Moore, K. A., Cornwell, G. C., Collins, D. B., Prather, K. A., Jayarathne, T., Stone, E. A., Azam, F., Kreidenweis, S. M. and DeMott, P. J.: A Dynamic Link between Ice Nucleating Particles Released in Nascent Sea Spray Aerosol and Oceanic Biological Activity during Two Mesocosm Experiments, *J. Atmos. Sci.*, 74, 151–166, doi:10.1175/JAS-D-16-0087.1, 2017.

Moffett, B., Hill, T. and DeMott, P.: Abundance of Biological Ice Nucleating Particles in the Mississippi and Its Major Tributaries, *Atmosphere (Basel)*, 9, 307, doi:10.3390/atmos9080307, 2018.

Moffett, B. F.: Fresh water ice nuclei, *Fundam. Appl. Limnol. / Arch. für Hydrobiol.*, 188, 19–23, doi:10.1127/fal/2016/0851, 2016.

Moum, J. N. and Smyth, W. D.: *Encyclopedia of Ocean Sciences*, 2001.

Murray, B. J., Broadley, S. L., Wilson, T. W., Atkinson, J. D. and Wills, R. H.: Heterogeneous freezing of water droplets containing kaolinite particles, *Atmos. Chem. Phys.*, 11, 4191–4207, doi:10.5194/acp-11-4191-2011, 2011.

Murray, B. J., O’Sullivan, D., Atkinson, J. D. and Webb, M. E.: Ice nucleation by particles immersed in supercooled cloud droplets, *Chem. Soc. Rev.*, 41, 6519–6554, doi:10.1039/c2cs35200a, 2012.

National Snow and Ice Data Center: IMS daily Northern Hemisphere snow and ice analysis at 1 km, 4 km, and 24 km resolutions, 2008.

Niedermeier, D., Hartmann, S., Shaw, R. A., Covert, D., Mentel, T. F., Schneider, J., Poulain, L., Reitz, P., Spindler, C., Clauss, T., Kiselev, A., Hallbauer, E., Wex, H., Mildenerger, K. and Stratmann, F.: Heterogeneous freezing of droplets with immersed mineral dust particles – measurements and parameterization, *Atmos. Chem. Phys.*, 10, 3601–3614, doi:10.5194/acp-10-

3601-2010, 2010.

Niemand, M., Möhler, O., Vogel, B., Vogel, H., Hoose, C., Connolly, P., Klein, H., Bingemer, H., DeMott, P., Skrotzki, J. and Leisner, T.: A Particle-Surface-Area-Based Parameterization of Immersion Freezing on Desert Dust Particles, *J. Atmos. Sci.*, 69, 3077–3092, doi:10.1175/JAS-D-11-0249.1, 2012.

O’Sullivan, D., Murray, B. J., Malkin, T. L., Whale, T. F., Umo, N. S., Atkinson, J. D., Price, H. C., Baustian, K. J., Browse, J. and Webb, M. E.: Ice nucleation by fertile soil dusts: Relative importance of mineral and biogenic components, *Atmos. Chem. Phys.*, 14, 1853–1867, doi:10.5194/acp-14-1853-2014, 2014.

O’Sullivan, D., Murray, B. J., Ross, J. F., Whale, T. F., Price, H. C., Atkinson, J. D., Umo, N. S. and Webb, M. E.: The relevance of nanoscale biological fragments for ice nucleation in clouds, *Sci. Rep.*, 5, 8082, doi:10.1038/srep08082, 2015.

Overland, J. E. and Wang, M.: When will the summer Arctic be nearly sea ice free?, *Geophys. Res. Lett.*, 40, 2097–2101, doi:10.1002/grl.50316, 2013.

Parsons, M. T., Mak, J., Lipetz, S. R. and Bertram, A. K.: Deliquescence of malonic, succinic, glutaric, and adipic acid particles, *J. Geophys. Res.*, 109, D06212–D06220, doi:10.1029/2003JD004075, 2004.

Prather, K. A., Bertram, T. H., Grassian, V. H., Deane, G. B., Stokes, M. D., DeMott, P. J., Aluwihare, L. I., Palenik, B. P., Azam, F., Seinfeld, J. H., Moffet, R. C., Molina, M. J., Cappa, C. D., Geiger, F. M., Roberts, G. C., Russell, L. M., Ault, A. P., Baltrusaitis, J., Collins, D. B., Corrigan, C. E., Cuadra-Rodriguez, L. A., Ebben, C. J., Forestieri, S. D., Guasco, T. L., Hersey, S. P., Kim, M. J., Lambert, W. F., Modini, R. L., Mui, W., Pedler, B. E., Ruppel, M. J., Ryder, O. S., Schoepp, N. G., Sullivan, R. C. and Zhao, D.: Bringing the ocean into the laboratory to probe the chemical complexity of sea spray aerosol., *Proc. Natl. Acad. Sci. U. S. A.*, 110, 7550–7555, doi:10.1073/pnas.1300262110, 2013.

Prenni, A. J., DeMott, P. J., Rogers, D. C., Kreidenweis, S. M., Mcfarquhar, G. M., Zhang, G. and Poellot, M. R.: Ice nuclei characteristics from M-PACE and their relation to ice formation in clouds, *Tellus, Ser. B Chem. Phys. Meteorol.*, 61B, 436–448, doi:10.1111/j.1600-0889.2009.00415.x, 2009a.

Prenni, A. J., Petters, M. D., Kreidenweis, S. M., Heald, C. L., Martin, S. T., Artaxo, P., Garland,

R. M., Wollny, A. G. and Pöschl, U.: Relative roles of biogenic emissions and Saharan dust as ice nuclei in the Amazon basin, *Nat. Geosci.*, 2, 402–405, doi:10.1038/ngeo517, 2009b.

Pruppacher, H. R. and Klett, J. D.: *Microphysics of clouds and precipitation*, edited by Springer-Verlag., 1997.

Rainville, L., Lee, C. and Woodgate, R.: Impact of Wind-Driven Mixing in the Arctic Ocean, *Oceanography*, 24, 136–145, doi:10.5670/oceanog.2011.65, 2011.

Rangel-Alvarado, R. B., Nazarenko, Y. and Ariya, P. A.: Snow-borne nanosized particles: Abundance, distribution, composition, and significance in ice nucleation processes, *J. Geophys. Res. Atmos.*, 120, 760–774, doi:10.1002/2015JD023773. Received, 2015.

Rogers, D. C., DeMott, P. J., Kreidenweis, S. M. and Chen, Y.: Measurements of ice nucleating aerosols during SUCCESS, *Geophys. Res. Lett.*, 25, 1383–1386, doi:10.1029/97GL03478, 1998.

Rogers, D. C., DeMott, P. J., Kreidenweis, S. M. and Chen, Y.: A continuous-flow diffusion chamber for airborne measurements of ice nuclei, *J. Atmos. Ocean. Technol.*, 18, 725–741, doi:10.1175/1520-0426(2001)018<0725:ACFDCF>2.0.CO;2, 2001.

Rosinski, J., Haagenson, P. L., Nagamoto, C. T. and Parungo, F.: Ice-forming nuclei of maritime origin, *J. Aerosol Sci.*, 17, 23–46, doi:10.1016/0021-8502(86)90004-2, 1986.

Rosinski, J., Haagenson, P. L., Nagamoto, C. T. and Parungo, F.: Nature of ice-forming nuclei in marine air masses, *J. Aerosol Sci.*, 18, 291–309, doi:10.1016/0021-8502(87)90024-3, 1987.

Rosinski, J., Haagenson, P. L., Nagamoto, C. T., Quintana, B., Parungo, F. and Hoyt, S. D.: Ice-forming nuclei in air masses over the Gulf of Mexico, *J. Aerosol Sci.*, 19, 539–551, 1988.

Sarmiento, J. L. and Gruber, N.: *Ocean Biogeochemical Dynamics*, Princeton University Press, New Jersey., 2006.

Saukko, E., Kuuluvainen, H. and Virtanen, A.: A method to resolve the phase state of aerosol particles, *Atmos. Meas. Tech.*, 5, 259–265, doi:10.5194/amt-5-259-2012, 2012.

Schnell, R. C.: Ice Nuclei in Seawater, Fog Water and Marine Air off the Coast of Nova Scotia: Summer 1975, *J. Atmos. Sci.*, 34, 1299–1305, 1977.

Schnell, R. C. and Vali, G.: Freezing nuclei in marine waters, *Tellus*, 27, 321–323, doi:10.3402/tellusa.v27i3.9911, 1975.

Schnell, R. C. and Vali, G.: Biogenic Ice Nuclei: Part I. Terrestrial and Marine Sources, *J. Atmos. Sci.*, 33, 1554–1564, doi:10.1175/1520-0469(1976)033<1554:BINPIT>2.0.CO;2, 1976.

Seinfeld, J. H. and Pandis, S. N.: Atmospheric Chemistry and Physics: From Air Pollution to Climate Change. [online] Available from: <http://www.knovel.com/knovel2/Toc.jsp?BookID=2126>, 2006.

Shinki, M., Wendeberg, M., Vagle, S., Cullen, J. T. and Hore, D. K.: Characterization of adsorbed microlayer thickness on an oceanic glass plate sampler, *Limnol. Oceanogr. Methods*, 10, 728–735, doi:10.4319/lom.2012.10.728, 2012.

Sieburth, J. M., Smetacek, V. and Lenz, J.: Pelagic ecosystem structure: Heterotrophic compartments of the plankton and their relationship to plankton size fractions, *Limnol. Oceanogr.*, 23, 1256–1263, doi:10.4319/lo.1978.23.6.1256, 1978.

Skamarock, W. C., Klemp, J. B., Dudhia, J., Gill, D. O., Barker, D. M., Wang, W. and Powers, J. G.: A description of the advanced research WRF version 2., 2005.

Steinke, I., Funk, R., Busse, J., Iturri, A., Kirchen, S., Leue, M., Möhler, O., Schwartz, T., Schnaiter, M., Sierau, B., Toprak, E., Ullrich, R., Ulrich, A., Hoose, C. and Leisner, T.: Ice nucleation activity of agricultural soil dust aerosols from Mongolia, Argentina and Germany, *J. Geophys. Res. Atmos.*, 121, 13559–13576, doi:10.1002/2016JD025160, 2016.

Stohl, A., Forster, C., Frank, A., Seibert, P. and Wotawa, G.: Technical note: The Lagrangian particle dispersion model FLEXPART version 6.2, *Atmos. Chem. Phys. Discuss.*, 5, 4739–4799, doi:10.5194/acpd-5-4739-2005, 2005.

Stokes, M. D., Deane, G. B., Prather, K., Bertram, T. H., Ruppel, M. J., Ryder, O. S., Brady, J. M. and Zhao, D.: A Marine Aerosol Reference Tank system as a breaking wave analogue for the production of foam and sea-spray aerosols, *Atmos. Meas. Tech.*, 6, 1085–1094, doi:10.5194/amt-6-1085-2013, 2013.

Ström, J., Umegård, J., Tørseth, K., Tunved, P., Hansson, H. C., Holmén, K., Wismann, V., Herber, A. and König-Langlo, G.: One year of particle size distribution and aerosol chemical composition measurements at the Zeppelin Station, Svalbard, March 2000-March 2001, *Phys. Chem. Earth*, 28, 1181–1190, doi:10.1016/j.pce.2003.08.058, 2003.

Szyrmer, W. and Zawadzki, I.: Biogenic and Anthropogenic Sources of Ice-Forming Nuclei: A Review, *Bull. Am. Meteorol. Soc.*, 78, 209–228, 1997.

Tan, I., Storelvmo, T. and Zelinka, M. D.: Observational constraints on mixed-phase clouds imply higher climate sensitivity, *Science*, 352, 224–227, 2016.

Tanaka, T. Y. and Chiba, M.: A numerical study of the contributions of dust source regions to the global dust budget, *Glob. Planet. Change*, 52, 88–104, doi:10.1016/j.gloplacha.2006.02.002, 2006.

Tremblay, G., Belzile, C., Gosselin, M., Poulin, M., Roy, S. and Tremblay, J. É.: Late summer phytoplankton distribution along a 3500 km transect in Canadian Arctic waters: Strong numerical dominance by picoeukaryotes, *Aquat. Microb. Ecol.*, 54, 55–70, doi:10.3354/ame01257, 2009.

Tunved, P., Ström, J. and Krejci, R.: Arctic aerosol life cycle: Linking aerosol size distributions observed between 2000 and 2010 with air mass transport and precipitation at Zeppelin station, Ny-Ålesund, Svalbard, *Atmos. Chem. Phys.*, 13, 3643–3660, doi:10.5194/acp-13-3643-2013, 2013.

Twomey, S.: Aerosols, clouds and radiation, *Atmos. Environ. Part A, Gen. Top.*, 25, 2435–2442, doi:10.1016/0960-1686(91)90159-5, 1991.

Usher, C. R., Michel, A. E. and Grassian, V. H.: Reactions on Mineral Dust, *Chem. Rev.*, 103, 4883–4939, doi:10.1021/cr020657y, 2003.

Vali, G.: Quantitative Evaluation of Experimental Results on the Heterogeneous Freezing Nucleation of Supercooled Liquids, *J. Atmos. Sci.*, 28, 402–409, 1971.

Vali, G.: Interpretation of freezing nucleation experiments: Singular and stochastic; Sites and surfaces, *Atmos. Chem. Phys.*, 14, 5271–5294, doi:10.5194/acp-14-5271-2014, 2014.

Vali, G., Christensen, M., Fresh, R. W., Galyan, E. L., Maki, L. R. and Schnell, R. C.: Biogenic Ice Nuclei. Part II: Bacterial Sources, *J. Atmos. Sci.*, 33, 1565–1570, doi:10.1175/1520-0469(1976)033<1565:BINPIB>2.0.CO;2, 1976.

Vasiliou, J. G., Sorensen, D. and McMurry, P. H.: Sampling at controlled relative humidity with a cascade impactor, *Atmos. Environ.*, 33, 1049–1056, doi:10.1016/S1352-2310(98)00323-9, 1999.

Vergara-Temprado, J., Murray, B. J., Wilson, T. W., O’Sullivan, D., Browse, J., Pringle, K. J., Ardon-Dryer, K., Bertram, A. K., Burrows, S. M., Ceburnis, D., DeMott, P. J., Mason, R. H., O’Dowd, C. D., Rinaldi, M. and Carslaw, K. S.: Contribution of feldspar and marine organic aerosols to global ice nucleating particle concentrations, *Atmos. Chem. Phys.*, 17, 3637–3658, doi:10.5194/acp-2016-822, 2017.

Wang, B., Laskin, A., Roedel, T., Gilles, M. K., Moffet, R. C., Tivanski, A. V. and Knopf, D. A.: Heterogeneous ice nucleation and water uptake by field-collected atmospheric particles below 273 K, *J. Geophys. Res. Atmos.*, 117, D00V19–D00V34, doi:10.1029/2012JD017446, 2012a.

Wang, B., Lambe, A. T., Massoli, P., Onasch, T. B., Davidovits, P., Worsnop, D. R. and Knopf, D. A.: The deposition ice nucleation and immersion freezing potential of amorphous secondary organic aerosol: Pathways for ice and mixed-phase cloud formation, *J. Geophys. Res. Atmos.*, 117, D16209–D16231, doi:10.1029/2012JD018063, 2012b.

Wang, X., Sultana, C. M., Trueblood, J., Hill, T. C. J., Malfatti, F., Lee, C., Laskina, O., Moore, K. A., Beall, C. M., McCluskey, C. S., Cornwell, G. C., Zhou, Y., Cox, J. L., Pendergraft, M. A., Santander, M. V., Bertram, T. H., Cappa, C. D., Azam, F., DeMott, P. J., Grassian, V. H. and Prather, K. A.: Microbial Control of Sea Spray Aerosol Composition: A Tale of Two Blooms, *ACS Cent. Sci.*, 1, 124–131, doi:10.1021/acscentsci.5b00148, 2015.

Welti, A., Lüönd, F., Kanji, Z. A., Stetzer, O. and Lohmann, U.: Time dependence of immersion freezing: An experimental study on size selected kaolinite particles, *Atmos. Chem. Phys.*, 12, 9893–9907, doi:10.5194/acp-12-9893-2012, 2012.

Welti, A., Müller, K., Fleming, Z. L. and Stratmann, F.: Concentration and variability of ice nuclei in the subtropical maritime boundary layer, *Atmos. Chem. Phys.*, 18, 5307–5320, doi:10.5194/acp-18-5307-2018, 2018.

Wentworth, G. R., Murphy, J. G., Croft, B., Martin, R. V., Pierce, J. R., Côté, J. S., Courchesne, I., Tremblay, J. É., Gagnon, J., Thomas, J. L., Sharma, S., Toom-Saunty, D., Chivulescu, A., Levasseur, M. and Abbatt, J. P. D.: Ammonia in the summertime Arctic marine boundary layer: Sources, sinks, and implications, *Atmos. Chem. Phys.*, 16, 1937–1953, doi:10.5194/acp-16-1937-2016, 2016.

Wex, H., DeMott, P. J., Tobo, Y., Hartmann, S., Rösch, M., Clauss, T., Tomsche, L., Niedermeier, D. and Stratmann, F.: Kaolinite particles as ice nuclei: Learning from the use of different kaolinite samples and different coatings, *Atmos. Chem. Phys.*, 14, 5529–5546, doi:10.5194/acp-14-5529-2014, 2014.

Wexler, A. S. and Clegg, S. L.: Atmospheric aerosol models for systems including the ions  $H^+$ ,  $NH_4^+$ ,  $Na^+$ ,  $SO_4^{2-}$ ,  $NO_3^-$ ,  $Cl^-$ ,  $Br^-$ , and  $H_2O$ , *J. Geophys. Res.*, 107, 4207–4221, doi:10.1029/2001JD000451, 2002.

Whale, T. F., Murray, B. J., O'Sullivan, D., Wilson, T. W., Umo, N. S., Baustian, K. J., Atkinson, J. D., Workneh, D. A. and Morris, G. J.: A technique for quantifying heterogeneous ice nucleation in microlitre supercooled water droplets, *Atmos. Meas. Tech.*, 8, 2437–2447, doi:10.5194/amt-8-2437-2015, 2015.

Wheeler, M. J., Mason, R. H., Steunenberg, K., Wagstaff, M., Chou, C. and Bertram, A. K.: Immersion freezing of supermicron mineral dust particles: Freezing results, testing different schemes for describing ice nucleation, and ice nucleation active site densities, *J. Phys. Chem. A*, 119, 4358–4372, doi:10.1021/jp507875q, 2015.

Wilson, T. W., Ladino, L. A., Alpert, P. A., Breckels, M. N., Brooks, I. M., Browse, J., Burrows, S. M., Carslaw, K. S., Huffman, J. A., Judd, C., Kilhau, W. P., Mason, R. H., McFiggans, G., Miller, L. A., Nájera, J. J., Polishchuk, E., Rae, S., Schiller, C. L., Si, M., Temprado, J. V., Whale, T. F., Wong, J. P. S., Wurl, O., Yakobi-Hancock, J. D., Abbatt, J. P. D., Aller, J. Y., Bertram, A. K., Knopf, D. A. and Murray, B. J.: A marine biogenic source of atmospheric ice-nucleating particles, *Nature*, 525, 234–238, doi:10.1038/nature14986, 2015.

Winkler, P.: Relative humidity and the adhesion of atmospheric particles to the plates of impactors, *J. Aerosol Sci.*, 5, 235–240, doi:10.1016/0021-8502(74)90058-5, 1974.

Wright, T. P. and Petters, M. D.: The role of time in heterogeneous freezing nucleation, *J. Geophys. Res. Atmos.*, 118, 3731–3743, doi:10.1002/jgrd.503652013, 2013.

Wurl, O., Miller, L., Röttgers, R. and Vagle, S.: The distribution and fate of surface-active substances in the sea-surface microlayer and water column, *Mar. Chem.*, 115, 1–9, doi:10.1016/j.marchem.2009.04.007, 2009.

Wurl, O., Wurl, E., Miller, L., Johnson, K. and Vagle, S.: Formation and global distribution of sea-surface microlayers, *Biogeosciences*, 8, 121–135, doi:10.5194/bg-8-121-2011, 2011.

Yamamoto-Kawai, M., Tanaka, N. and Pivovarov, S.: Freshwater and brine behaviors in the Arctic ocean deduced from historical data of  $\delta^{18}\text{O}$  and alkalinity (1929–2002 A.D.), *J. Geophys. Res. C Ocean.*, 110, 1–16, doi:10.1029/2004JC002793, 2005.

Young, K. C.: *Microphysical Processes in Clouds*, Oxford University Press, New York., 1993.

Yun, Y. and Penner, J. E.: An evaluation of the potential radiative forcing and climatic impact of marine organic aerosols as heterogeneous ice nuclei, *Geophys. Res. Lett.*, 40, 4121–4126, doi:10.1002/grl.50794, 2013.

Zhang, Z., Liu, L., Liu, C. and Cai, W.: Studies on the sea surface microlayer: II. The layer of sudden change of physical and chemical properties, *J. Colloid Interface Sci.*, 264, 148–159, doi:10.1016/S0021-9797(03)00390-4, 2003.

Zobrist, B., Marcolli, C., Peter, T. and Koop, T.: Heterogeneous ice nucleation in aqueous solutions: the role of water activity., *J. Phys. Chem. A*, 112, 3965–75, doi:10.1021/jp7112208, 2008.

## Appendices

### Appendix A

#### A.1 Classical nucleation theory: homogeneous ice nucleation

The concepts and equations used to describe atmospheric ice nucleation in the following section follow those of Young (1993). Additional descriptions of classical nucleation theory are available in Murray et al. (2012), Pruppacher and Klett (1997), and Seinfeld and Pandis (2006). To simplify the theory it is assumed that the ice clusters, sometimes called ice embryos, are spherical. The Gibbs free energy of the formation of a spherical ice embryo,  $\Delta G_{\text{hom},i}$ , of radius  $r_i$  in a supercooled water droplet is expressed as:

$$\Delta G_{\text{hom},i} = -\frac{4\pi r_i^3}{3} N_i k T \ln \left( \frac{e_{s,w}}{e_{s,i}} \right) + 4\pi r_i^2 \sigma_{LI} \quad (\text{A.1})$$

Where  $N_i$  is the molecular concentration in the volume of the ice embryo;  $k$  is the Boltzmann constant;  $T$  is the temperature in Kelvin; and  $\sigma_{LI}$  is the interfacial tension between the liquid and ice phase. Eq. (A.1) demonstrates the dependence of the Gibbs free energy on the formation of a new phase (ice), and the work required to create an interface between these two phases.

Figure A.1 shows the change in Gibbs free energy as a function of the radius of the ice embryo. A cluster of water molecules will not form a stable ice embryo if their collective radius is smaller than the critical radius,  $r^*$ , because the addition of water molecules to the embryo will cause the free energy of the system to increase. Once the cluster reaches a critical size, growth of an ice crystal will be spontaneous because the addition of water molecules to the embryo results in a negative value of the Gibbs free energy.

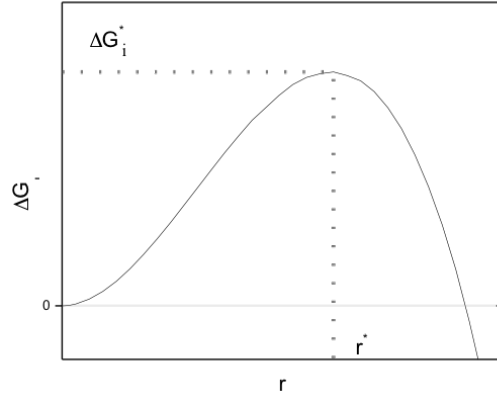


**Figure A.1** Change in  $\Delta G_i$  as a function of the radius of the ice embryo.  $\Delta G_i^*$  is the activation energy required for a critical cluster of water molecules to form an ice embryo; the radius,  $r^*$ , is the critical radius.

The formation of an ice embryo with radius  $r^*$  is the rate-determining step in ice nucleation. The homogeneous rate of nucleation,  $J_{hom}$ , can then be determined as follows:

$$J_{hom} = A_{hom} \exp \left\{ -\frac{\Delta G_{hom,i}^* + \Delta g}{kT} \right\} \quad (\text{A.2})$$

Where  $A_{hom}$  is the pre-exponential factor and  $\Delta g$  is the activation energy of self-diffusion, which is associated with the energy used to break the intermolecular hydrogen bonds in liquid water.

## A.2 Classical nucleation theory: heterogeneous ice nucleation

The equation used for calculating the Gibbs free energy for ice embryo formation via immersion ice nucleation is determined as follows:

$$\Delta G_{het,imm,i} = V_i \left( -N_i kT \ln \left( \frac{e_{s,w}}{e_{s,i}} \right) + C \epsilon^2 \right) + \sigma_{LI} A_{IL} + (\sigma_{IN} - \sigma_{LN}) A_{IN} \quad (\text{A.3})$$

Where  $V_i$  is the volume of the ice embryo;  $C$  is the elastic strain coefficient;  $\epsilon$  is the elastic strain of the ice lattice, a product of any crystallographic mismatch that may exist between the

embryo and substrate;  $\sigma_{IN}$  and  $\sigma_{LN}$  are the interfacial tensions of the ice-substrate and liquid-substrate phases, respectively; and  $A_{IL}$  and  $A_{IN}$  are the areas of the ice-liquid and ice-substrate interfaces.

The three interfacial tensions are connected by the contact angle,  $\theta$ , which exists between the ice embryo and the particle surface:

$$\hat{m} = \cos \theta = \frac{\sigma_{LN} - \sigma_{IN}}{\sigma_{LI}} \quad (\text{A.4})$$

The contact angle can be used to determine  $V_i$ ,  $A_{IL}$ , and  $A_{IN}$  using  $r_i$  as the radius of the spherical ice embryo. Substituting Eq. (A.4) into Eq. (A.3) yields a simplified function for the Gibbs free energy change of forming an ice embryo presented as Eq. (A.5). The geometric factor  $f(\hat{m})$  is given in Eq. (A.6).

$$\Delta G_{het,imm,i} = f(\hat{m}) \left[ \frac{4\pi r_i^3}{3} \left( -N_i kT \ln \left( \frac{e_{s,w}}{e_{s,i}} \right) + C \in^2 \right) + 4\pi r_i^2 \sigma_{LI} \right] \quad (\text{A.5})$$

$$f(\hat{m}) = \frac{(2 + \hat{m})(1 - \hat{m})^2}{4} \quad (\text{A.6})$$

The activation energy for immersion freezing can be calculated from the following equation:

$$\Delta G_{het,imm,i}^* = \frac{-16\pi f(\hat{m}) \sigma_{LI}^3}{3 \left[ N_i kT \ln \left( \frac{e_{s,w}}{e_{s,i}} \right) - C \in^2 \right]^2} \quad (\text{A.7})$$

The equation for the rate of formation of ice embryos with a critical radius via the immersion mechanism is analogous to Eq. (A.2) and is shown here:

$$J_{het,imm} = A \exp \left\{ \frac{(\Delta G_{het,imm,i}^* + \Delta g)}{kT} \right\} \quad (\text{A.8})$$

In classical nucleation theory there is a dependence of ice nucleation on temperature, surface area, and time. For the purpose of this dissertation we assume a time-independent approach to calculating the concentrations of INPs (Vali, 1971) i.e. there is a dependence on only temperature and surface area.

## **Appendix B**

### **B.1 Corrections for freezing temperature depression**

The water activity of the sample was calculated from the salinity of the sample and using the online Extended AIM Aerosol Thermodynamics Model (<http://www.aim.env.uea.ac.uk/aim/aim.php>; Friese and Ebel, (2010); Wexler and Clegg, (2002)). Then the water activity of a salt solution in equilibrium with ice at the median freezing temperature of the sample was determined. From the difference of these two water activities, the freezing temperature in the absence of salts was calculated. For further details see Fig. 1 of Koop and Zobrist (2009).

**Table B.1: Conditions at sampling stations.**

Station	Photos	Notes	Station	Photos	Notes
2		Behind iceberg and sheltered from wind. Sunny day, relatively flat sea surface. Macroalgae spotted approx. 75m away from sampling area. Wind speed: 4.6 m/s.	7		A little wavy, close to ice. Wind speed: 6.7 m/s.
4		Very flat, calm, glassy looking open water. No icebergs in sight. Wind speed: 1.4 m/s. Slick	8		Approx. 200m away from ice island. Partly cloudy. Calm and glassy sea surface. Wind speed: 0.7 m/s. Slick
5		Wavy, open water. Foggy. Wind speed: 3.1 m/s.	9		Overcast and raining. ~15m away from ice with brown material (possible animal faeces). Flat, calm and glassy sea surface. Wind speed: 2.4 m/s.
6		Uniform sea surface, near ice. Overcast. Wind speed: 2.4 m/s.	10		Glassy sea surface. Macroalgae floating approximately 5 m away. Partly sunny. Wind speed: 4.6 m/s. Slick

**Table B.2: Correlation analyses between chemical or physical properties of bulk seawater and T<sub>50</sub>-values for the bulk seawater samples. Numbers in bold represent correlations that are statistically significant (p < 0.05).**

Chemical and physical properties	T <sub>50</sub> -value		
	R	p	n
Dimethyl sulfide concentration	-0.4	0.167	8
Bacterial abundance	-0.2	0.319	6
Phytoplankton abundance	-0.3	0.268	6
Temperature	0.2	0.313	8
pH	-0.2	0.293	8
Salinity	<b>-0.8</b>	<b>0.006</b>	<b>8</b>

**Table B.3: Correlation analyses between phytoplankton and bacterial abundance in the microlayer and bulk seawater and T<sub>10</sub>-values for the microlayer and bulk seawater.**

Biological variable	Microlayer T <sub>10</sub> -value			Bulk seawater T <sub>10</sub> -value		
	R	p	n	R	p	n
Phytoplankton abundance	-0.7	0.058	6	-0.5	0.138	6
Bacterial abundance	-0.7	0.071	6	-0.4	0.189	6



**Figure B.1: Photo of sampling with the glass plate (Harvey and Burzell, 1972).**

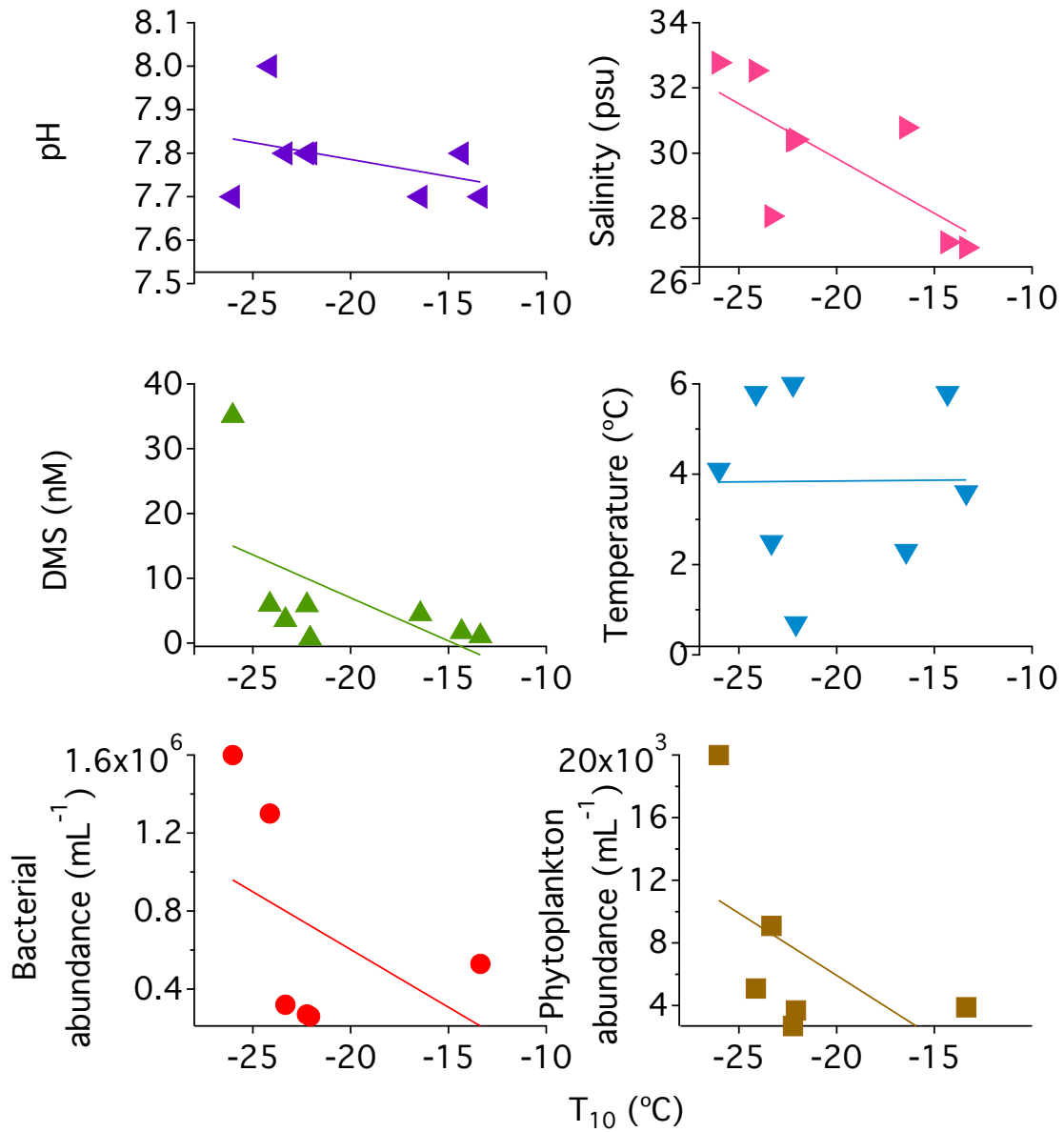
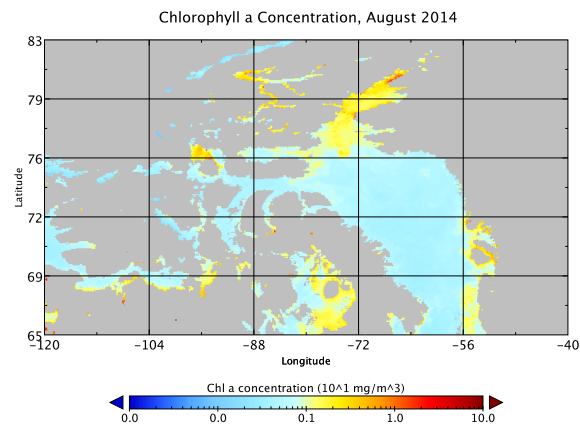
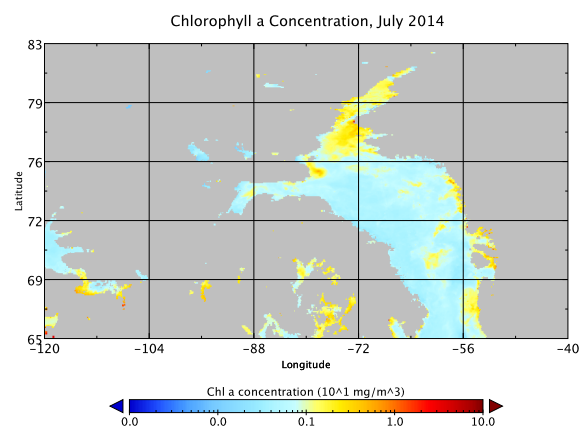
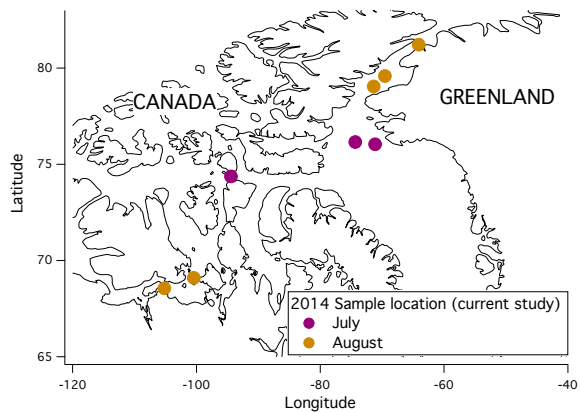
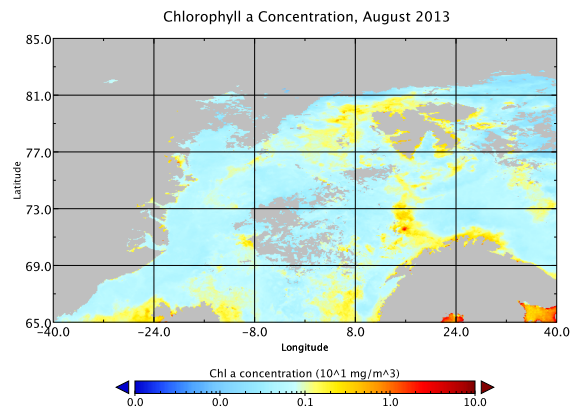
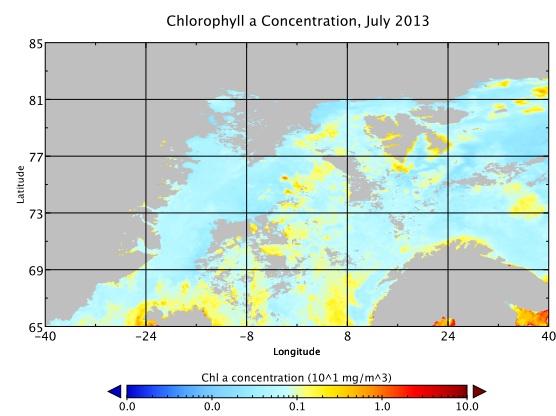
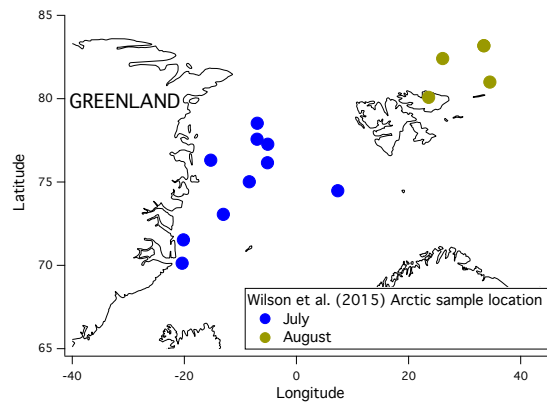


Figure B.2: Correlation plots between chemical and physical properties, and  $T_{10}$ -values in the bulk seawater. R and p values can be found in Table 2.2 in the main text.



**Figure B.3: Sample locations and monthly average chlorophyll *a* concentrations for sampling during the current study. Chlorophyll *a* concentrations were obtained from the NASA Ocean Biology Distributed Active Archive Centre (OB.DAAC).**



**Figure B.4: Sample locations and monthly average chlorophyll *a* concentrations for sampling during the Wilson et al. (2015) study in the Arctic. Chlorophyll *a* concentrations were obtained from the NASA OB.DAAC.**

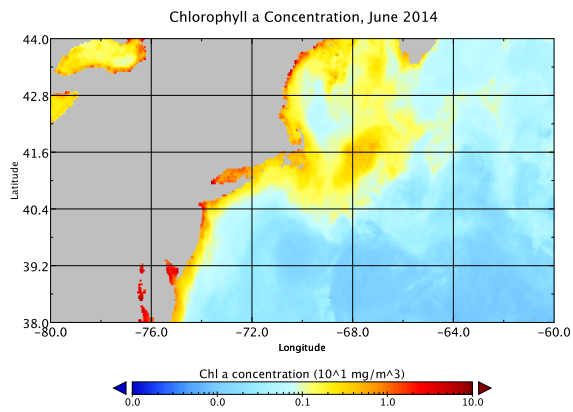
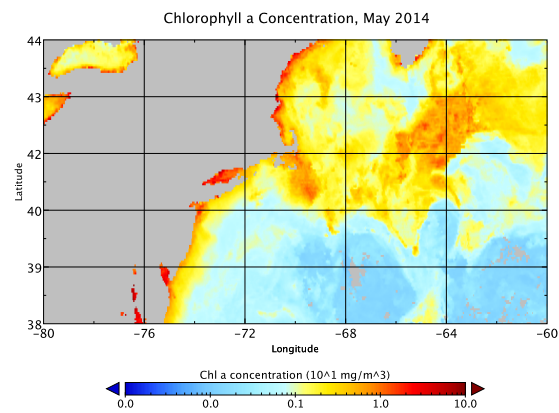
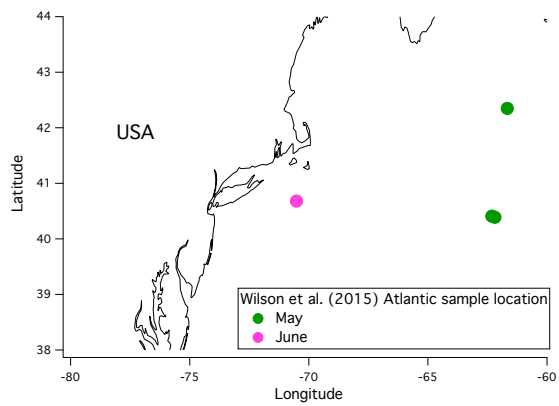


**Figure B.5: Sample locations and monthly average chlorophyll *a* concentrations for sampling during the Wilson et al. (2015) study in the Atlantic. Chlorophyll *a* concentrations were obtained from the NASA OB.DAAC.**

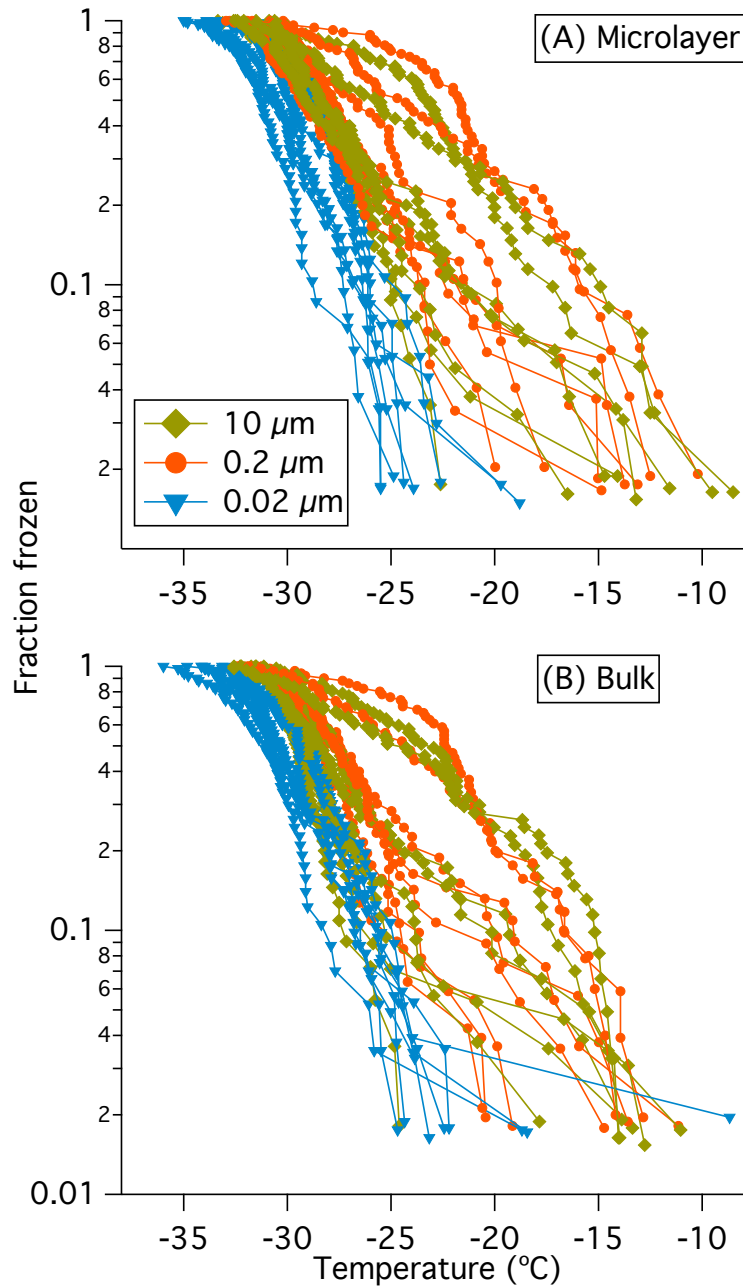


Figure B.6: Plots of the fraction of droplets frozen (in the immersion mode) versus temperature for samples filtered with 10  $\mu\text{m}$ , 0.2  $\mu\text{m}$  and 0.02  $\mu\text{m}$  filters in A) the microlayer, and B) bulk seawater. Each set of line and markers represents results for 3 repeat experiments of each sample or “blank”, adding up to a total of between 45 to 60 freezing events in each set. All microlayer and bulk seawater freezing points have been corrected for freezing point depression to account for dissolved salts in seawater (Section 2.2.4). The uncertainty in temperature is not shown but is  $\pm 0.3$   $^{\circ}\text{C}$ .

## **Appendix C**

### **C.1 Non-colligative effects of seawater on freezing temperatures**

Two ml of a microlayer sample stored at  $-80\text{ }^{\circ}\text{C}$  for less than 6 months (station 4) was mixed with 2 ml of a solution of Instant Ocean salt in ultrapure water. Instant Ocean is a commercially available sea salt replica used regularly by aquariums to mimic ocean composition (Atkinson and Bingman, 1997). The microlayer sample was mixed with three different concentrations of the Instant Ocean solution (26, 55, and 77 g of salt per kg of water) to make three salinity-altered microlayer samples. The freezing temperatures of the three salinity altered microlayer samples and the freezing temperatures of the three Instant Ocean solutions were measured and are shown in Fig. C.8.

**Table C.1: Conditions at sampling stations.**

Station	Photos	Notes	Station	Photos	Notes
1		Foggy. Rippled sea, small swell. Beaufort scale (BS) ~3-4. Wind speed 3.8 m/s.	7		A lot of ice and icebergs. Starting to spit rain. Polar bears in vicinity. Wind speed 0.3 m/s.
2		Sunny. Next to ice island. Icebergs approx. 100m away. BS ~2. Wind speed 6.1 m/s.	8		Overcast. Ice bits around. BS ~1. No polar bears...yet. Wind speed 3.5 m/s.
3		Partly sunny. A few icebergs approx. 200m away. BS ~3. Wind speed 6.6 m/s.	9		Sunny, ice bits, 1/10 <sup>th</sup> ice. BS 0. Clouds 1/9 <sup>th</sup> cirrus. Wind speed 1.3 m/s.
4		Can see Greenland. Overcast, rippled sea surface, bit of a swell. Wind speed 0.7 m/s.	10		BS ~4, sunrise, clear skies, very wavy conditions. Wind speed 6.9 m/s.
5		Sunny, slight swell, rippled surface. BS ~3/4. Wind speed 2.8 m/s.	11		BS ~3, sunrise, mostly cloudy. Wind speed 5.6 m/s.
6		Sunny, rippled waves. Icebergs >2miles away. BS 2. Wind speed 4.4 m/s.			

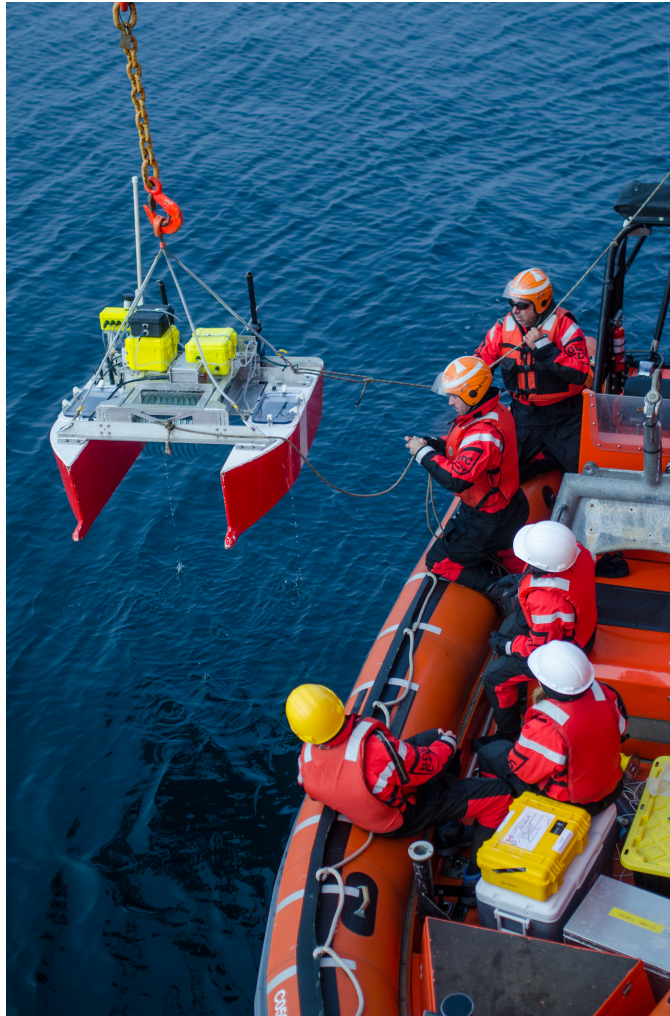


**Figure C.1: Photo of the automated sampling catamaran being lowered to the side of the zodiac. Photo credit: Robin B nard.**

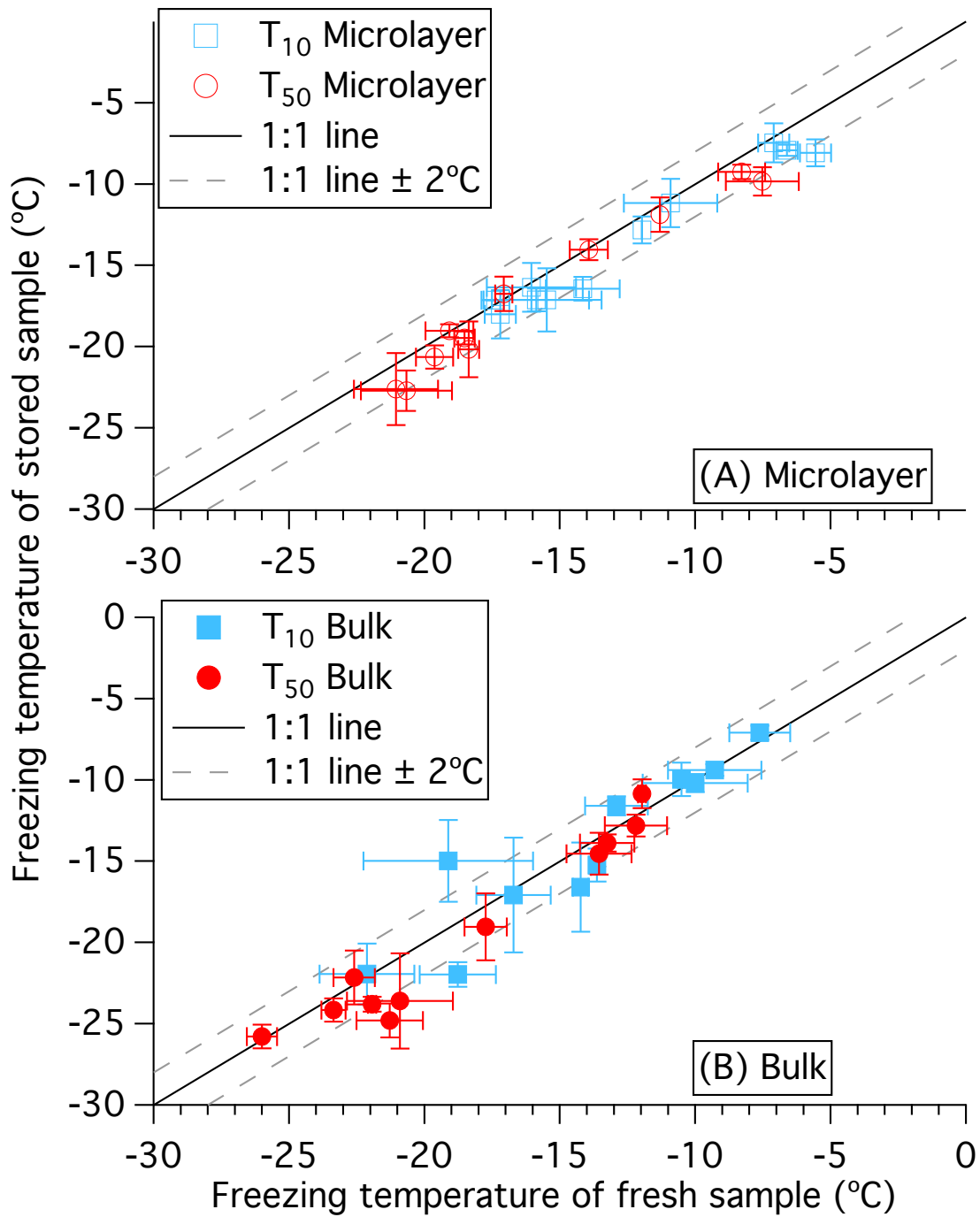
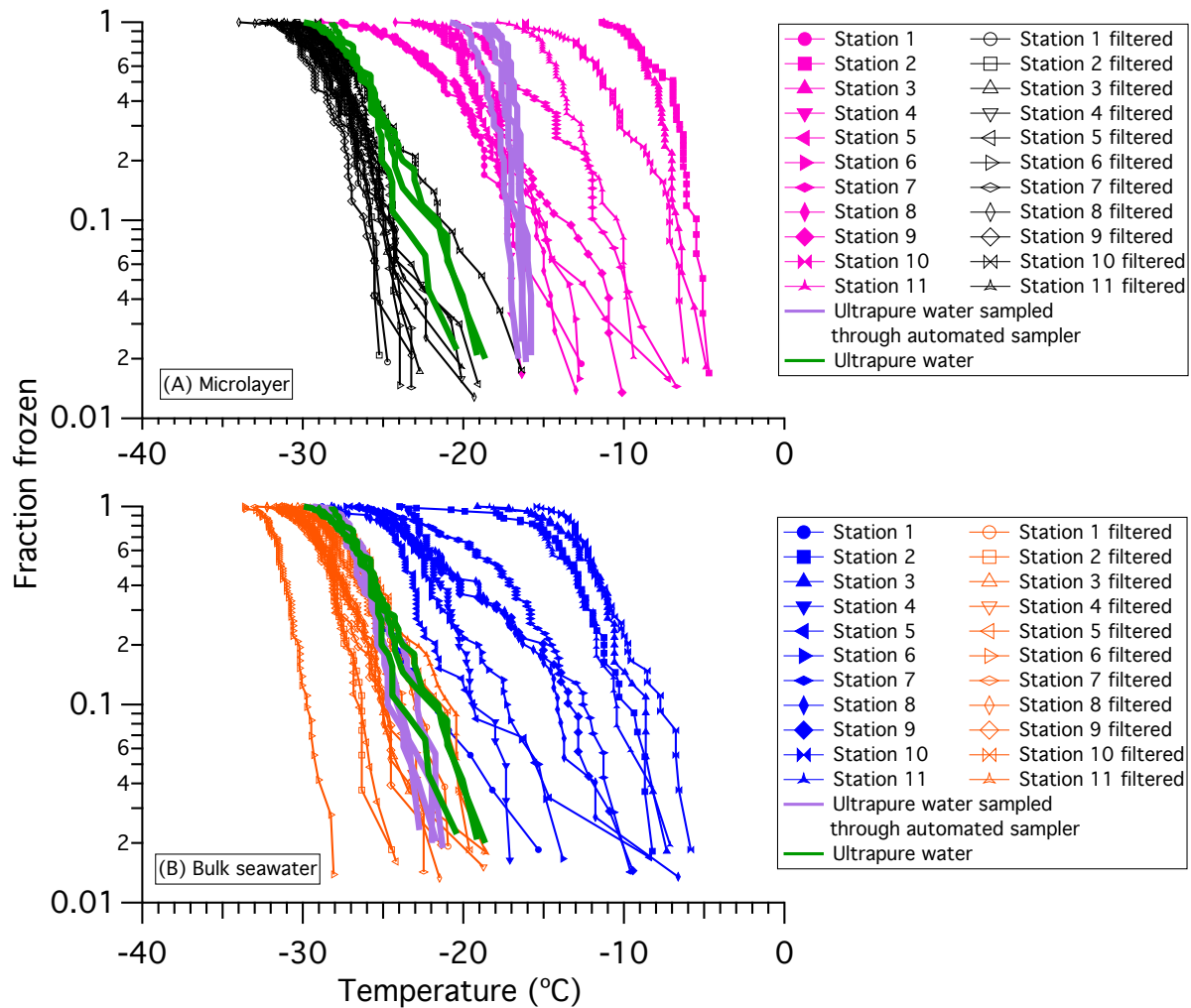
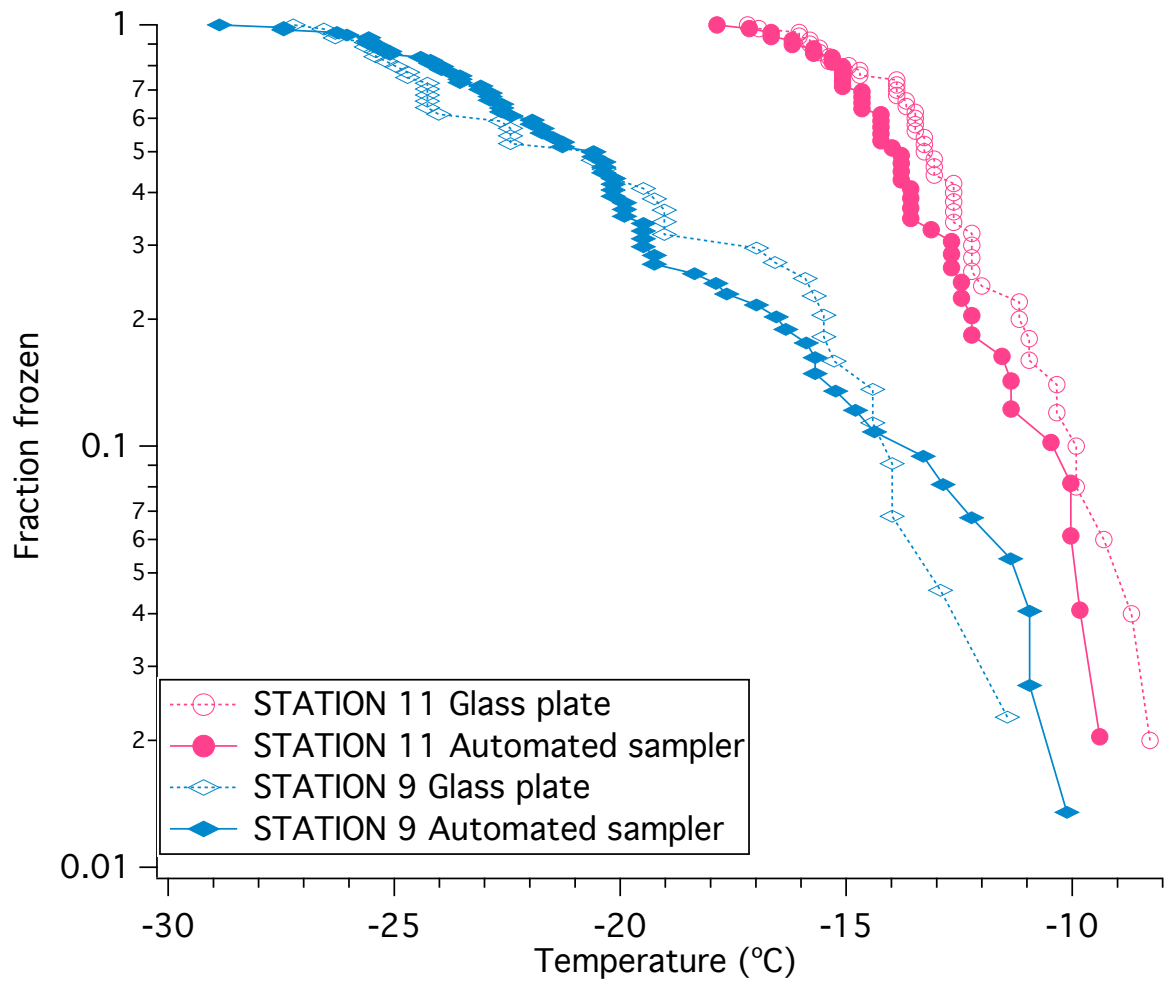


Figure C.2: Plots comparing the  $T_{50}$ -values and  $T_{10}$ -values for duplicate samples not frozen or stored (i.e. fresh) and samples stored at  $-80^\circ\text{C}$  for up to six months. A) Microlayer samples and B) bulk seawater samples. Data points are the average  $T_{50}$ -values and  $T_{10}$ -values from three repeat experiments. Error bars are the 95 % confidence interval for three repeat experiments. With experimental variability, all microlayer and bulk seawater samples lie within the  $1:1$  line  $\pm 2^\circ\text{C}$ .



**Figure C.3: Fraction of droplets frozen (in the immersion mode) versus temperature in A) the microlayer, and B) bulk seawater. Each set of line and markers represents the results for 3 repeat experiments of a sample or a sample passed through a 0.02  $\mu\text{m}$  filter, adding up to a total of between 45 to 60 freezing events in each set. Each data point corresponds to a single freezing event in the experiments. Also included are the results for ultrapure water and for ultrapure water sampled through the automated sampler (procedural blanks). All microlayer and bulk seawater freezing points have been corrected for freezing point depression to account for dissolved salts in seawater. The uncertainty in temperature is not shown but is  $\pm 0.3$  °C. The freezing properties of the samples after 0.02  $\mu\text{m}$  filtration may still contain some small particles ( $< 0.02$   $\mu\text{m}$  in diameter) that can act as INPs (Dreischmeier et al., 2017; O’Sullivan et al., 2015).**



**Figure C.4: Preliminary data comparing the fraction of frozen droplets from the glass plate method to the fraction of frozen droplets from the automated sampling method. Data from stations 9 and 11 are used. Data are not corrected for freezing point depression.**

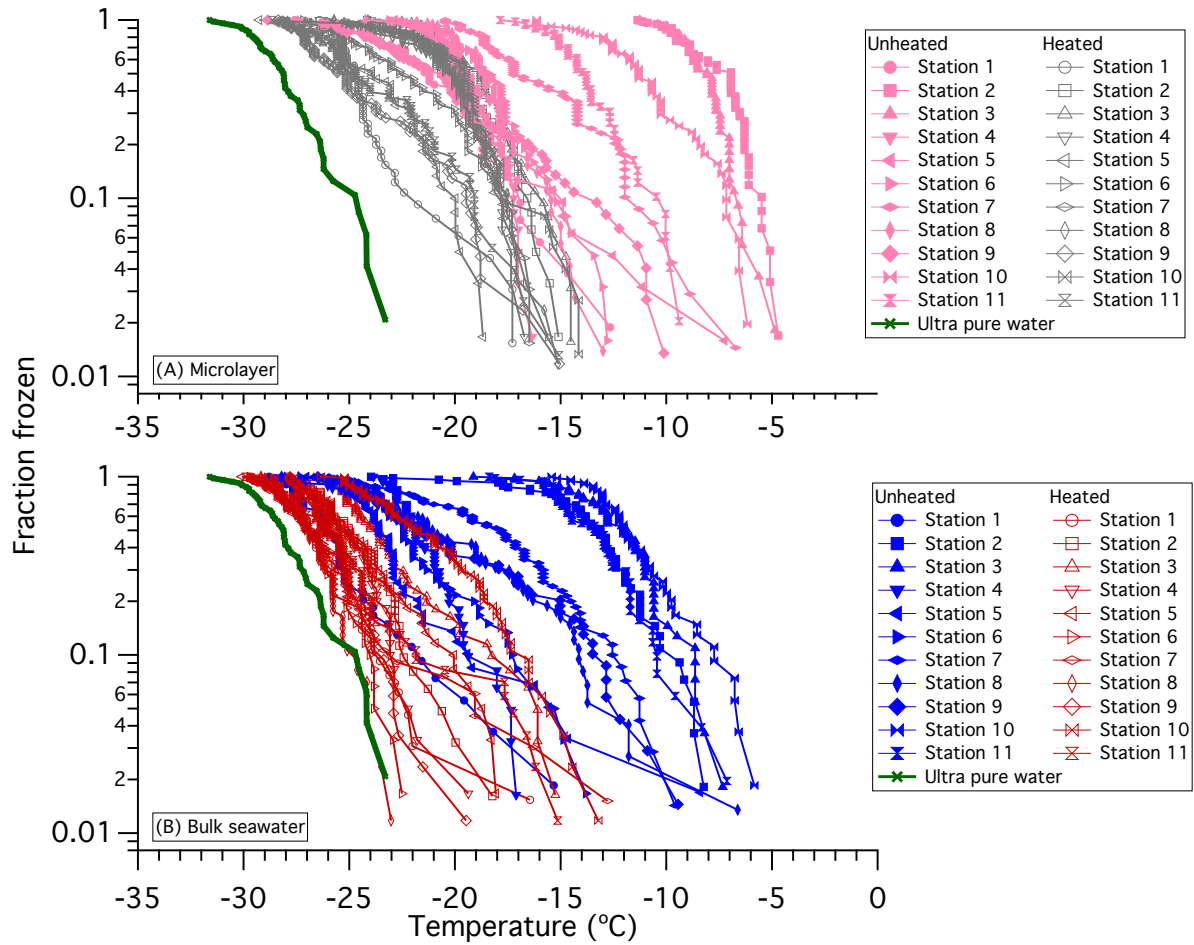
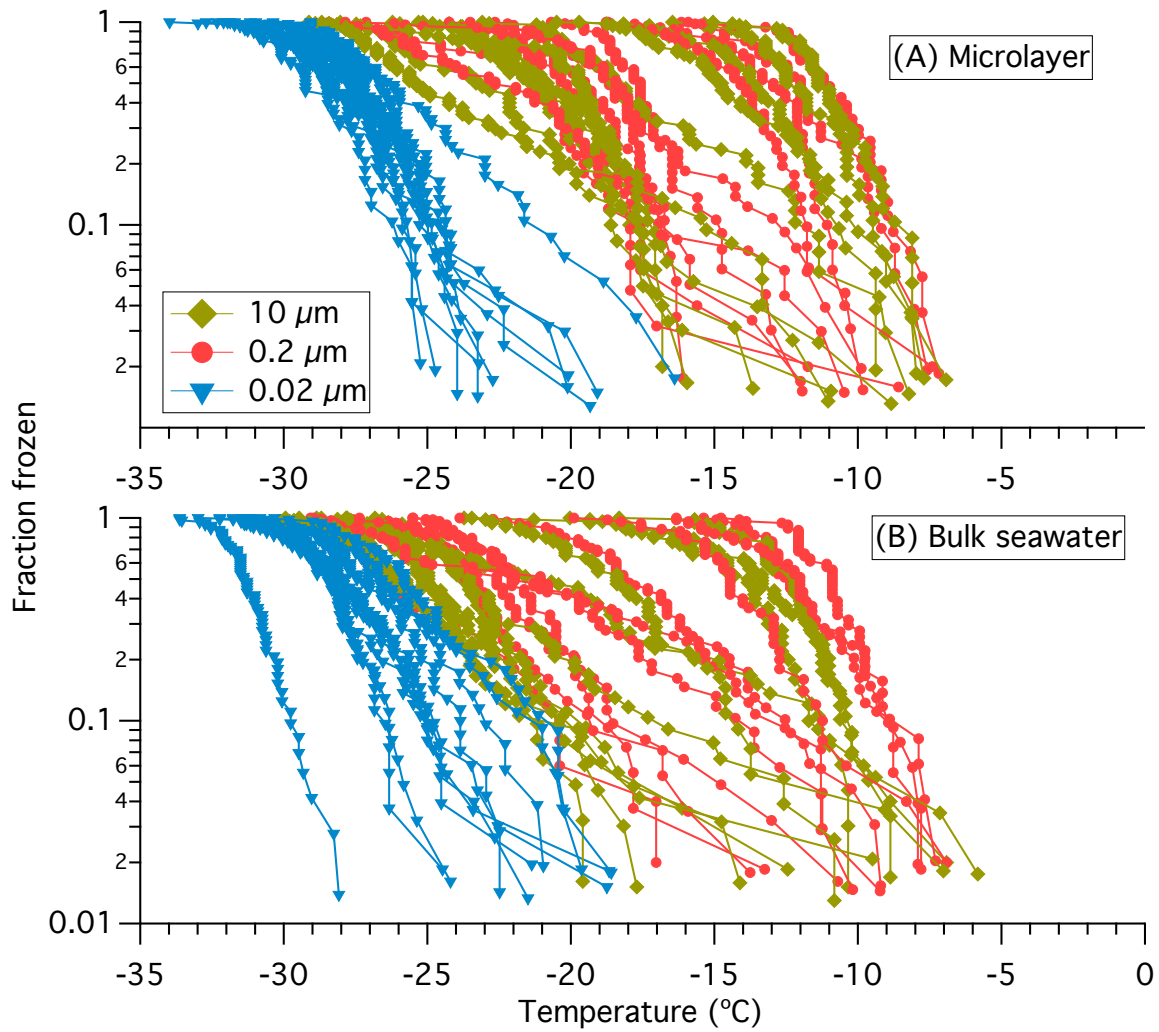
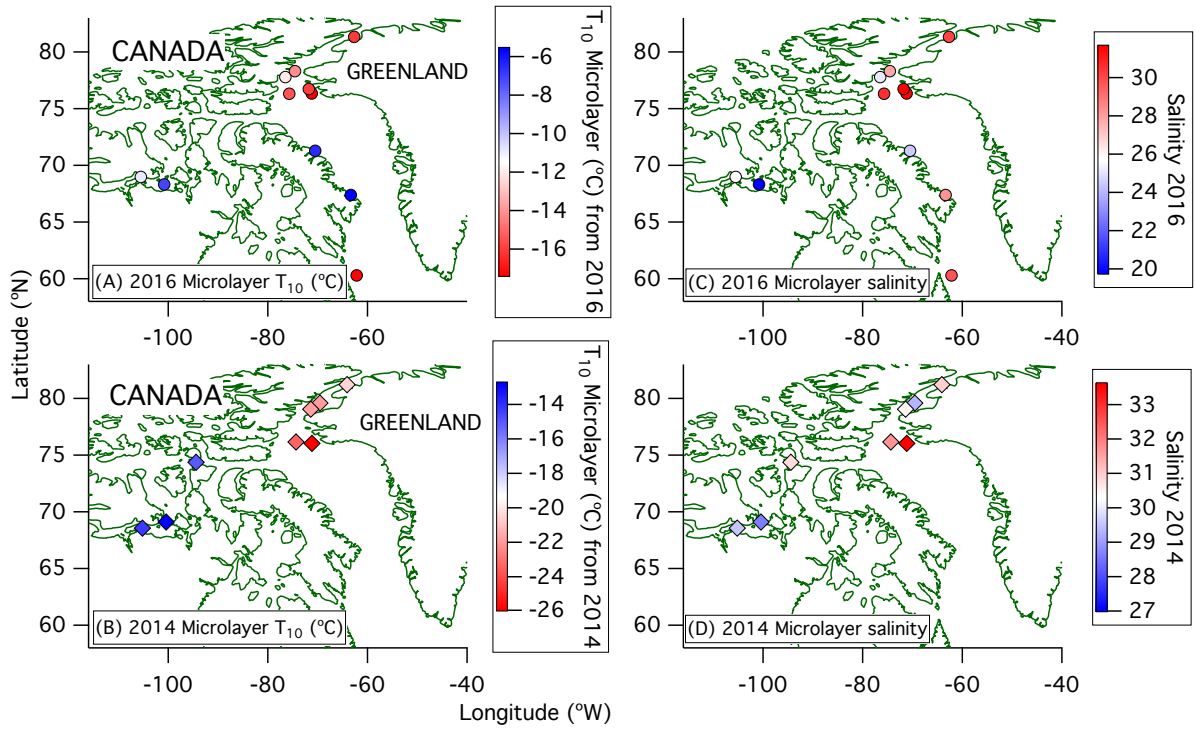


Figure C.5: Effect of heating on the fraction frozen curves for unfiltered samples from A) the microlayer, and B) bulk seawater. Each data point corresponds to one droplet freezing event. All data have been corrected for freezing point depression.



**Figure C.6: Fraction of droplets frozen as a function of filter pore size in A) microlayer samples, and B) bulk seawater samples. Filter pore sizes used in the experiments were 10 μm (yellow diamonds), 0.2 μm (red circles) and 0.02 μm (blue triangles). All data have been corrected for freezing depression.**



**Figure C.7: Spatial patterns of (A, B)  $T_{10}$ -values and (C, D) salinities in (A, C) 2016 and (B, D) 2014 for the microlayer.**

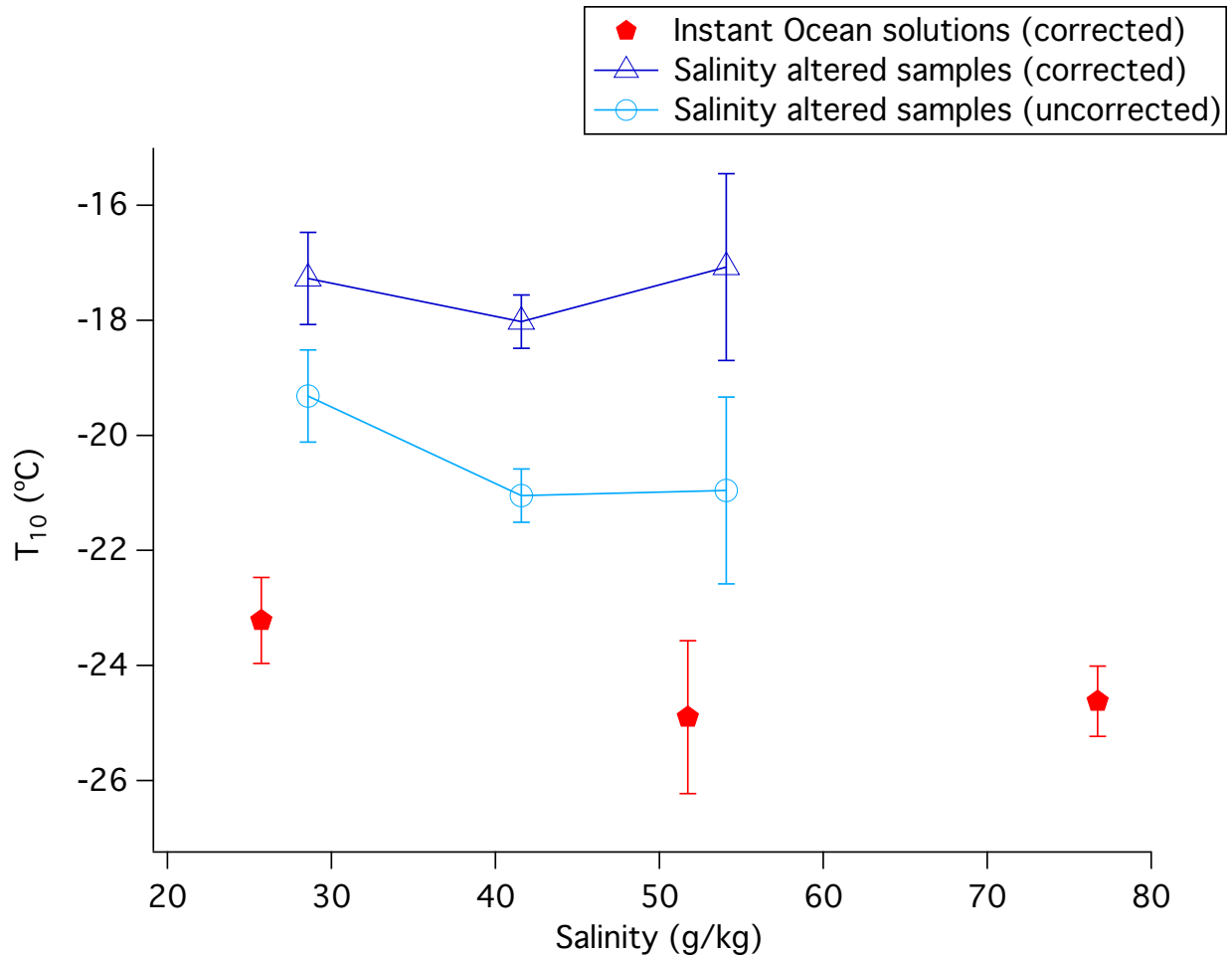


Figure C.8: Plot of the  $T_{10}$ -values of microlayer sample from station 4 as a function of salinity. The salinity was adjusted by adding solutions of Instant Ocean in ultrapure water to the samples. Data points represent averages and error bars represent the 95 % confidence intervals of 3 repeat experiments. Light blue circles represent  $T_{10}$ -values uncorrected for freezing point depression. Dark blue triangles represent  $T_{10}$ -values after correcting for freezing point depression by the presence of salts as described in Section 2.3.3. Red pentagons represent  $T_{10}$ -values for solutions of Instant Ocean in ultrapure water, after correcting for freezing point depression.

## Appendix D

### D.1 Calculation of $n_s$ -values of Niemand et al. (2012) and DeMott et al. (2016)

At -25, -20, and -15 °C, the exponential function from Niemand et al. (2012) predicts  $n_s$ -values of 307263 cm<sup>-2</sup>, 39092 cm<sup>-2</sup>, 1810 cm<sup>-2</sup>, respectively. Errors were calculated from the 95 % prediction band.

A linear fit was applied to the  $n_s$ -values reported in DeMott et al. (2016) for laboratory conditions only. At -25, -20, and -15 °C, the  $n_s$ -values were 123 cm<sup>-2</sup>, 10 cm<sup>-2</sup>, and 1 cm<sup>-2</sup>, respectively. Data for laboratory bloom conditions were not accounted for in this study as the reported chlorophyll *a* concentrations during the bloom experiment in DeMott et al., (2016) were much higher than average monthly chlorophyll *a* concentrations during this cruise. Errors were calculated from the 95 % prediction band of the linear fit.

**Table D.1: Dates, times, and locations of sampling.**

DATE	Time mid-sample (UTC)	Longitude (°)	Latitude (°)
14 <sup>th</sup> July	12:51	-61.085	67.240
15 <sup>th</sup> July*	17:33	-64.847	69.359
16 <sup>th</sup> July*	21:52	-71.117	71.702
17 <sup>th</sup> July	19:29	-79.464	73.982
18 <sup>th</sup> July	20:37	-81.018	73.569
19 <sup>th</sup> July	16:18	-83.976	74.110
21 <sup>st</sup> July	14:21	-92.225	74.237
22 <sup>nd</sup> July	12:23	-94.859	74.324
23 <sup>rd</sup> July	14:41	-94.526	74.547
24 <sup>th</sup> July	21:48	-94.912	74.620
25 <sup>th</sup> July	19:50	-86.998	74.428
26 <sup>th</sup> July*	17:13	-75.270	73.926
27 <sup>th</sup> July	17:47	-63.609	73.281
28 <sup>th</sup> July*	22:08	-57.885	73.261
29 <sup>th</sup> July	13:40	-61.610	75.402
30 <sup>th</sup> July	19:59	-72.193	76.260
31 <sup>st</sup> July*	17:15	-73.272	76.317
1 <sup>st</sup> August	16:44	-76.097	76.340
2 <sup>nd</sup> August	20:03	-72.689	78.934
3 <sup>rd</sup> August	12:41	-64.180	81.367
4 <sup>th</sup> August	14:57	-69.213	80.150
5 <sup>th</sup> August	22:47	-71.690	79.078
7 <sup>th</sup> August	12:50	-78.381	74.701
8 <sup>th</sup> August	14:22	-96.151	74.191
9 <sup>th</sup> August	14:10	-98.507	74.421
10 <sup>th</sup> August	16:27	-96.235	72.926
11 <sup>th</sup> August	14:07	-99.243	70.090
12 <sup>th</sup> August	14:11	-105.472	68.971

\*Indicates dates included in the (DeMott et al., 2016) study

**Table D.2: Total number of particles analysed, and fractions of the total number of particles classified as either dust or sea salt using CCSEM-EDX.**

Date	Total number of particles analysed	Fraction of total number of particles classified as sea salt	Fraction of total number of particles classified as dust
21 <sup>st</sup> July	2180	0.09	0.01
25 <sup>th</sup> July	1004	0.50	0.11
29 <sup>th</sup> July	516	0.32	0.08

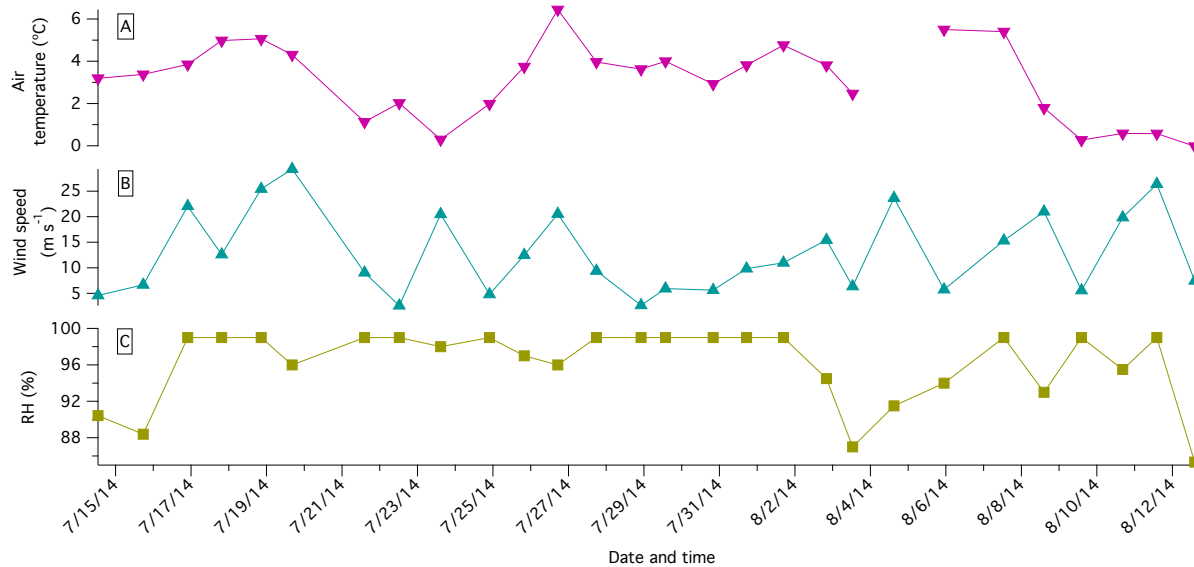
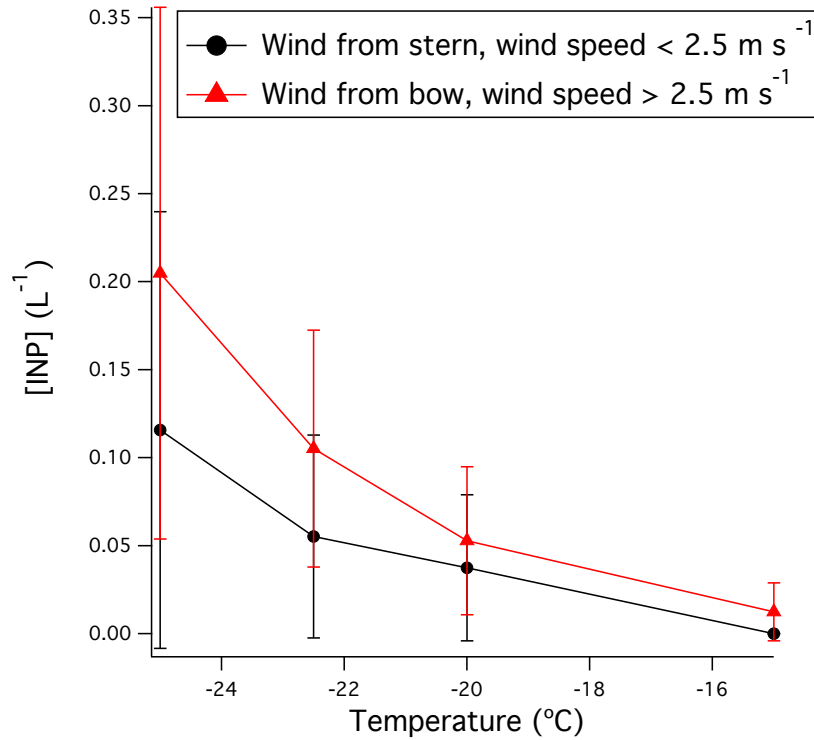


Figure D.1: A) Air temperature, B) wind speed, and C) relative humidity (RH) during sampling.



Figure D.2: Photo of the MOSSI (top shelf), and TSP inlet on the bridge of the CCGS *Amundsen*.



**Figure D.3: Comparison of [INP] (L<sup>-1</sup>) when the wind direction measured on the ship was coming from the bow of the ship (between 0-90° and 270-360°, where 0°/360° = bow of ship) and when the minute average wind speed was higher than 2.5 m/s (in red) to the [INP] (L<sup>-1</sup>) when the wind direction was from the stern of the ship (between 90°-270°) or when the minute average wind speed was less than 2.5 m/s (in black). Error bars represent the 95 % confidence interval.**



Figure D.4: WRF domain used in FLEXPART

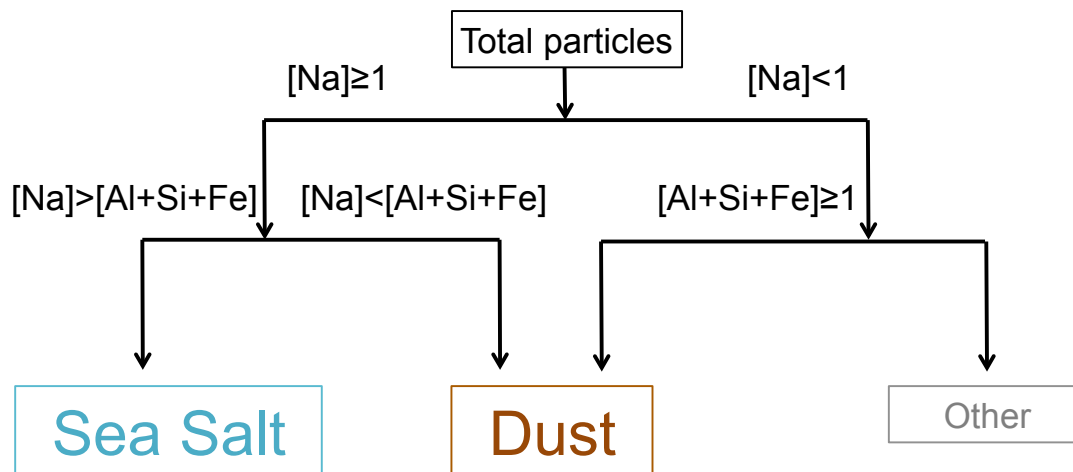
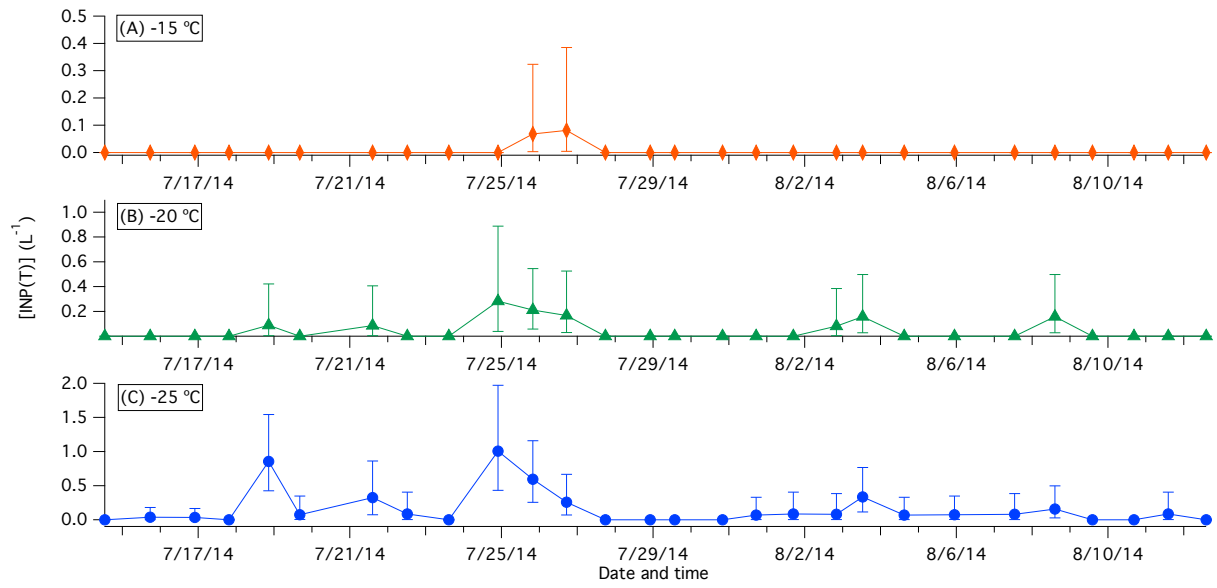
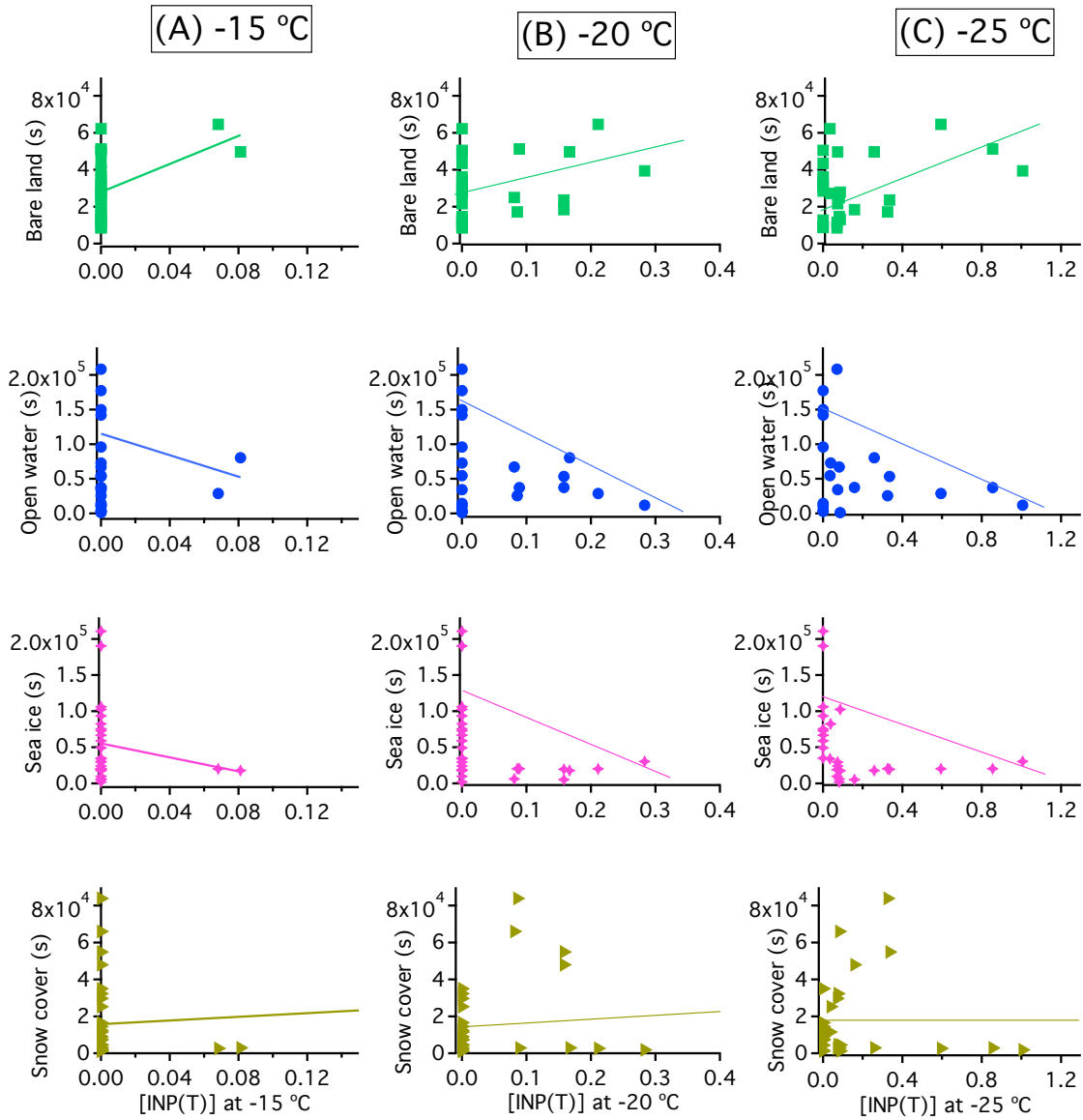


Figure D.5: CCSEM-EDX particle classification scheme. Numbers represent atomic percentage.



**Figure D.6: Time series of [INP(T)] (L<sup>-1</sup>) at A) -15 °C, B) -20 °C, and C) -25 °C. Error bars were calculated using nucleation statistics following Koop et al. (1997).**



**Figure D.7:** Plots for correlation analyses between the time the air mass spent over different surface types within 0-300 m of the surface and [INP(T)] at A) -15 °C, B) -20 °C, and C) -25 °C. Correlation statistics for analyses can be found in Table 4.1.